Analysis of Pile-Concrete Connections in Near-Shore Applications

S. Belfroid

TUDelft

Delft
University of
Technology

Analysis of Pile-Concrete Connections in Near-Shore Applications

In partial fulfilment of the requirements for the degree of

Master of Science

In Civil Engineering at Delft University of Technology

by
S. Belfroid
September 2015

Thesis Committee:

Prof. ir. F.S.K. Bijlaard	TU Delft, Steel Constructions (Chairman)
Ir. R. Abspoel	TU Delft, Steel Constructions
Dr. ir. drs. C.R. Braam	TU Delft, Concrete Structures
Dr. ir. M.A.N. Hendriks	TU Delft, Structural Mechanics
Ing. F. van der Woerdt MBA	Ballast Nedam Engineering

An electronic version of this thesis is available at http://repository.tudelft.nl/.

Faculty of Civil Engineering and Geosciences (CiTG)
Delft University of Technology

Summary

Tubular steel sections are used as foundation piles in near-shore applications like jetties or bridgeworks. The steel tubes are connected to a concrete capping beam or pile cap which transfers the forces from the structure to the piles. Multiple options for this connection type have been developed over the years with varying specifications. Constructability, costs and construction time are of high importance when adopting an alternative.

The possible options have been identified by means of a literature survey. These alternatives follow from various disciplines like pile-footing, pile-to-cap and concrete filled tubes (CFT). Design issues or problems are acknowledged and a consideration is made about the applicability. A further distinction is made by introducing the trade-off aspects like the costs, the construction time and the manufacturability.

The concrete plug connection seems the most used and suitable option. Only in a few situations, this connection is not applicable. A major design problem is the relatively unknown bond strength between the concrete plug and the steel pile. This bond stress is examined in more detail and most influences are identified. Current design expressions, including pile-sleeve formulations, are elaborated by a comparative study in relation to the influences on bond strength found in testing. Furthermore, a new analytical model for the bond strength for circular tubes is proposed. Based on the stresses and strains of both the steel and the concrete, this formulation is obtained by solving the equations. This newly derived formulation (DF) is verified using 61 selected test specimens with the appropriate failure mechanism. When comparing the outcome of this analysis with other bond expressions, the new formulation results in the largest prediction for the 61 specimens with the lowest standard deviation. In combination with the correction factor, this formula calculates safely the bond capacity between the steel pile and the concrete core.

The model is expanded to allow for shear keys in the connection. Unfortunately, this expression cannot be verified as in the case of the bond capacity due to the lack of experimental data. Lastly, a proposition is done for the bending moment capacity of the connection. Two major assumptions in this model need to be verified with testing.

Preface & Acknowledgements

This document is the Master's thesis report to finalize the Master Structural Engineering at Delft University of Technology. This document is established in cooperation with Ballast Nedam Engineering. I first came in contact with Ballast Nedam Engineering on the company fair at the civil engineering faculty. I had a very interesting talk with one of the employees about internships and graduation projects. Infected with enthusiasm, I contacted the engineering department for an appointment.

During the first interview, an idea arose for the graduation topic: the connection between steel piles and concrete elements in near-shore applications. What intrigued me the most concerning this topic is the interface between the steel and the concrete. Multiple disciplines are involved which results in great and numerous difficulties. Right after a very interesting conversation with the professor, I accepted the challenge.

I am really grateful for the opportunity that I got at Ballast Nedam Engineering. Special thanks go to my supervisor Frank van der Woerdt. I want to thank you for the inspiring meetings we had and for the wisdom you provided. Furthermore, I want to thank all members of the committee for guiding me through this process. I found the consultations very interesting and inspirational.

Of course, I want to thank my parents, family and friends for the support. Not only during completion of this thesis but also during the rest of my study and beyond. Mam, pap, de laatste is dan ook eindelijk afgeleverd. Ik kan jullie niet genoeg bedanken voor alles wat jullie voor mij hebben gedaan. Anne-Michelle, thanks for all the support during completion of this work. You could always get my mind off when I needed it. I could not thank you enough.

Delft, University of Technology,   Bas Belfroid
September 2015

Contents

Chapter 1

Problem Description

Near-shore structures are generally founded on circular steel pipe piles. These pipe piles transfer the loading from either a bridge pier or a deck structure to the bearing soil layer. Different aspects favour these tubes like the high bearing capacity, the high torsional resistance, fast installation and the variety in available dimensions. The forces from e.g. a bridge pier or a deck structure are transferred through water, through compressible soil to the bearing soil- or rock layer. Individual piles are connected with a capping beam or a pile cap to form a pile group. The connecting element distributes the loads from the structure over the piles within the group. Due to high corrosion rates offshore, concrete is preferred as a construction material over steel for these elements. This results in the problem of connecting the steel piles to the concrete element.

Several options for this type of connection have been developed and applied in practice. However, it is not a clear decision on which alternative to adopt. Engineers tend to rely on practical experience from previous projects, usually not considering this decision at all. Some alternatives are conceived and tested for specific situations, for instance seismic regions. The usability for other situations for these connections is questionable. Furthermore, a number of alternatives suffer from great constructability impracticalities or are costly to make.

1.1 Motivation

This report is established in cooperation with Ballast Nedam Engineering. Ballast Nedam Engineering is a leading engineering company with major experience in different design fields. Their experience is not just limited within the Netherlands but they executed projects all over the world. Also in the field of application of near shore construction, the experience is vast. Multiple jetty and mooring structures have been realized internationally with great success. To remain competitive in the industry, constant innovation and development is required. Clever designs or new solutions to existing problems might give a reduction in construction costs which generates advantage over the competition.

1.2 Research objectives

The aim of this research is to collect current knowledge about the pipe pile to concrete element connections. This includes possible alternatives, experimental research, design issues and practical experiences. Furthermore, with this information a distinction will be made between alternatives with a trade-off analysis. The design issues of the chosen alternative will be tackled. The purpose of this thesis will be to offer substantiated advice on the pile to concrete element connections. The main question that embraces this research is formulated as:

What is the best strategy of connecting a steel pipe pile to a concrete element in different near-shore situations dealing with unknown/inconsistent factors and with respect to trade-off aspects such as economy, durability and manufacturability?

To answer this question, a literature research will be carried out about possible joining options. With the help of the expertise within Ballast Nedam Engineering, more information about practical experience, like costs, manufacturability etc. will be obtained.

1.3 Outline

The outline of this document is as follows:

The general picture concerning the near-shore structure is given in Chapter 2. Aspects to take into account in making a proper decision are identified. The developed alternatives are listed and subdivided into the production method of the capping beam in Chapter 3. Chapter 4 deals with the decision model in which a distinction is made between the remaining options from Chapter 3. Trade-off aspects like the manufacturability, costs and construction times are considered.

The analysis results in one single alternative which is preferred on this basis. The behaviour of this connection is deepened in Chapter 5. A distinction is made between two axial load transfer methods. The first one, about the natural bond stress, is elaborated in more detail in Chapter 6. An analytical bond model is proposed in Chapter 7 and verified to test data in Chapter 8. The second transfer method is deepened in Chapter 9. The following chapter discusses a proposition for the bending moment capacity. In the final chapter, the main conclusions are presented and recommendations for future research are given.

Applications & Background

The considered pipe pile to concrete element connections are applied in multiple applications with varying properties. Structures in which the joints are adopted are briefly discussed together with more background information regarding production methods of the pile and the concrete element, design influences and the loading which can be expected. This will reveal a number of issues to keep in mind for further design.

2.1 Applications

The function of the steel pipe piles is to transfer the loading from the superstructure to the more compact and less compressible soil- or rock layer (Tomlinson et al. (2008)). In offshore situations, this is through water, through compressible soil to the bearing sand- or rock layer. The structure is connected via a so-called capping beam (jetty) or a pile cap (bridgeworks). Illustrations of these constructions are given in Figure 2.1.

One of the functions of this concrete element is to deviate the forces over multiple piles. The number of piles connected to one concrete element is called a pile group. For the case of a bridge structure, the pile cap supports usually one single bridge pier. A second common structure adopting the pile connections is a jetty structure. In case of cargo jetties, the piles must be able to carry resistance from the cargo handling equipment like quay- or gantry cranes, the weight of the cargo and the berthing forces from vessels (Tomlinson et al. (2008)). Berthing forces can be counteracted in two several manners; forces can be absorbed by a so-called dolphin structure, which works independently from the jetty structure or with fender piles. Fender piles are applied as the first row of piles which are connected with a rubber cushion to the deck of the jetty structure. Impact forces from vessels are transferred and distributed via the deck to the foundation piles. The pier system and jetty structure are typical examples in which pipe piles are connected to concrete elements. Other applications are machinery foundations, abutments, dolphins, mooring structures or retaining walls.
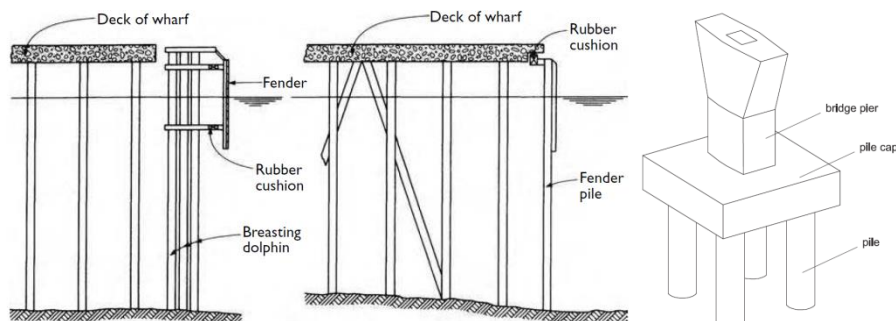
Figure 2.1: Typical constructions in which steel pipe piles are connected to concrete elements (Tomlinson et al. (2008)).

2.1.1 Force deviation

The forces are distributed over the piles within one group by the capping beam. This can be done in two ways according to Hsiao (2012):

- The first method assumes that only a part of the horizontal load is resisted by the inclined piles (a.k.a. batter piles) (traditional statical method).
- The second method assumes that the horizontal load is resisted by the inclined piles. This means that the vertical piles carry none of the horizontal load.

The vertical force (V_i) in the piles equals

$$V_i = \frac{P}{n} \pm \frac{M}{\Sigma(x_i{}^2)} x.$$
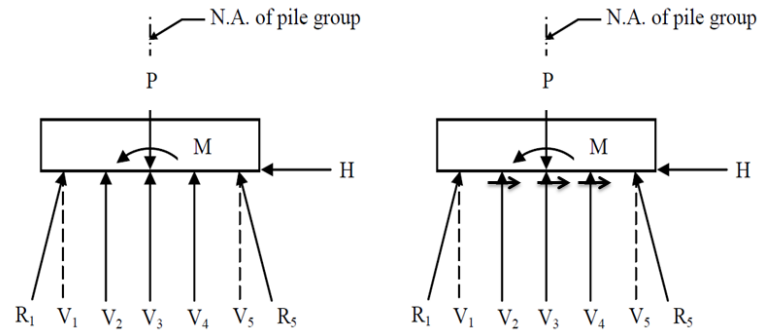
(Eq. 2.1)

Figure 2.2: Pile cap with three vertical piles and two batter piles, on the left the first method and on the right the second method. (Hsiao (2012)).

The vertical force, as expressed in (Eq. 2.1), is a function of the number of piles (n), the distance from the pile to the centre of the capping beam (x_i) and the bending moment (M) as shown in Figure 2.2. With the first method, the slope of the batter piles can be chosen freely. When for instance a slope of 1:8 is assumed, the force in the batter pile will be

$$R_{b,i} = V_i \left(\frac{\sqrt{(8)^2 + (1)^2}}{8} \right)$$

(Eq. 2.2)

in which $R_{b,i}$ is the resultant in the batter pile and V_i as defined in (Eq. 2.1). With the second method, the angle of the batter piles cannot be chosen freely. The magnitude of the horizontal load determines this angle. Both distribution methods have been examined by Hsiao (2012) by means of modelling. Three different scenarios, each with a different ratio between vertical and inclined piles, are verified. The connection to the capping beam is both assumed pinned and clamped for each scenario (Figure 2.3). By comparing both methods for all three scenarios (with pinned and clamped connections), the second method gives more equivalent outcomes to the modelling results (SAP2000). The first method gives large computational errors.
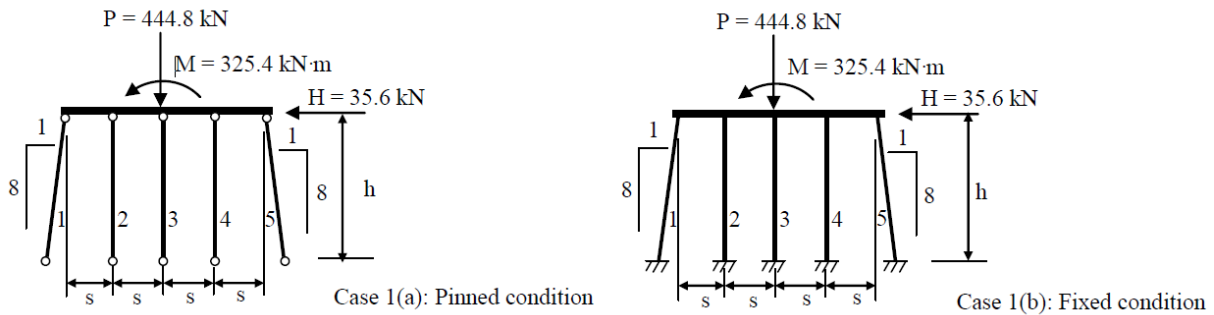
Figure 2.3: Both pinned and clamped connections for scenario one (Hsiao (2012)).

2.1.2 Loading

Depending on the application, the loads are induced due to several reasons. Tomlinson et al (2008) made a list of all the loads which can be exerted and which will result in an axial force in the piles (P), bending moments (M) and shear force (H). The loads are summarised for the two main structures namely the jetty and the bridge pier.

Jetty:
- Dead load,
- Berthing loads including fendering,
- Lateral loads due to pull of mooring ropes,
- Loads from wave forces,
- Current drag and moored ships,
- Lateral loads from wind on mooring ships, cargo or handling equipment,
- Dead load of the structure and the handling equipment,
- Compressive and uplift forces due to overturning movements,
- Loadings from ice or earthquake excitation have to be taken into account when present.

Bridge pier:
- Dead- and live load on the superstructure,
- Dead load of the superstructure,
- Earth pressure on the abutments,
- Creep and shrinkage of the concrete,
- Temperature variations of the superstructure,
- Traffic forces (like braking, accelerating and transverse forces),
- Wind- and eventual seismic loadings,
- Collisions (from traffic or locomotives, vessels etc.),
- Construction loads,
- Current- and wave forces,
- Impact from garbage.

2.2 Pipe piles

As stated in the introduction of this thesis, circular piles are advantageous due to several reasons. Circular tubes can resist high forces to which they can be driven into place. This is performed by use of an impact hammer (diesel, hydraulic or water impact hammer) or, when limited penetration is needed, by vibration. Several driving techniques have been developed over the years to improve on the installation time and impact consequences. Another feature of the driving process is that the soil properties around the pile change. The fabric of the soil is rearranged, the soil density is changed and the larger particles can be crushed into smaller parts resulting in a change in grain-size distribution in case of sand. This does not hold for clay and rock layers (Kraft (1991)).

Furthermore, the circular piles are available in a large range of dimensions (diameter, wall thickness and length) and provide a high flexural strength for horizontal berthing forces and environmental loads. On top of the previous, the sections are relatively light and therefore the transportation is relatively easy and economical. Lastly, the analytical methods of establishing the bearing capacity of the piles are improved over the years (Tomlinson et al. (2008)). These models result in greater assurance of long-term performance. The concept of redistribution in a pile group allows the piles to be shorter and a reduction in cross-sectional dimensions can be achieved.

Three different pipe piles can be distinguished according to the chosen installation method (Tomlinson et al. (2008)). These are the large displacement-, the small displacement- and the replacement piles. The first category contains all driven piles with a closed-end. Timber (round or square), precast concrete and steel tubes (with closed-end) are examples of this category. Examples of the small

displacement piles are open-ended steel pipes or open-ended prestressed or precast concrete piles. The pile is called open-ended when the soil is able to enter the pile (no further provisions are given). Nonetheless, this research is limited to steel piles only.

Pipe piles transfer the forcing to the bearing soil layer via either the tip of the pile (point bearing piles), friction (friction piles), and lateral force transfer or tension forces via shaft friction. Due to overturning moments (due to wind or berthing loads), piles can be loaded in tension which can be permanent or temporally. The resistance of such a tension pile contains the own weight of the pile, the friction between the pile shaft and the surrounding soil and the adhesion between pile and soil (FinnRa (2000)).

2.2.1 Production methods

The production process of the piles is depicted in Figure 2.4. The pile is formed through spiral welding of steel sheets during production. The first steps in the process are the uncoiling, forming and levelling of the sheets. Subsequently, the steel is welded (on the in- and outside) and inspected visually. The dimensions are checked and the ends are bevelled. Furthermore, the piles are ultra-sonically tested and the last checks are performed by X-ray and visual inspection. The final step is applying the appropriate corrosion protection in the form of a coating after which the pile can be used. Instead of spirally welding, longitudinal welding is also an option. The steel plates are pushed and rolled into the desired shape followed by the welding process. A third method for production is by rolling steel sheets and welding them together. The pieces are welded longitudinal and to create the piles, the specimens are welded circumferential. The so-called 'cans' can be produced up to diameters of eight meters (Skyline (2013)). These piles are applied in deep-sea foundations as in the case of monopiles.
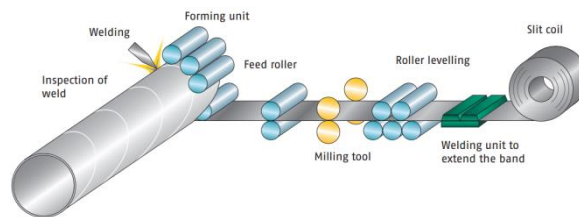
Figure 2.4: Production process of the steel pipe piles (RUUKKI (2014)).

According to supplier's information (RUUKKI (2014)), diameters of the spirally welded pipe piles differ from 406mm to 1220mm with thickness varying from 8 to 20mm (depending on the pile forming equipment). Available steel grades are S355, S440 and S550. Piles can naturally be produced with varying lengths. The production range of Arcelor Mittal (2010) varies from diameters of 864mm till 2997mm with wall thicknesses ranges from 10 to 25mm. The top quality is X70 which corresponds with a minimum yield strength of 485N/mm^2. Piles can be produced up to a length of 53m without splice welds.

2.2.2 Driving tolerances

It is almost impossible to install the pipe piles exactly in the intended position. The pile tips will deviate due to obstructions in the ground or tilting of the piling frame leaders. Furthermore, piles can cause horizontal ground movements by which the location of the tip deviates from the intended position. This misalignment should be prevented as much as possible since this will otherwise conflict with the congested reinforcement within the capping beam/pile cap or it can cause interference between the collaboration within a pile group. When during construction the tolerances are exceeded, the pile cap should be redesigned or additional piles should be installed to ensure that the working load is within project tolerances (Tomlinson et al. (2008)). Deviations can be decreased by pulling the piles afterwards to a more vertical position.

The Eurocode (ECS (2001)) prescribes that tolerances above water should be according to the specification requirements with a maximum of 100mm. The skew cannot be more than 0.04mm/m

pile. These values need to be adopted for both vertical- and batter piles installed as displacement piles. According to ECS (2011e), the maximum deviation is 100mm for pipe piles with a diameter (D_p) smaller then 1.0m, $0.1D_p$ for 1.0m≤D_p≤1.5m and 150mm for D_p>1.5m in case of bored piles.

2.2.3 Corrosion

Steel pipe piles are susceptible to corrosion, especially in marine conditions. Corrosion is an electro-chemical process caused by moisture and oxygen. In near-shore situations, salt is normally present which accelerates the diffusion of electrons. In offshore usage, corrosion protection is of extra importance. A second form is bacterial corrosion, which can occur even without the presence of oxygen. Morley et al. (1983) divided the pipe pile in different zones according to corrosion rates (Figure 2.5). The buried zone is where the pile is embedded into the soil. Almost no oxygen is present, which limits the amount of corrosion. Therefore, there is less need for corrosion measures.
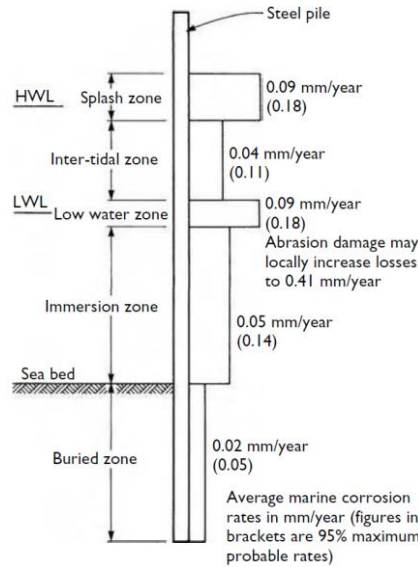
Figure 2.5: The different zones with the corrosion rates (Morley et al. (1983)).

The immersion zone of the pile is continuously submerged in the water. In this zone, high corrosion rates are expected. Adequate protection methods are anodes or applying a protection layer. A third option is to omit any coating but to increase the wall thickness. The thickness will then be a function of the corrosion rate to achieve a certain life span. With this method, the protection can be less or even omitted (ECS (2007)). The anode protection is realized with either a sacrificial system or with power-supplied anodes. Marine growth in the form of weeds and barnacles can interfere with the suture of the applied coating. The highest corrosion rate is present in the splash zone (the surface where waves hit the pile). In this area, corrosion rates up to 0.18mm/year can be found. Adequate protection is of high significance. Coatings (with reapplying every 10-15 years), encasement or sacrificing the steel tube are sufficient options.

2.2.4 Capacity

The capacity of the pipe piles is relevant for the connection design since in seismic design spirits, the structure must provide sufficient ductility and deformation capacity (AASHTO (2012)). When the pipe pile has more strength than anticipated, the connection might be the weaker section after which non-anticipated failure modes occur. The three most influential aspects are the installation method and the soil- and pile parameters. The latter two determine the buckling capacity, since the following equation holds (ECS (2008))

$$L_{crit} = k \cdot L_{pile}. \qquad \text{(Eq. 2.3)}$$

The buckling length (L_{pile}) is a function of the length above the firm soil and the stiffness of the connection (k). In the case of soft soil, the firm layer is far down after which a long buckling length is found. The connection design can counteract this effect.

One last phenomenon that might influence the capacity is scour around the piles. This phenomenon is the removal of soil around the piles due to current or transportation of particles (Figure 2.6). According to Hosseini et al. (2015), scour is the main cause of bridge failure worldwide. Scour can either be a local or general effect.
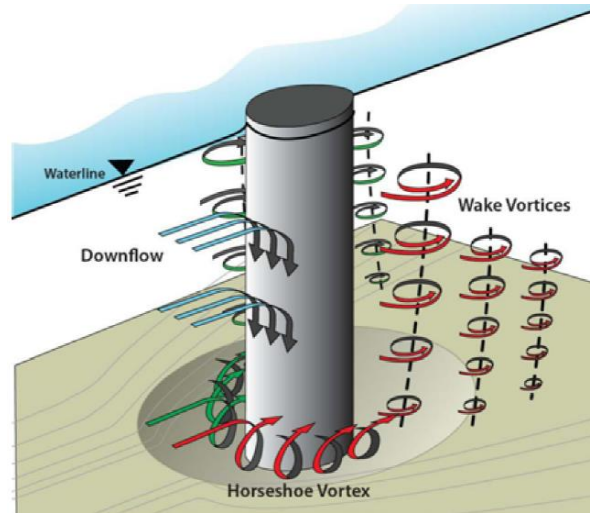
Figure 2.6: Scour around piles in near-shore construction (Hosseini et al. (2015)).

2.3 Capping beam/pile cap

The concrete element connecting the piles to the structure can be made of reinforced or prestressed concrete (Shritharan (2005)). Steel elements may also be applied due to the relative lightness and flexibility. For economic and practical reasons, these elements are not considered in this research.

The capping beam is placed at the level of low tide or low river height in the case of over-water bridges. This location is adopted since during a collision, a vessel would hit one single pile rather than dividing the load over multiple piles. Furthermore, ships cannot get trapped between the piles. A second reason is that garbage and litter will not gather around the piles which is aesthetically not appealing (Tomlinson et al. (2008)).

Production methods of the concrete element are in-situ casting, prefabrication or a combination of the two. In case of the former, the construction is separated from the river by a cofferdam to create a dry building dock. After placement of the formwork, the element is casted on the building location. A combination of prefab and in-situ casting is achieved with a precast box structure. After installation of the precast box and placement of the reinforcement, it is filled with in-situ concrete. Such a solution can be adopted when the lifting weight becomes too large. This solution can also be convenient in tidal rivers (Tomlinson et al. (2008)).

2.3.1 Reinforcement design

Capping beams or pile caps transfer high forces exerted by the superstructure. Congested reinforcement lay-outs might be required to make sure that these forces can be transferred and that crack widths are within the limits. Three different design methods are applicable for this matter namely bending theory (Euler-Bernoulli), truss analogy and the strut and tie model (STM). The difference between the latter two is found in how it is dealt with non-linear effects. The truss model does not take cracking and reinforcement yielding into account while STM does (Yap (2012)). The three different possibilities are a point of discussion in current research with varying results regarding the most economical design.

Raj et al. (2008) conducted an experiment on all three different theories and concluded that the STM leads to the lowest cost regarding reinforcement. Contrary to the conclusion from Raj et al. (2008), is the result from Nori et al. (2007). They state that an STM will result in <u>more</u> flexural reinforcement than the beam theory (bending theory). The reason for this difference is that no shear reinforcement is needed. This conclusion is based on strut and tie models for pile caps with different numbers of piles and with different loading situations. Furthermore, they conclude that an STM cannot be used for loading situations which include bending moments.

According to Souza et al. (2009), this inconsistency in test results between Raj et al. (2008) and Nori et al. (2007) can be explained by two factors. The first is the position of the critical section for bending and the second is the position of the nodal zone underneath the column. Therefore it is difficult to state that the STM is more efficient in general. Added to this conclusion is that the strut and tie model represents the flow of forces better than the sectional design methods.

2.4 Conclusion

The backgrounds concerning the steel piles, the concrete element and the possible applications are investigated in this chapter. Important issues are pile tip deviations up to 150mm, steel corrosion, capacity of the piles and the reinforcement design of the concrete element. These matters should definitely be taken into account.

The connection type investigated in this report, finds its application in for instance jetty structures, bridgeworks and mooring structures. Due to the several possible applications, multiple designs have been made over the years. These are examined in the following chapter.

Alternatives

Resulting from the multiple applications to which the considered connections are applicable, numerous alternatives have been developed over the years. These variants are subjected to a great deal of research about failure mechanisms, strength properties and seismic behaviour. An overview of the current knowledge is reported and alternatives are listed.

3.1 Design strategies

During this literature research, two design strategies are acknowledged. Most of the found research concerns the usability in areas with seismic activity. The intention for those areas is completely different since it focusses on different principles.

3.1.1 Seismic design strategy

Seismic design is aimed at ductility within the connection/system. According to the AASHTO (2012), the piles are the members that are able to provide this capacity the most. Their reasoning is that the piles provide a high energy-dissipation and rotation capacity. Prior to failure of the connection, the piles should have formed plastic hinges. As seen in the left of Figure 3.1, the pile tends to buckle to which plastic hinges are formed. The pile will tear at the location of the local buckle when the load is further increased as displayed in the right of Figure 3.1.

Experimental research for seismic purposes is aimed at demonstration of the proper failure mechanism. These seismic systems are called capacity-protected, since the connection provides higher cyclic loading strength in comparison to the adjacent members (NCHRP (2011)).

Figure 3.1: Local buckling of the pipe piles on the left and tearing of the tube at the position of the local buckle at the right (Stephens et al. (2014)).

Due to the unpredictable character of seismic activity, design forces are taken twice the expected magnitude. An overstrength factor is introduced to make sure that the correct failure mechanism occurs. This factor increases the column capacity by 1.25 in order to make sure that all other parts in the system are stronger than the column. It happens that columns are stronger than accounted for due to miscommunications or delivery reasons (AASHTO (2012)).

3.1.2 Non-seismic design strategy

Non-seismic design aims at adequate strength during service and exceptional conditions. Components should be designed according to the appropriate design code to provide adequate levels of safety. Choosing between alternatives is based on practical and economic reasons in contrast to the previous paragraph. These alternatives are likely to be too expensive in non-seismic application.

3.2 Connection alternatives

To be able to make a distinction between the options, the construction method of the capping beam is used. Following from the previous chapter, it is seen that this element can be produced either in-situ or prefab. The results from experimental research are added for every connection design.

3.2.1 In-situ capping beam/pile cap

3.2.1.1 Monolithic connection

The monolithic connection type, like depicted in Figure 3.2, is made in combination with an in-situ capping beam. The idea behind this connection actually follows from column-footing details, however literature states that it can be used for pile to cap applications (Stephens et al. (2014)).

With this connection, the pile is cast into the concrete element. The length of the pile within the capping beam is called the embedment length (or embedment depth) of the connection. An annular ring is welded onto the pile to provide sufficient shear resistance of the pile. This connection is widely used in American bridge structures, mostly in combination with concrete filled tubes (CFT).
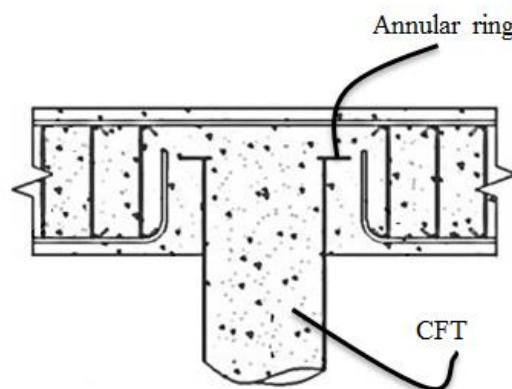
Figure 3.2: Monolithic connection (Stephens et al. (2014)).

Experimental research

Multiple tests have been conducted by Roeder et al. (2008), Lehman et al. (2012), Richards et al. (2011) and Rollins et al. (2010) concerning the bending moment capacity of this connection. The bending moment capacity is, according to the authors, attributed to the pressure of the pile against the concrete (Figure 3.3). When the pile starts to rotate, the concrete exerts a pressure on both sides of the pile. This pair of horizontal forces gives the bending moment capacity. It is clear that with increased embedment length this bending moment capacity increases. Findings indicate that, in case of a shallow embedment (0.6 times the pile diameter), the footing starts to crack at the location of the interface (Roeder et al. (2008)). By increasing this embedment length, the desired failure mode occurred (yielding of the pile).
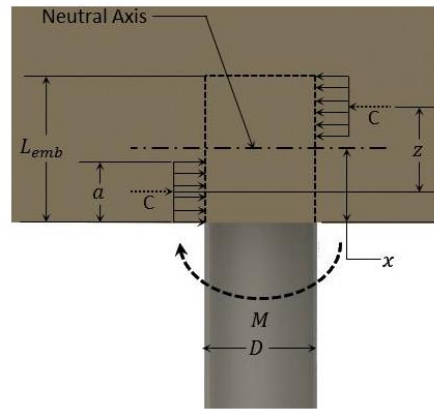
Figure 3.3: Bending moment capacity of the connection (Kappes et al. 2013)).

Richard et al. (2011) state that the connection is still able to transfer significant bending moments with shallow embedment. This is, according to the authors, attributed to the friction between the pile and the concrete as shown in Figure 3.4. This conclusion is contrary to the earlier statement by Roeder et al. (2008)). Rollins et al. (2010) tested piles which did not have a concrete infill (hollow piles). With sufficient embedment, acceptable capacities are found. All the conducted research led to design expressions for the monolithic connection. These formulations are presented in Appendix A.
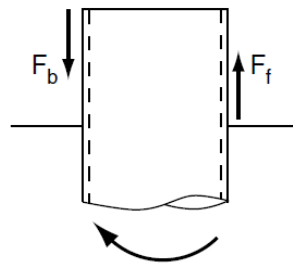
Figure 3.4: Friction between the pile and the concrete resulting in bending moment capacity (Richard et al. (2011)).

Design issues

Embedding the pile into the concrete results in critical design- and practicality problems. Stephen et al. (2014) denoted that the embedded pile conflicts with the congested reinforcement within the capping beam and to make this alternative a success, this issue should be resolved. In this research domain, piles can have diameters up to around 1200-1500mm. This would mean that the longitudinal reinforcement of the concrete element should be deviated around or extended through the piles. A design method of the former solution is added in Appendix A. The latter solution requires lots of manual labour which will enhance the construction costs. Furthermore, the concrete beam should have sufficient height to provide enough resistance against punching shear. This leads to more material usage and therefore more transportation, more environmental unfriendly designs and cost enhancements.

3.2.1.2 Encased fixed-based detail

A second option for the connection in combination with an in-situ capping beam or pile cap is the connection developed by Marson et al. (2004). This connection (Figure 3.5) contains of a steel frame welded onto the pile. After the pile is positioned, the top plate is slipped over the pile. Two U-shaped channels are welded onto this top plate and finally the bottom plate is welded against these channels. This total frame is subsequently casted into the concrete.
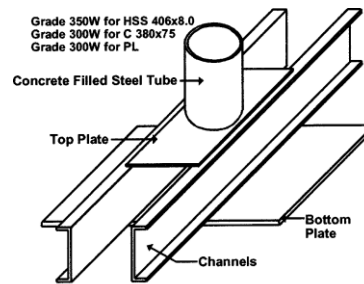
Figure 3.5: Fixed-based connection detail (Marson et al. (2004)).

Experimental research

Only four test specimens are reported in literature with diameter over thickness ratio of the pile (D_p/t_p) ranging from 34 to 64. Steel plates with a thickness of 30mm are adopted. According to Marson et al. (2004), no extra pile-to-cap reinforcement is needed since the steel sections are able to transfer the loads. Experimental research shows the ability for seismic purposes.

Design issues

Just like the monolithic connection, the interference with the capping beam is a major concern. Also the constructability and practicality while constructing above water, is highly questioned. Lastly, there is a significant amount of welding to perform on site, which will result in high construction costs.

3.2.1.3 Other options

On top of the previous two options for an in-situ capping beam, the Eurocode gives one more example for a possible connection type (Figure 3.6). Shear studs are welded onto the outside perimeter of the pile which will provide resistance against shear and pull-out of the pile. No conducted research has been found about this possibility in literature. Similar connections are adopted in the field of underwater concrete floors. The top part of the piles is treaded to provide for sufficient friction between anchor and concrete.
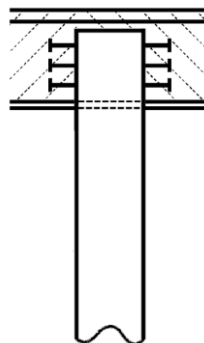
Figure 3.6: Option adopting shear studs by ECS (2008).

3.2.2 Prefab capping beam/pile cap

3.2.2.1 Isolated connection

The isolated connection (Figure 3.7) is very similar to the monolithic connection, only now it is adopted in combination with a prefab concrete element. Recesses are left open in the capping beam in which the piles are positioned. These recesses are made with a corrugated pipe to serve as formwork during casting of the concrete element. These recesses are filled with high strength grout on site to form the connection with the pipe piles. No additional pile-to-cap reinforcement is required.
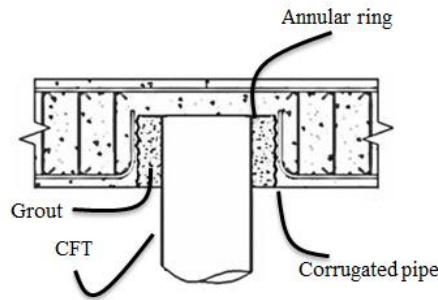
Figure 3.7: Isolated connection (Stephens et al. (2014)).

Experimental research

Research about the isolated connection is associated with research of the monolithic from section 3.2.1.1. The results as presented in Appendix A are also applicable to this connection type.

Design issues

The same design issues apply to the isolated connection as to the monolithic variant due to the similarities. Adopting this connection in a pile-to-cap construction, the recesses should provide for the ability of pile deviations. A problem arises when these deviations are larger than the recesses can provide. Secondly, the grout is poured immediately after the element is positioned, which gives cause to new issues. The space around the pile should be closed and sealed, to which the grout is poured from either below or above the capping beam. This results in impracticalities at the workplace.

3.2.2.2 Embedded base plate

A totally different option is the one developed by Steunenberg et al. (1998). This connection (Figure 3.8) contains of a thick steel plate which is embedded into the capping beam and bonded with anchor bars. Forces are transferred via these anchors to the plate and subsequently to the pile. This means that the plate will be loaded in bending. The capacity is a function of the strength and ductility of the anchors, the connecting welds, the bending stiffness of the plate and the flexural behaviour of the top of the pile. Thicknesses of 30-50mm for the steel plate are commonly adopted due to this reason. On site, the piles are levelled and bevelled with great precision. The plate is welded to the pile with a full penetration overhead weld after placement of the cap.
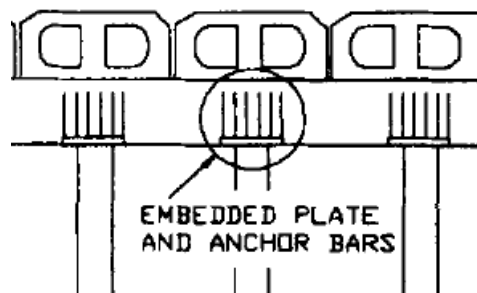
Figure 3.8: Embedded plate and anchor bars (Steunenberg et al. (1998)).

When designing for seismic regions, the pile is compact and relative small in order to prevent that either the weld, the plate or the anchors will fail. With the mentioned thickness for the steel plate, the plates should be tested for lamellar tearing by means of ultra-sonic testing. Lamellar tearing is a material failure in which small inclusions are present in the steel. Cracking in the steel is induced by the non-metallic manganese-sulphide inclusions. Failure can be avoided by the use of proper steel with lower sulphur content (Steunenberg (1996)). The anchorage is designed as if it is a reinforced concrete beam (the capping beam) (Steunenberg et al. (1998)). According to the design, the strains are assumed to be linearly along the length of the plate. Therefore, the plate should have sufficient bending moment resistance.

The welding of the steel plate to the circular pile has to be performed by a qualified welder with the appropriate inspection afterwards. When weld faults are found, it needs to be repaired and rechecked.

Experimental research

Research has been performed by Steunenberg et al. (1998). Only one test specimen is examined with a diameter of 324mm and a wall thickness of 12.7mm. The yield strength of the pile appeared to be almost 30% higher than expected which indicates the usefulness of the overstrength factor (like explained in section 3.1.1). Despite the exceedance of this factor, the connection still fulfilled the requirements and the appropriate failure mechanism was found.

Design issues

The large thickness of the plate is cause for ultra-sonic testing and high workshop specifications. The required tools to handle such a plate are expensive and not present in every region. Holes are drilled in the plate in which the anchor bars are positioned. This means double welding of the anchor bars on both sides of the plate, which is costly to perform. Furthermore, deviations in pile tip position need to be accounted for in the anchor plan resulting in a lot of anchors and large plate dimensions. The plates are welded to the piles with overhead welds on site. Only special trained and licensed workmen may perform this weld. Nonetheless the quality of the welders, weld defects are hard to prevent.

3.2.3 Both prefab and in-situ

3.2.3.1 Plug connection

For both a prefab and cast in-situ capping beam, a concrete plug connection (Figure 3.9) can be used. The pile is partly filled with concrete to which the load is introduced. The concrete transfers the load via the natural bonding (bond stress) or shear keys which are welded on the inside of the tube. The concrete within the pile is reinforced for practical reasons.
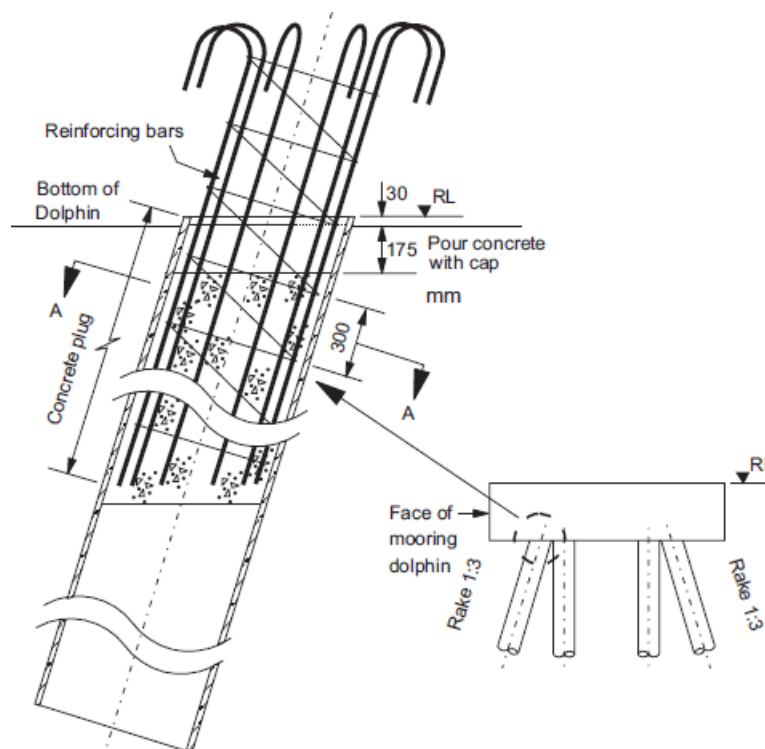
Figure 3.9: Plug connection for a batter pile (Nezamian et al. (2006)).

Experimental research

Lots of experimental research is conducted about two topics concerning this connection type. The first subject is the pile-to-cap reinforcement, particularly the shape. In Figure 3.9, it can be seen that the top of the reinforcement bars are bended outwards. Other possibilities can be inward bended bars or straight bars with spiral reinforcement like seen in Figure 3.10, right figure. This reinforcement lay-out is a point of discussion. According to Ferritto et al. (1999), the inward bend dowels are to be preferred over the outward bent variant. The reason is that the outward bended dowels transfer high tensile stresses to a region which is already subjected to high tensile forces from joint shear forces. Roeder et al. (2005) found opposite results.

The second research topic comprises the natural bond stress between the concrete core and the steel pile. It seems that small differences in parameters result in large effects on the axial capacity of the plug connection. A more detailed description of this issue is given in Chapter 6.
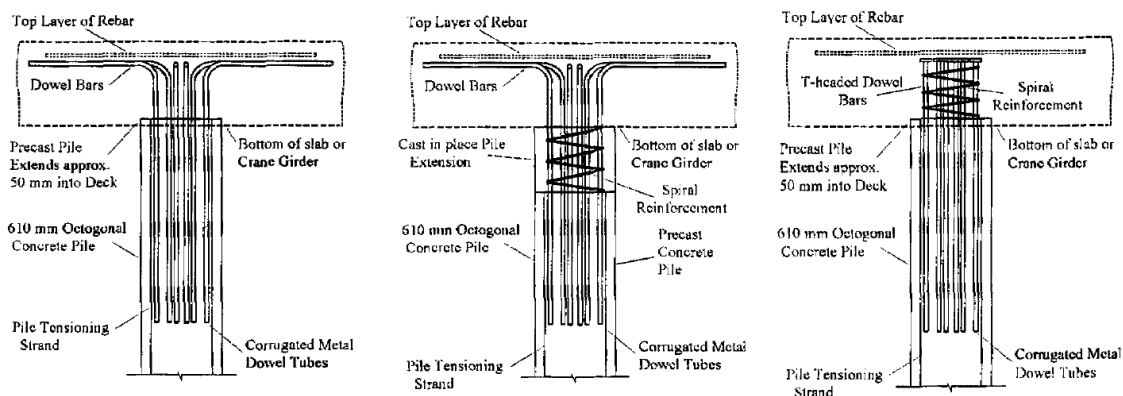
Figure 3.10: Three typical plug connections (Roeder et al. (2005)).

Design issues

The major issue with this connection is the highly uncertain bond stress and the way of connecting it to the capping beam. Bond seems to rely on a vast range of parameters with varying influences on the capacity. One way to dodge this issue is to apply shear keys. It should be noted that these keys are welded on the inside of the pile, this means that it should physically be possible to reach this location and still be able to perform high quality welding.

3.2.3.2 Reinforcement welded to steel shell

In this connection, the pile-to-cap reinforcement is welded to the steel pile (Figure 3.11). This can either be on the inside or the outside of the pile. The adopted reinforcement bars can only be straight since otherwise, it is impossible to position the capping beam (see Figure 3.12). If the pile would have been inclined, the reinforcement cannot be guided into the recess. Inclinations due to the driving process can also result in impractical situations. In extreme situations, reinforcement bars are dismissed because they cannot be positioned into place.

Since the hole in the capping beam needs to be filled with concrete afterwards, it is usual practice to partly fill the pile as in the case of the plug connections. Figure 3.11 is based on the same principle as the isolated connection with associated drawbacks. The principle of Figure 3.12 is deemed more practical.
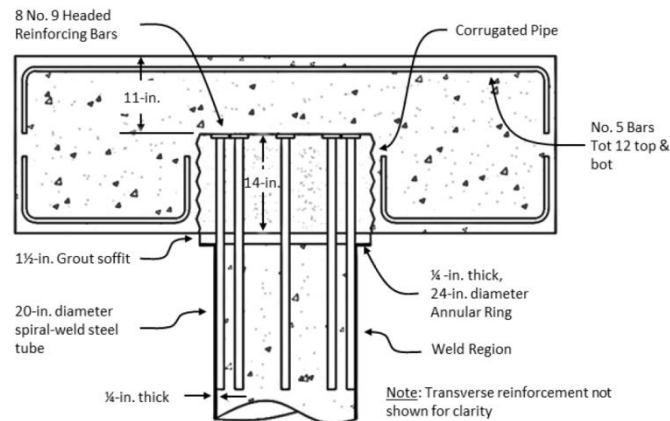
Figure 3.11: Reinforcement welded to steel shell (Berg (2014)).

Figure 3.12: Principle of connecting the reinforcement bars to the cap (NCHRP (2011)).

Experimental research

Very little research on this connection type is found in literature. Berg (2014) tested one specimen with the dowels welded to the inside of the steel pipe pile for CFT columns. The pipe pile, with 508mm diameter, is connected to the capping beam with eight reinforcing bars. The reinforcing bars extend over 355.6mm into the capping beam. The one specimen did not achieve the desired failure mechanism to fulfil the seismic design requirements.

Design issues

This connection has great similarities with the plug connection type, only now the load is not transferred via bond or shear keys. The greatest concern is the economic part, lots of welding is required which has to be performed on site. Furthermore, all installations for pouring the concrete need to be present just like in case of the concrete plug connection.

3.2.3.3   Inverted t-beam

Propositions for pile-to-cap connections are done by Stephen et al. (2014). Based on the knowledge of pile-footing details, they developed CFT pier cap beam connections with the use of a precast inverted-t cap beam element (Figure 3.13). Proposal A and C are based on earlier described principles. Proposal B uses dowels to connect the pile via a bearing pad to the prefabricated element. Option D is an example of a pinned connection.
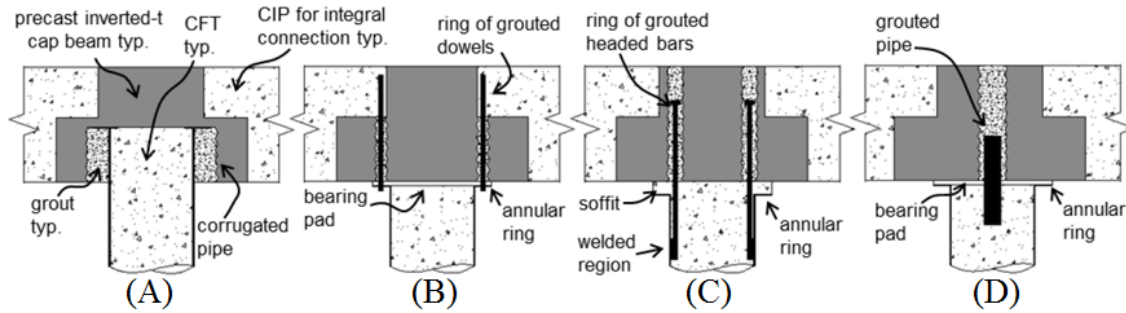
Figure 3.13: Proposal by Stephens et al. (2014).

3.3   Suitability for seismic regions

Now all the possibilities are identified, a separation is made by Harn et al. (2010) for the seismic usage. The adaptability in seismic region is dependent on the ability to form plastic hinges in the pile. According to Harn et al. (2010), the embedded connections (monolithic and isolated) and the embedded plate connection are suitable for these purposes. The result of their analysis is listed in Table 3.1. Full-moment means that the pile will form plastic hinges and partial moment means connection failure. Not all options are adopted in the table since they are not considered in their analysis or there is a lack of experimental data to come to a conclusion.

Table 3.1: Pile-to-Deck connections (Harn et al. (2010)).

Connection Type	Full Moment	Partial Moment
Embedded pile	X	
Embedded plate	X	
Plug connection		X

3.4   Conclusion

All possible alternatives have been listed according to the production method of the concrete element. Eight different options are found based on pile-footing details, pile-to-cap and CFT applications. By comparison with the specifications found in Chapter 2, design issues are detected for each. A summary of all connections and the associated issues are given in Table 3.2.

The embedded connections result in highly impractical designs. When piles are adopted with a diameter in the range of 1000mm and taking into account possible deviations of 150mm, a substantial amount of longitudinal bars needs to be deviated around the pile. This causes additional design challenges but also a high labour intensive reinforcement lay-out. On top of the previous, punching shear causes increased beam heights which result in more material usage. Based on these reasons, the embedded connections like the monolithic, encased fixed-based detail, the ECS (2008) example and the isolated option are dismissed. In the next chapter, there will be continued with the embedded plate, the concrete plug and the reinforcement welded to steel shell connection.

Table 3.2: Summary of the found connections with the associated issues.

Production method	Issues
In-situ capping beam	
Monolithic	Reinforcement interference
	Punching shear - large beam height
Encased fixed-based detail	Reinforcement interference
	Lot of welding on site
ECS (2008) method	No test data found
	Lot of welding on site
	Reinforcement interference
Prefab capping beam	
Isolated	Reinforcement interference
	Pile deviations
	Sealing and placement grout
Embedded plate	Workshop specifications
	Adequate workforce required
Both	
Concrete plug	Bond stress
	Connection to cap
Reinforcement welded to steel shell	Lot of welding on site
	Expensive
Inverted t-beam	Only a proposal
	Reinforcement interference

Decision Model

Choosing between the presented alternatives is directly related to the situation at hand. In practice, experience plays an important role in this decision. Knowledge within a company is obtained about a few alternatives by means of development, testing and adaptation. A distinction will be made between the remaining options from the previous chapter. A decision scheme is proposed which can be used by engineers to adopt an alternative. It should be noted that this is a general scheme in which general assumptions are done. In particular situations, specifications can change to which the outcome may be different. One project is not like another. The information within this chapter is mostly obtained with interviews within Ballast Nedam.

4.1 Design influences

Multiple influences on the decision for a connection are already found in Chapter 2. The final decision follows from minor decisions during the design process. If for example a jetty construction is considered, the construction method of the capping beams is chosen for economic reasons, which subsequently influence the connection type. Sticking with this jetty, if this structure is realized in an area where large tidal differences are expected, assembly time is of importance. For this example, the embedded base plate by Steunenberg et al. (1998) will probably be best suited. However, suppose that this same jetty is used for transportation of liquefied natural gas. This -180 degrees fluid will cause brittle failure of the welds during leakages. In that situation, the proposed connection can definitely not be used. This simple example already shows the vast range of influences on the connection design.

4.1.1 Aspect groups

The influences found during this analysis are organised within groups. Arising from available project data within Ballast-Nedam Engineering, the following clusters are established. A detailed description, possible examples and a list of influences is given in Appendix B.

- Construction aspects,
- Function,
- Loading,
- Availability,
- Possible lifting weights,
- Local conditions,
- Capacity and installation method piles,
- Practical experience.

4.2 Advanced decisions

The design issue is subdivided into multiple decisions prior to the connection consideration. How this simplification is performed, is elaborated in Appendix B (section B.2). These decisions include

- The type and magnitude of loading (following from e.g. the function),
- The production method of the capping beam,
- Type of pile (including capacity),
- Speed of construction.

4.3   Decision scheme

With the simplifications that are proposed in section B.2 of Appendix B, a decision scheme can be formulated to which a decision for a connection can be made (Figure 4.3). This scheme is composed with the help of the expertise within Ballast-Nedam Engineering. Three options remained from Chapter 3 namely, the embedded plate connection by Steunenberg et al. (1998), the concrete plug connection and the reinforcement which is welded to the steel shell. The embedded options are dismissed due to the capping beam reinforcement and economic reasons.

The alternatives are numbered in order to give more insight in the appearance (Figure 4.1). Alternative 1 equals a concrete plug with long interface length, 2 medium length, 3 short length, 4 is the embedded plate connection and 5 the reinforcement welded to the steel tube. It should be added that the short plug should at least have a length of 1200mm to provide enough anchorage length for the pile-to-cap reinforcement bars.
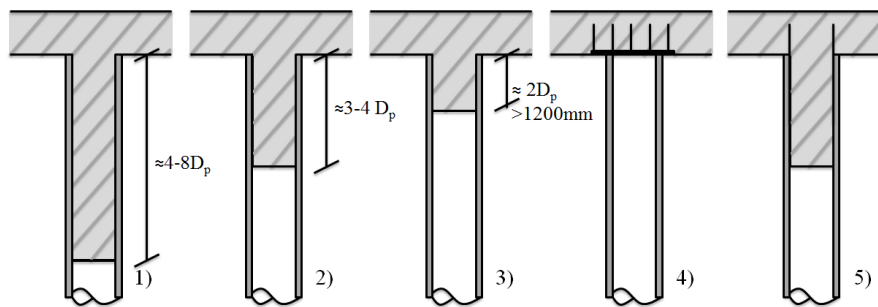
Figure 4.1: The numbering of the alternatives.

4.3.1   Instructions

The scheme starts at the bold printed box. The design questions from Appendix B are used as guidance through the scheme. One question has been added which follows from the function of the object. Mass is required when fire conditions might happen. Therefore, the scheme is started with this topic to exclude this question in further progress.

Possible answers are formulated in the small text boxes at the arrows (two options are given). When all questions are completed, a rounded box is reached which will give an indication for the possible option(s). Again, it is pointed out that this is general representation of the real process. Some simplifications have been made to reach this result.

4.3.2   Demonstrations

Two examples are composed to demonstrate the function of the scheme. The first example contains of a bridge pier with large forces (axial force and bending moments). Fire conditions are very unlikely to occur and the soil conditions are reasonable. Let's assume that the bridge is used for traffic and that horizontal forces are induced due to breaking, accelerating etc. The following path can be taken for this example:
Start at Pipe pile concrete connection ─ no fire conditions ─ inclined piles (due to the horizontal loading) ─ capping beam in-situ (probably made as a box and filled on site) ─ there are bending moments and the capacity of the piles is high. This results in a concrete plug with medium length.

The second example exists of a jetty structure for mooring of vessels. This can be used for cruise ships, loading and unloading etc. Mooring- and breasting dolphins are used, such that the horizontal loading on the jetty is minor. Due to economic reasons, a fast construction is needed. For this case the following path is taken:
No fire conditions ─ vertical piles (only very little horizontal force is expected) ─ Prefab capping beams (size will be sufficient in order that prefab capping beams are economical) ─ almost no bending

moments ─ fast construction and workshop conditions are sufficient. This results in an embedded plate connection.

4.3.3 Appearance

Based on the presented scheme, a ratio has been formulated for the appearance chances of each connection type. Based on experience, the embedded plate is used in approximately 5-10% of all cases. The reinforcement which is welded to the steel shell is only used rather limited. This seems logical considering the numbers of steps to be taken during fabrication (this is elaborated in detail in section 4.4.1.2). In almost all other cases, the concrete plug connection is adopted. This is by far the most popular alternative.

4.4 Trade-off

The design influences and a general scheme are given for the decision on which connection to adopt. However, this does not involve aspects like the construction process, the erection time or the costs. Therefore, research has been done to clarify these so-called trade-off aspects.

4.4.1 Manufacturability

The manufacturability describes the process and the steps which should be taken to complete the production. It includes transportation, hoisting and lifting, placement difficulties etc. For each alternative used in Figure 4.3 the complete process is described.

4.4.1.1 Concrete plug

The concrete plug can be made in two ways depending on the plug length. For long plugs the following method is normally used:

Long plug

At first, the piles are placed according to project descriptions with respect to the capacity and the allowable pile tip deviations. A working platform is installed (welded onto the piles) and the piles are flame cut and bevelled to align for further construction. The concrete within the pile is casted in two stages. The first stage is prior to placement of the capping beam/pile cap. Formwork (steel- or concrete plate) is lowered into the pile which is connected with hooks to the top of the pile. The reinforcement cage is positioned within the pile and the first part of the plug is casted (Figure 4.2). A length of 40 times the reinforcement bar diameter below the pile tip remains hollow. This space accounts for the anchorage length of the pile-to-cap reinforcement.
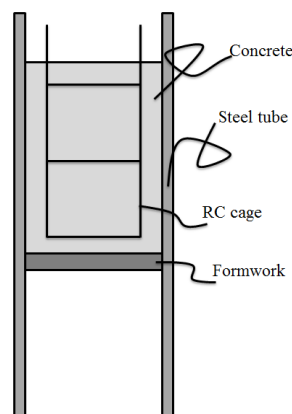
Figure 4.2: Casting of the first part of the concrete plug.

Figure 4.3: Flowchart based on experience.
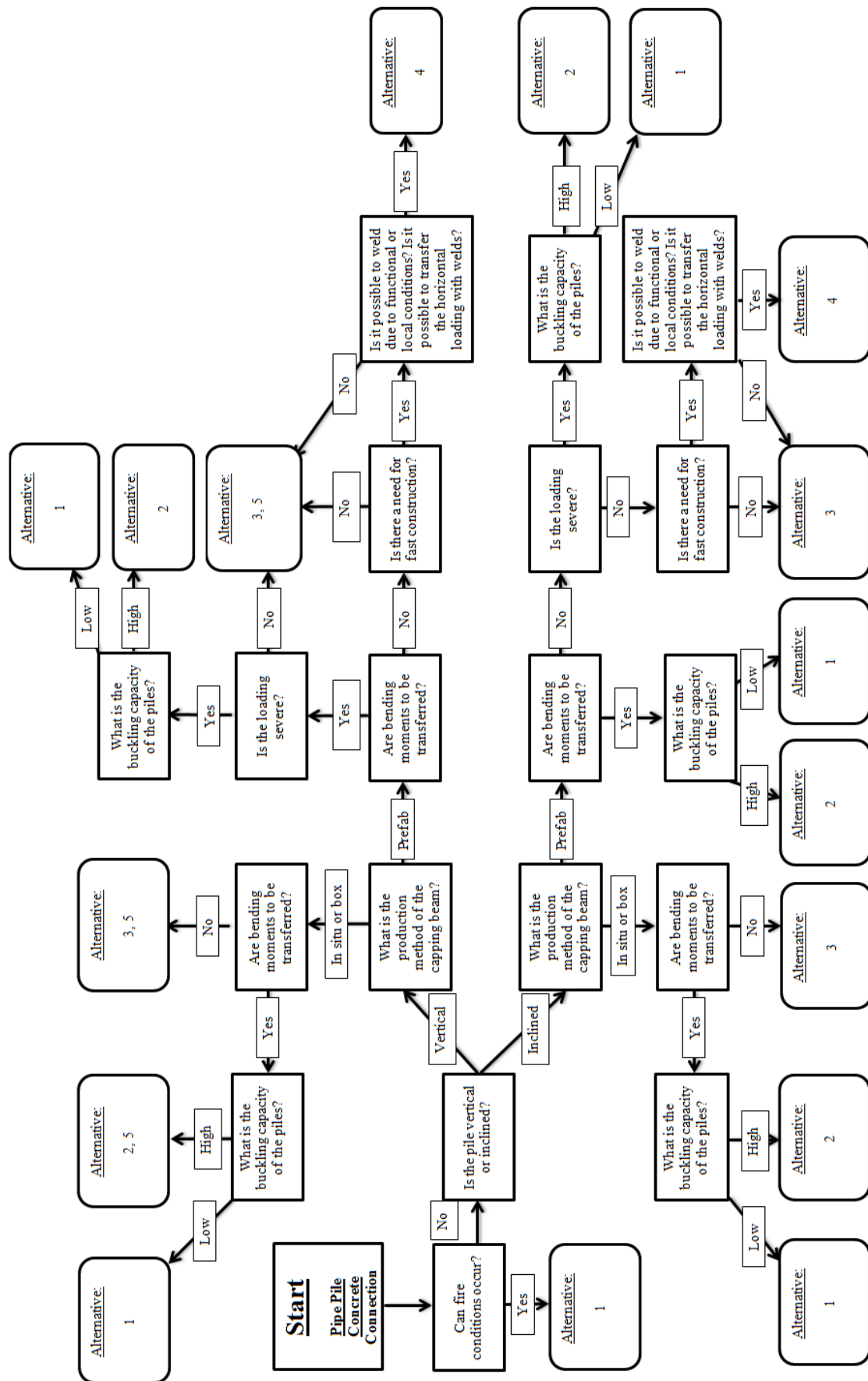
After pouring the first stage, the capping beam is positioned on top of the piles. The longitudinal reinforcement within this capping beam supports the weight of this element. If this is not possible, steel bars are cast in the capping beam to fulfil this function. A distinction between the two is made on basis of equilibrium and strength.

The pile-to-cap reinforcement bars (bended or straight bars) are lowered between the longitudinal bars of the capping beam and stuck into the remaining hollow space in the pile (Figure 4.4, part B). Bars of Ø.32 or Ø.25 are often required for this function. The remaining space in the capping beam and pile is filled in the second pouring stage (Figure 4.4, part C). A recess of Ø.200 is required for the pouring hose to reach the level of the pile. The final steps include cleaning, potential repair jobs and removal of the temporary working platform.
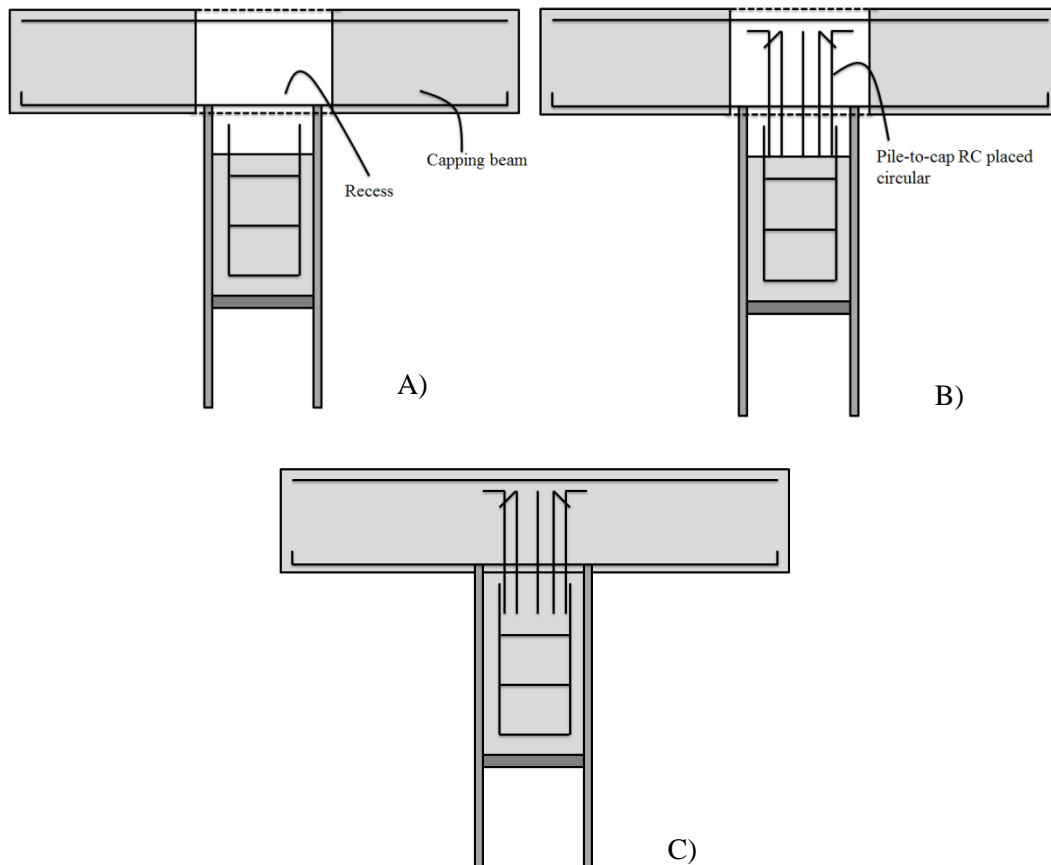
Figure 4.4: Production of the long plug (working platform not drawn), A) placement of the capping beam, B) installation of the pile-to-cap RC and C) the final result.

Short plug
The second method can only be adopted for short plugs. The minimum plug length is 1200mm due to the anchorage length of the reinforcement bars (40 Ø). This minimal length is only used when pile-to-cap reinforcement is present.

The steps of the process are equal to the first production method. However this time, the plug is casted in one pour instead of two. Only the pile-to-cap brackets are used as reinforcement so no additional reinforcement case is needed. This production process is shown in Figure 4.5.
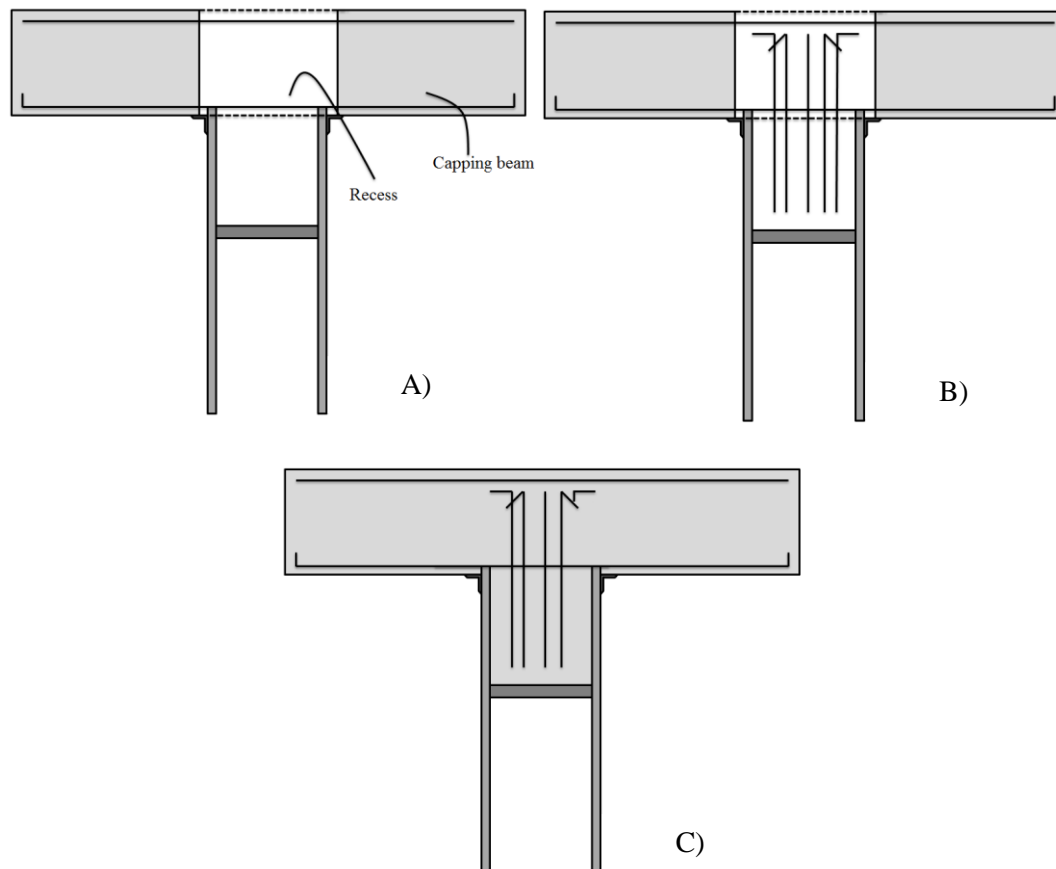
Figure 4.5: Production of the short plug (working platform not drawn), A) placement of the capping beam, B) installation of the pile-to-cap RC and C) the final result.

4.4.1.2 Reinforcement welded to steel shell

During erection, the first steps are similar to the plug connection. The piles are positioned, cut and bevelled, a working platform is installed and formwork is lowered into the pile. Production starts to differ at this point in comparison to the plug connection. The straight reinforcement bars are welded to the pile wall on either the inside or the outside of the pile (Figure 4.6, part A). Only straight bars can be used in combination with vertical piles, since otherwise the capping beam cannot be lowered onto the piles. Again, diameters of 25 or 32mm are commonly used. Right after welding, the capping beam is slid over the bars into place (like depicted in Figure 3.12 and Figure 4.6, part B). The recess and the remaining space in the pile are casted in one pour (Figure 4.6, part C). The final steps include cleaning, optional repair jobs and removal of the working platform.
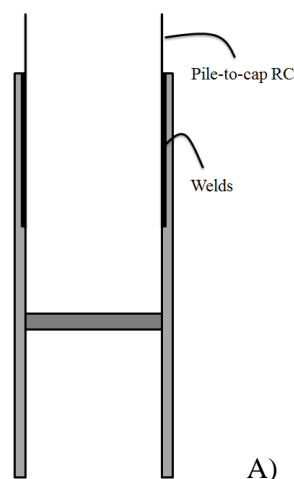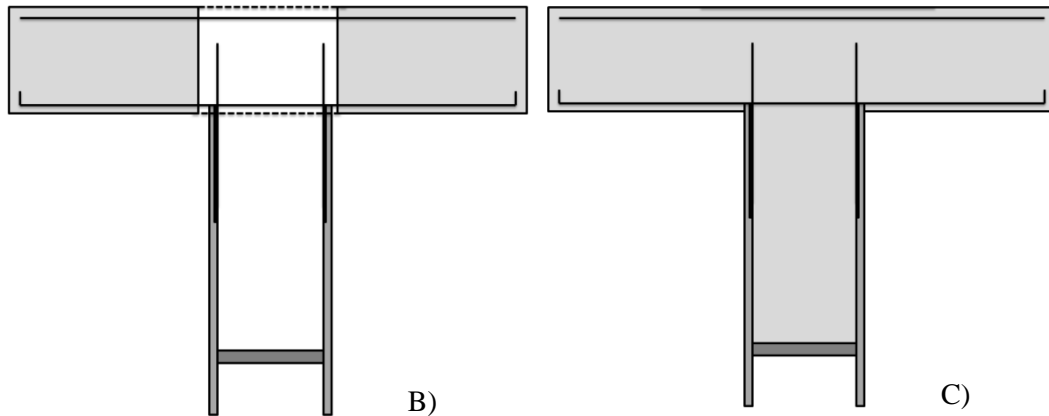
Figure 4.6: Production of the welded reinforcement connection, A) welding of the bars, B) placement of the capping beam and finally, C) pouring of the concrete.

4.4.1.3 Embedded plate connection

The last remaining option is the embedded plate connection proposed by Steunenberg et al. (1998). The embedded plate is connected via studs to a prefabricated concrete element. On site, the piles are levelled and bevelled with much greater precision in comparison to the two previous alternatives. The capping beam is positioned directly onto the piles. Small misalignments will result in inclinations of the concrete beam. After placement of the capping beam (including the embedded plate), the piles are welded to the steel plates (Figure 4.7). Afterwards, the welds are checked with ultrasonic testing and eventual repair jobs are performed. A more detailed figure of the weld connecting the pile to the plate is given in Figure 4.8.
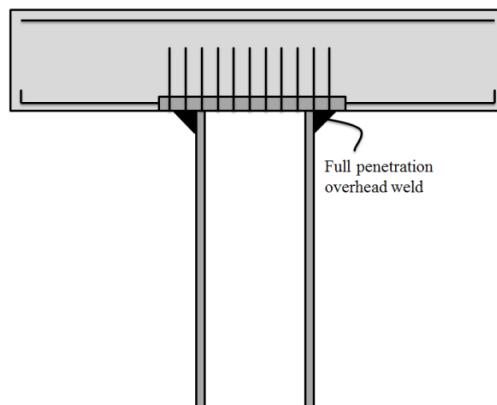
Figure 4.7: Embedded plate connection.
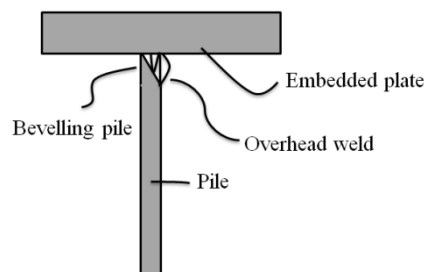
Figure 4.8: The full penetration overhead weld in more detail.

The plate itself has a thickness of approximately 30-50mm. The studs are connected, through holes, via double welding to the plate (Figure 4.9). These studs can either be placed in a grid or circular pattern. Drilling and welding equipment for this kind of work should be present in the work area just

like the proper testing equipment. To allow for pile deviations (section 2.2.2), the dimensions of the plate are larger than that of the pile. A pile diameter of 1016mm will result in approximately a 1500x1500mm steel plate. Length of the studs, dependent on the required anchorage length, will be around 900mm.
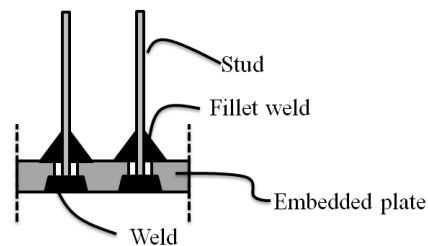
Figure 4.9: Detail of the studs welded to the embedded plate.

4.4.1.4   Conclusion

The reinforcement which is welded to the steel shell is dismissed at this point in this analysis. The number of steps is more than the concrete plug whilst the capacity is at most equal. The pile is still partly filled with concrete which means that pontoons and tug boats are still required. Besides, the reinforcement has to be welded on site which is expensive to do and it cannot be used with batter piles. These limitations results in omitting of this alternative in further analysis.

4.4.2   Durability

Durability is defined as the amount of maintenance which is needed during the lifespan of the structure. Nowadays, maintenance is often included in the construction contract.

The most important factor is corrosion. Average corrosion rates up to 0.09mm/year are found in the splash zone like seen in section 2.2.3. When for example a life span of 50 years is adopted, 4.5mm of the pile wall thickness is gone. Hence, there is a real need for protection. For the embedded plate connection, coating, cathode protection or thickness of the pile wall can be adopted. A major disadvantage of coating is that it needs to be reapplied every 10-15 years (Tomlinson et al. (2008)). This is not only costly to do but can also result in impractical situations (like in case with a jetty structure where the middle piles can almost not be reached). A second method would be to use piles with increased wall thicknesses which allow for corrosion during the life span. The pile wall thickness is than a function of both the load transfer and the maximum expected corrosion rate.

For the plug connection, a completely different solution can be used. The plug within the pile can be made longer after which it reaches a zone of low corrosion rates (Tomlinson et al. (2008)). This means that a part of the pile is allowed to corrode away over time (right of Figure 4.10). In the low corrosion zones, the pile can be protected with anodes or with a coating application. During the first stages (left of Figure 4.10), the interface length is the complete plug length. Naturally, this length needs to be adequate for the load transfer. This system requires almost none maintenance but will cost more material in the first place.
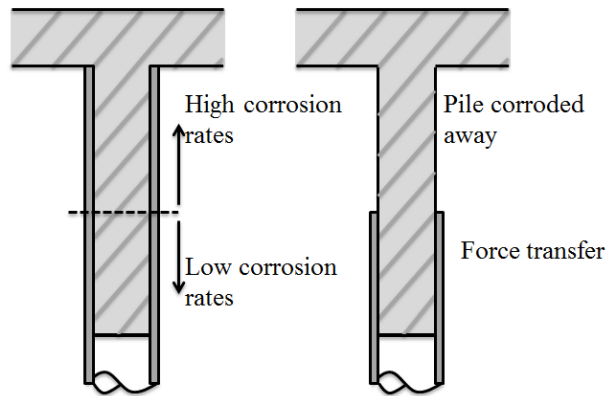
Figure 4.10: A possible corrosion principle of the plug connection. On the left the situation at the first stage and on the right the stage after which the pile corroded away.

4.4.3   Construction time

In the considered research field of near-shore construction, planning is of great importance because construction above water is very costly. An example is created to obtain the planning of both the embedded plate and the plug connection.

In this example, a jetty construction is considered with capping beams which connect four piles (Figure 4.11). Two of those piles are vertical and two are batter piles. A service road is present at the right part of the jetty and on the left pipelines for transportation usage. For the plug connection, a long plug is assumed.
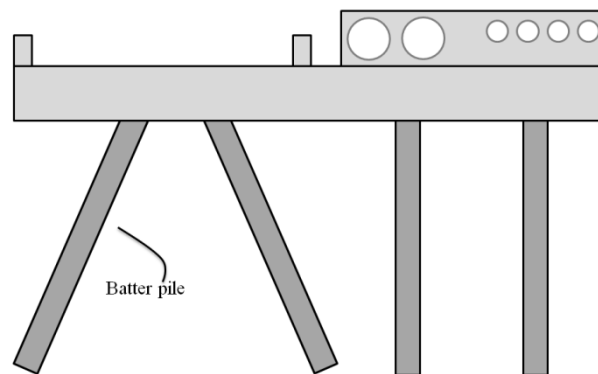
Figure 4.11: Fictitious jetty example.

The steps from the construction process, as is described in section 4.4.1, are maintained. The result for the embedded plate connection is shown in Table 4.1 and the planning for the plug connection in Table 4.2. These two schedules are compiled in consultation with an expert. As seen for the embedded plate alternative, the welding of the piles takes most of the time. Welding takes approximately 1.5 days per pile with two classified welders. The total cycle time per capping beam is approximately two weeks. The same cycle time is found for the concrete plug connection. A notable detail is that only two days are planned for casting and curing of the concrete is accounted for. A spare day is included for both schedules, which accounts for possible delays, repairs or circumstances.

Table 4.1: Planning for the embedded plate connection.

Embedded plate connection	1	2	3	4	5	6	7	8	9	10	11	12	13	14
	M	T	W	T	F	S	S	M	T	W	T	F	S	S
Install temporary platform	█													
Cutting piles & bevelling piles		█	█											
Placement of the capping beam				█										
Welding of the piles					█	█		█						
Ultra-sonic testing									█					
Repair welding										█				
Repair /apply coating											█			
Spare or delay												█		
Remove temporary platform													█	

Table 4.2: Planning for the concrete plug connection.

Concrete plug connection	1	2	3	4	5	6	7	8	9	10	11	12	13	14
	M	T	W	T	F	S	S	M	T	W	T	F	S	S
Install temporary platform	█													
Cutting piles		█												
Placement of the capping beam			█											
Placement formwork				█										
Placement rebar cages					█									
Cast plug phase 1						█								
Curing phase 1							█							
Placement rebar cages								█						
Cast plug phase 2									█					
Curing phase 2										█				
Repair/cleaning											█			
Remove temporary platform												█		
Spare or delay													█	

4.4.4 Costs analysis

In general, it is hard to provide accurate costs estimations. This difficulty of predicting the costs follows from the several relations within the system and the varying ratio between material and labour costs. It might be economical to adopt more time consuming alternatives in countries with low wages and vice versa. General site costs are not included in this analysis; it is purely a distinction between the two remaining options.

The costs are subdivided into four categories namely: labour, permanent materials, temporary materials and plant & equipment costs. Temporary materials include the formwork for casting the plug and welding materials. Transportation and installation costs are included. The example of Figure 4.11 is used again for this analysis. It must be noted that generalised numbers are used in the comparison of Appendix C. The comparison will change for every situation.

4.4.4.1 Embedded plate

When doing the same for the embedded plate results:
- Labour: 60%
- Materials permanent: 27%
- Materials temporary: 0 %
- Plant & equipment: 13%

4.4.4.2   Plug connection

For the plug connection, the following partition is found:
- Labour: 6%
- Materials permanent: 65%
- Materials temporary: 17%
- Plant & equipment: 12%

4.4.4.3   Mutual differences

When comparing the plug connection to the embedded plate connection, the plate is around 20-30% more expensive. The reason is the amount of required manual labour just to make the plate and perform the welding. Testing is required and coating is required which needs to be reapplied every 10 years (Tomlinson et al. (2008)). The plug connection is relative simple to make since only few specialized operations are required.

4.5   Conclusion

A general decision scheme is proposed based on the influential aspects. These aspects are subdivided into a number of decisions to make. These are the construction method of the capping beam, the construction speed, the function and the capacity of the piles.

Generally seen, the concrete plug is the most suitable solution for the design issue. This is due to the fact that this connection is cheaper in comparison to the embedded plate connection, the production is relatively simple and the producing time is comparable with the embedded plate connection. Only in some situations (determined by local conditions) the embedded plate is more favourable, since it is constructed in a different manner. Thus from eight possible options, the concrete plug connection will be examined in more detail in the following chapters.

Behaviour Plug Connection

Resulting from the previous chapter, the concrete plug connection is the most economical and practical solution for the design problem. The behaviour and mechanisms of this connection will be identified in more detail. Two load transfers for the axial capacity have been identified in section 3.2.3.1, namely by natural bond or by shear keys.

5.1 Axial behaviour without shear keys

The axial behaviour of the plug connection is subdivided into the pull-out and the push-out behaviour. Pull-out means that a tensile force is exerted on to the plug which tries to pull the plug out of the pile. Push-out is the opposite; a compressive force is exerted by which the plug is pushed further into the pile. The axial load introduction is depicted in Figure 5.1, for the push-out case. The plug is attached to the capping beam because it is poured at once as seen in section 4.4.1.1. Large pressures appear just above the steel pile due to the small contact surface. It is likely that the concrete compressive strength is reached at these locations. Consequently, the axial force is transferred via the concrete plug to the pile.
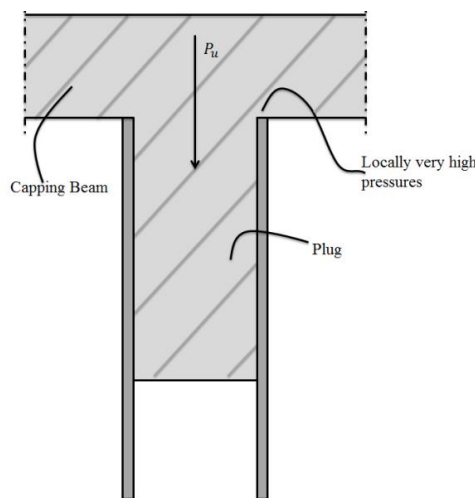
Figure 5.1: Concrete plug connection with axial load introduction.

5.1.1 Pull-out

Pull-out means a tensile load onto the plug as depicted in Figure 5.2. This tensile force can only be introduced to the plug via pile-to-cap reinforcement and is introduced into the concrete plug over the anchorage length of the reinforcement bars.

All tensile force is transferred to the pile at the bottom of the plug (the stress in the concrete is zero). The pile is tended to move inwards (necking of the pile) due to this high tensile load. This radial movement of the pile exerts a pressure onto the concrete. At the top of the plug (at the tip of the pile), the opposite mechanism occurs. The plug carries all tensile force whereas the pile experiences almost none. This behaviour is also seen in Figure 5.2.

Al-Mahaidi et al. (1999) found another effect in their testing series. Deformed bars were used as reinforcement. With a high tensile load on the bars, the ribs tend to impart a pressure on the concrete in the shape of a wedge. This effect enhances the frictional behaviour according to the authors.
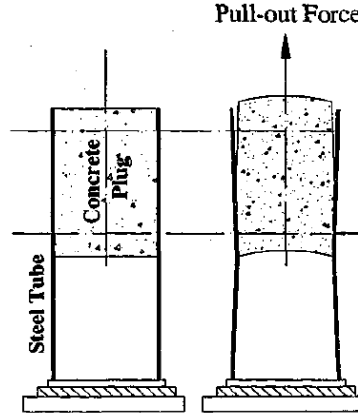
Figure 5.2: Pull-out behaviour (Nezamian (2003)).

5.1.1.1 Ultimate pull-out capacity

The ultimate capacity in pull-out is determined by Nezamian et al. (2003). During testing, he found that during pull-out the plug breaks at the level of the reinforcement as shown in Figure 5.3.
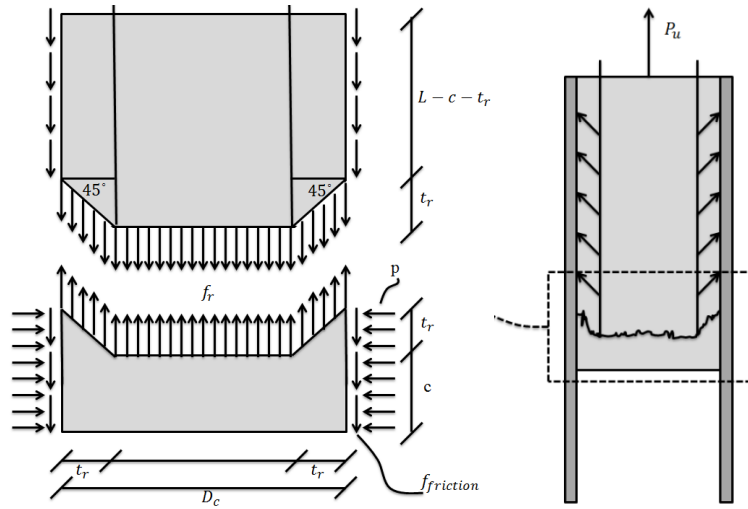
Figure 5.3: Tensile splitting of the plug (Nezamian (2003)).

Tensile splitting of the plug is illustrated in the right of Figure 5.3. This tensile crack is depicted in more detail in the left of Figure 5.3. Nezamian (2003) proposed the following formulation for the ultimate capacity (P_u) in pull-out, based on equilibrium based on the tensile strength (f_r) of the concrete

$$P_u = f_{friction}(L - c - t_r)\pi D_c + f_r\pi(0.5D_c + (\sqrt{2} - 1)t_r)^2. \qquad \text{(Eq. 5.1)}$$

Only the ultimate capacity has been derived by Nezamian (2003). Based on equilibrium, the following can be obtained

$$f_{friction}\pi D_c(c + t_r) = f_r\pi(0.5D_c + (\sqrt{2} - 1)t_r)^2. \qquad \text{(Eq. 5.2)}$$

Applying the Mohr-Coulomb friction model, the pressure (p) is a function of the friction like

$$f_{friction} = \mu \cdot p \qquad \text{(Eq. 5.3)}$$

$$\mu p D_c(c + t_r) = f_r(0.5D_c + (\sqrt{2} - 1)t_r)^2. \qquad \text{(Eq. 5.4)}$$

Substituting (Eq. 5.3) into (Eq. 5.4) and rearranging the variables results in the following expression for the wall pressure at the bottom part of the plug.

$$p = \frac{0.25f_r\left(2\left(\sqrt{2}-1\right)t_r + D_c\right)^2}{\mu D_c(c + t_r)}.$$

(Eq. 5.5)

5.1.2 Push-out

The push-out mechanism means that the plug is loaded in compression and pushed into the tube (Figure 5.4). At the top location, the concrete experiences high compressive stresses. Due to the Poisson ratio, the plug exerts a horizontal pressure onto the pile. The pile carries all compressive force at the bottom of the plug. This causes an expansion of the pile diameter resulting in low contact between plug and pile. This mechanism is found in testing without a concrete beam on top of the pile, otherwise the plug will not be able to move far away into the pile.
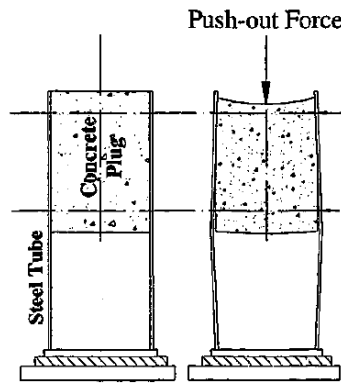
Figure 5.4: Push-out behaviour (Nezamian (2003)).

5.1.2.1 Ultimate capacity

In the pull-out case, a clear failure mechanism is seen where the concrete failed under tensile stresses around the tip of the reinforcement. Push-out failure is really a bond failure, the pile widens at the bottom of the plug meaning that the plug can slip through.

5.1.3 Design capacity

The design capacity for the plug connection without shear keys is a matter of solely the bond capacity (in case without shear keys). In pull-out, the ultimate capacity of the connection is a function of the frictional forces between the pile and the plug at the bottom location (like depicted in Figure 5.3). With these high forces, it is likely that the bond has been broken. When the connection is unloaded again, the capacity is reduced to zero (since the bond is broken). Therefore, the design capacity should only be the bond capacity of the system. Test data which represent the ultimate pull-out failure will report higher values than which should be adopted in design. This does not hold for the push-out failure mechanism since this is purely a bond failure.

5.2 Axial behaviour with shear keys

In contrast to the bond capacity (without shear keys), the behaviour with shear keys is relatively unknown. No reported test data is found in literature about the plug connection with shear keys. This is probably related to the minimum required size of the steel tube. A diameter of approximately 900mm is needed to be able to weld the shear keys on the inside of the pile (BN (2015)). Testing such sizes will result in costly experiments.

5.2.1   Pile-sleeve systems

Another system in which shear keys are used, are the so-called pile-sleeve systems. An example of this connection is given in Figure 5.5. Pile-sleeve connections are typically used in oil platforms or in monopile foundations. The pile, which can have diameters up to eight meters, is driven into place. The sleeve, to which the mill is attached, is grouted to this foundation pile. In Figure 5.5, shear keys are welded on both the pile and the sleeve.
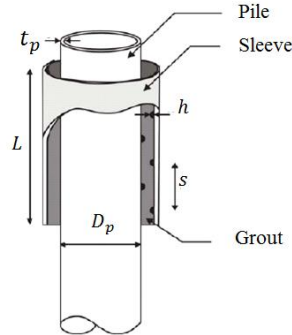
Figure 5.5: Typical grouted pile-sleeve connection.

The shear keys are welded horizontally along the perimeter of the pile and the sleeve. Three possible configurations are given by Krahl et al. (1985). Possibility (a) of Figure 5.6 is a weld bead which acts as a shear key. Options (b) and (c) are steel strips welded to the inner pile wall (with filled welds).
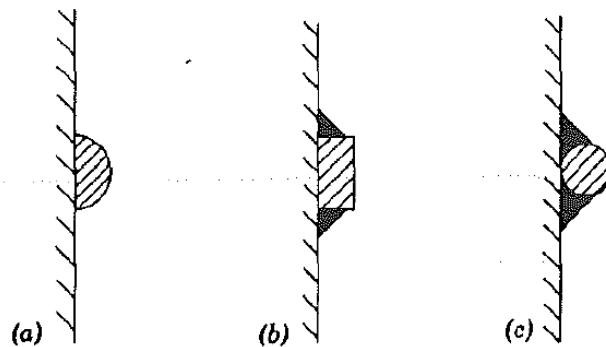
Figure 5.6: Possible shear key configurations (Krahl et al. (1985)).

The detailing of the shear keys should be in accordance with the following requirements (API (2003)):
- The shear key may be circular hoops or a continuous helix,
- The keys should be applied at sufficient length to ensure that enough are present in the required length,
- Both the key and the welds should be designed at the basic allowable stresses of 1.7 times f_{ck}. This is to make sure that the keys will not fail before the concrete starts to crush,
- The spacing between the keys is constant.

5.2.1.1   Failure mechanism

In contrary to the plug connections, test data is reported about the pile-sleeve systems adopting shear keys. The failure mechanism which is found in testing is shown in Figure 5.7. The natural bond is broken and the concrete above the shear key is crushed. Furthermore, diagonal cracks are observed from one shear key to the corresponding opposite key (Krahl et al. (1985)).

Four empirical formulations are developed for this behaviour. These are discussed in the next chapter. The applicability of these expressions for the plug connection will be investigated in more detail.
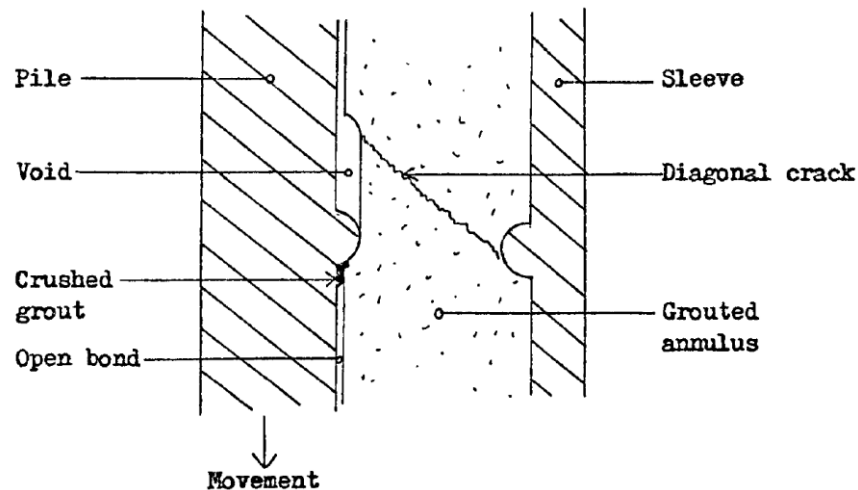
Figure 5.7: Shear key failure in a pile-sleeve system (Chilvers (1984)).

5.3 Bending moment and shear behaviour

Unfortunately, only little is found about the bending moment and shear capacity of the plug connection. The conducted research about the bending moment capacity is aimed at verifying the right failure mechanism and load-slip curves like seen in Chapter 3. On top of that, some of this research has been performed in combination with concrete piles rather than steel ones.

Just as with the shear keys, research about the bending moment capacity has been conducted in pile-sleeve applications. Some of this conducted research can provide valuable data for the plug connections. The research is conducted due to the fatigue behaviour of the monopile connection. In the past these connections were made without shear keys. Due to cyclic loading, a significant number of these towers settled. The force transfer changed and the grout started to crack under fatigue loading. It is assumed that the largest part of the bending moment is transferred by horizontal contact pressures with the associated vertical friction (Lotsberg et al. (2012)).

It is rather odd that only so little is known about the bending moment capacity. This loading is almost always present in all kinds of situations. In the current standards, a method is adopted where the bending moment capacity is based on the axial strength. This is elaborated in section 6.5.3.1.

5.4 Conclusion

Main conclusions are that the push-out failure is truly a bond failure whereas with pull-out, multiple other mechanisms are involved. Research about the axial capacity without shear keys is numerous in contrast to the axial capacity including shear keys and the bending moment capacity. This is remarkable since bending moments are almost always present. For the shear keys, pile-sleeve systems will provide more information. These load transfers are elaborated in more detail in the next chapters.

Chapter 6

Axial Capacity Without Shear Keys

There are two possible methods of transferring the axial force between the plug and the pile as seen in Chapter 5. One method is by the natural bonding between the two materials and the second with the help of shear keys. The former force transfer method is subject of a long list of research. A vast number of influences have been found during testing and contradictory conclusions have been stated. This chapter deals with the list of effects on bond and the currently available design expressions are given.

6.1 Bond

The natural bond stress (f_b) between the steel pile and the concrete core is defined as follows

$$f_b = P_u/(2\pi R_c L) \tag{Eq. 6.1}$$
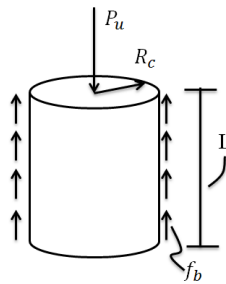
Figure 6.1: Definitions of the bond stress.

in which P_u is the maximum axial load, R_c is the inner radius of the pipe pile and L is the interface length (Roeder et al. (1999)). These definitions are displayed in Figure 6.1. A typical bond failure mode is given in Figure 6.2, the concrete core is pushed into the steel tube to which bond is broken and a relative longitudinal displacement occurred.
.

Figure 6.2: Typical bond failure mode found by Radhiki et al. (2012).

The bond strength is a function of both chemical adhesion and micro friction due to the roughness of the steel tube and possible shape variations. When this bond is broken, macro-friction mechanisms provide some remaining capacity (Nezamian et al. (2006)). Design values for the bond capacity vary, according to literature, from 0.2 to 1.0N/mm^2. A typical load-slip curve is displayed in Figure 6.3, in which the bond is given as the first part of the graph (micro-friction and bond). After the peak at

1.25mm, the mechanism changes to macro-friction. This means friction of the plug due to welding seams, deviations from the circular form of the pile or other imperfections.
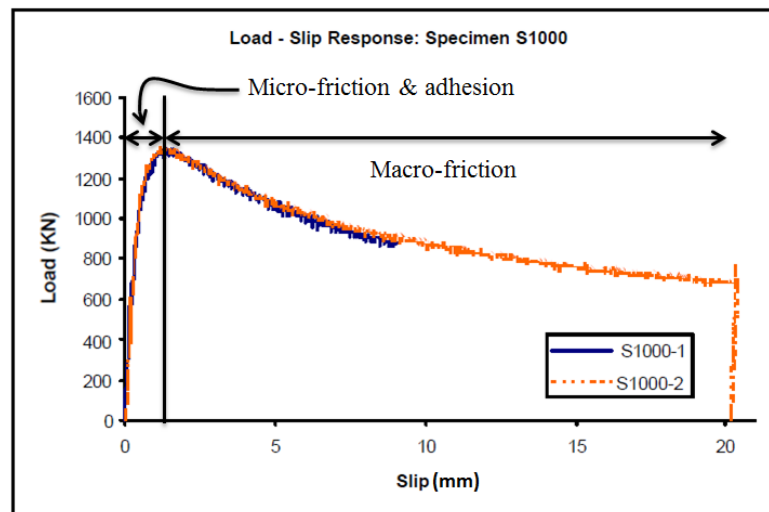
Figure 6.3: Typical load-slip curve for bond (Nezamian et al. (2002)).

6.2 Parameter study

Numerous influences are investigated in previous research on the bond stress in circular piles. Test results from multiple research teams are analysed and summarized in this section. Research started in 1980 by Virdi and Dowling towards circular piles. In a later stage, Shakir-Khalil and Roeder et al. started experimenting on the subject. Even nowadays, multiple researches can be found which try to improve on this bond strength. Multiple influential parameters will be discussed in this section.

6.2.1 Concrete compressive strength

The concrete compressive strength is tested with eighteen specimens by Virdi et al. (1980). Six different compressive strengths are used varying from 24 to 41N/mm^2. In contrast to bond in combination with reinforcement, the bond between pile and plug does not seem to be influenced by the concrete compressive strength. According to Virdi et al. (1980), this effect is due to the increased shrinkage properties of the higher strength concrete which seems to counteract the increased strength. Roeder et al. (1999) collected data of push-out tests on concrete plugs in relation to the concrete compressive strength. This collection is extended with more recent research which results in Figure 6.4. The great scatter in results is due to multiple varying parameters during testing. Roeder et al. (1999) agrees with the conclusion from Virdi et al. (1980). In contrast, Aly et al. (2009) conclude differently and stated that the bond strength becomes lower with higher strength concretes.
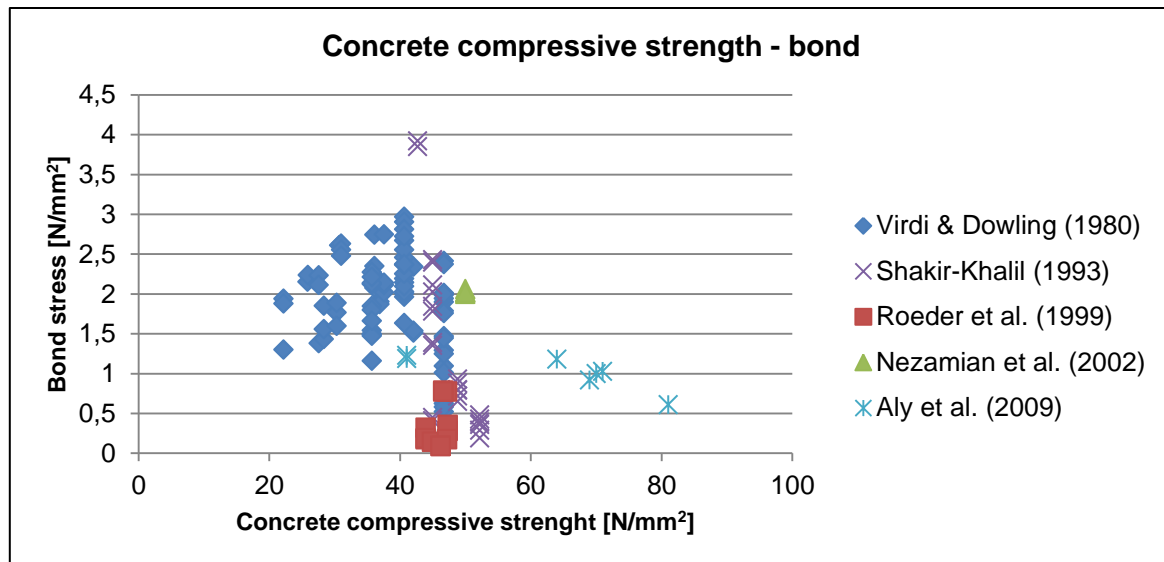
Figure 6.4: Concrete compressive strength in relation to bond strength.

6.2.2 Interface length/diameter

Researchers believe that the interface length influences the axial strength of the connection. Virdi et al. (1980) tested fifteen specimens with varying lengths. Conclusion is that this length did not seem to influence the capacity. Al-Mahaidi et al. (2002) found opposite results and concluded that with increasing interface length/diameter, the bond capacity lowers. Test results have been collected and the results are given in Figure 6.5. The test data shows large scatter regarding the interface length.
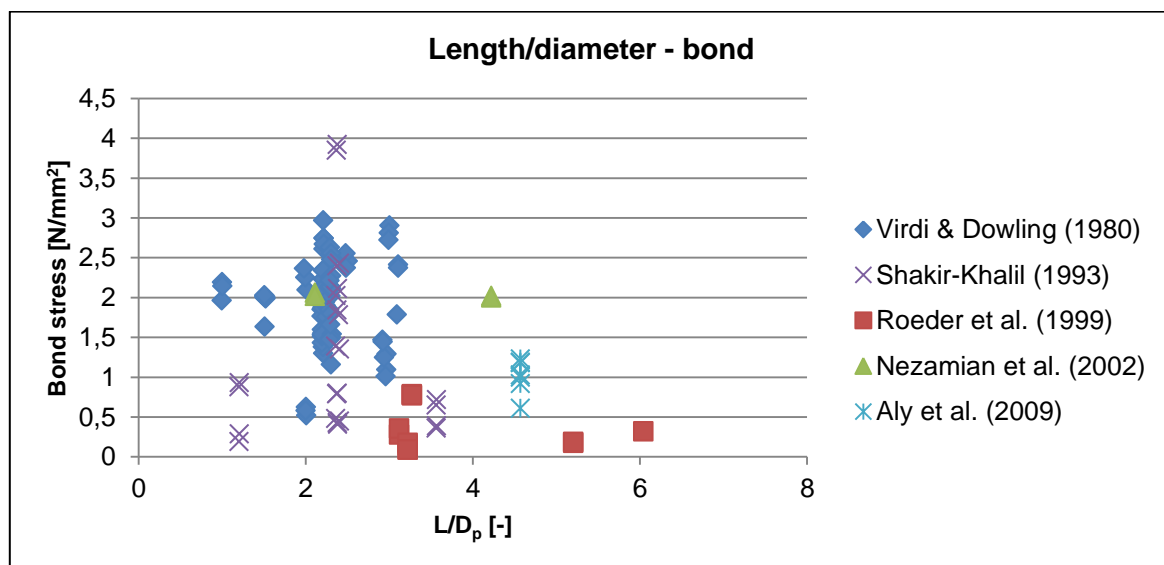
Figure 6.5: Influence of the plug length on the bond stress.

6.2.3 Pipe pile diameter

Shrinkage is denoted as one of the major influences by Virdi et al. (1980) and Roeder et al. (1999). With an increased pile diameter, this shrinkage effect grows substantially. Limited research data has been found concerning large diameter piles. Only three specimens have diameters exceeding 600mm, whilst in practice diameters up to 1500mm are adopted. Based on the current knowledge, scale effects are hard to predict accurately. The relation between the diameter and the bond is depicted in Figure 6.6. The tendency within this figure is clearer in relation to the previous two figures.
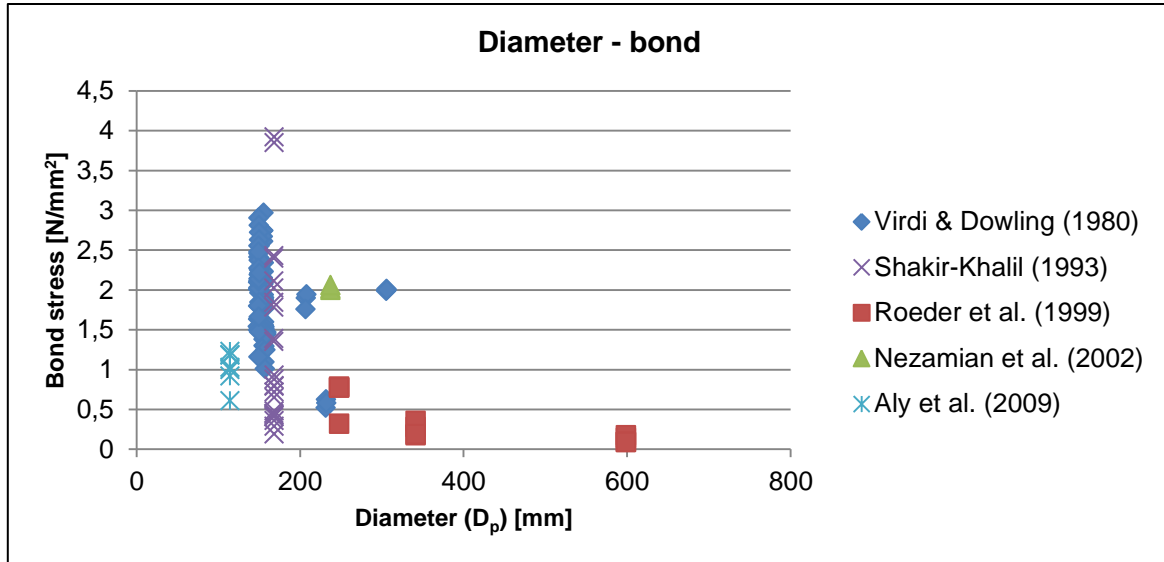
Figure 6.6: Relation between the diameter (D_p) and the bond strength.

In agreement with Figure 6.6, is the relation between the diameter over thickness ratio and bond strength (Figure 6.7). With increasing D_p/t_p, the bond strength seems to be reduced spectacularly. Once more, limited data is present with large diameter over thickness ratios.
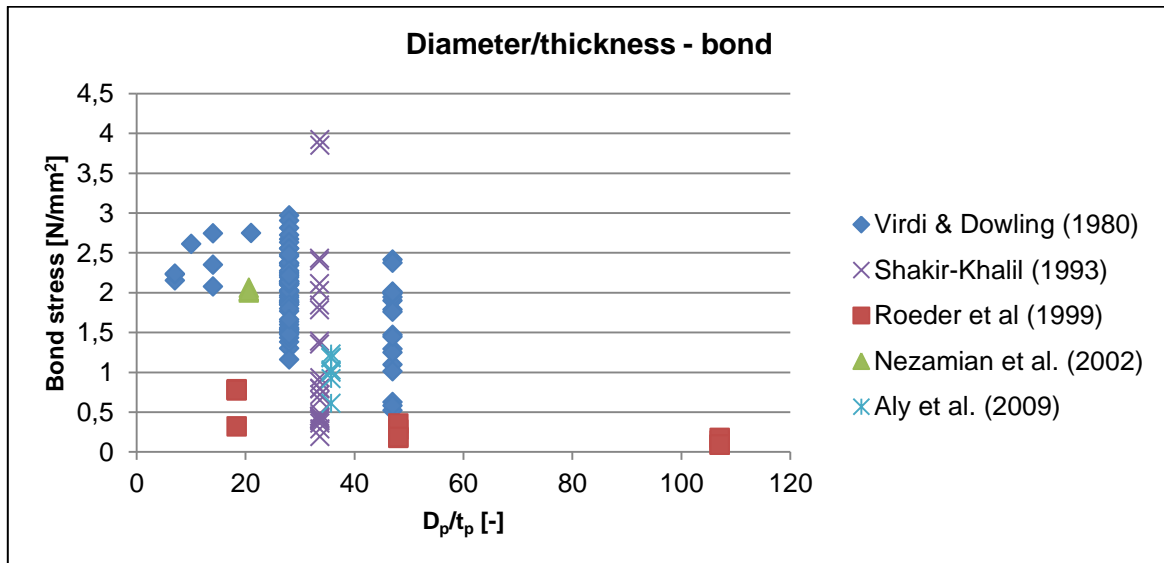
Figure 6.7: Effect of the diameter over thickness on bond.

6.2.4   Shrinkage

Shrinkage is mentioned to have a detrimental on the connection capacity. Three different states are distinguished by Roeder et al. (1999) concerning shrinkage:

- State A: $\Delta_1 + \Delta_2 > 0$,
- State B: $\Delta_1 + \Delta_2 < -\Delta_3$,
- State C: $0 \geq \Delta_1 + \Delta_2 \geq -\Delta_3$.

In the formulation, Δ_1 is the radial enlargement of the tube due to pressure induced by the concrete core. Shrinkage of the core can be expressed as

$$\Delta_2 = (-cD_p)/2 \qquad \text{(Eq. 6.2)}$$

in which c is the linear shrinkage strain of the concrete and D_i is the inside diameter of the pile. The amplitude of the rugosity of the inner surface of the steel tube is included via Δ_3. In state A, the concrete conducts a pressure against the inner surface of the steel tube and the resistance is formed by natural bond. If the force keeps increasing and the natural bond is exceeded, then the force can still increase due to the mechanical interlock. State B, the two materials are separated after the shrinkage of the concrete. A relative rigid body motion can occur, which results in low bond strength. State C is an intermediate state, the adhesion is reduced just as the mechanical interlock.

The trend in literature is to test specimens after 28 days. This seems inconvenient regarding the previous statements concerning shrinkage. Concrete age in relation to bond strength is presented in Figure 6.8.
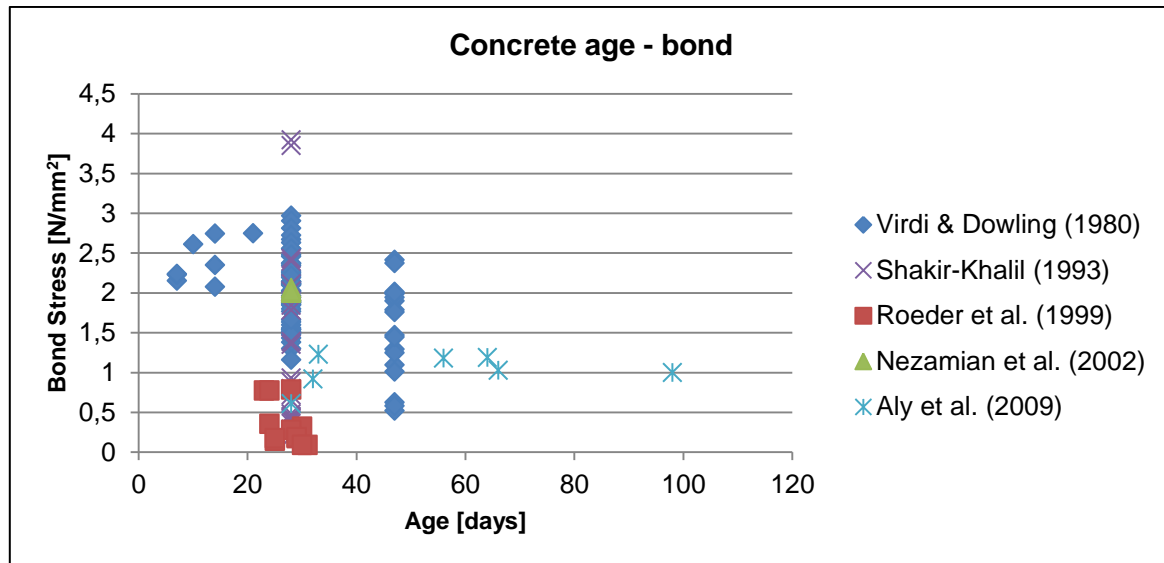
Figure 6.8: Concrete age in relation to the bond strength.

6.2.5 Compaction of the concrete

Higher compaction levels of the concrete result in an improved micro-friction. The concrete is forced into the steel surface irregularities. This effect has only been tested by Virdi et al. (1980) and showed expected results. Higher compaction levels resulted in higher bond.

6.2.6 Surface roughness

Continuing on the previous, the effect of surface roughness has been examined. Shakir-Khalil (1993) tested several pieces with oiled interfaces and Virdi et al. (1980) examined specimens with machined smooth-out tubes. Specimens with a smooth inner surface performed considerably worse compared to specimens without any treatment at all. Right after the point where the bond stress is exceeded, the concrete slipped through the pipe pile. The micro-friction effect is considerably reduced.

6.2.7 Eccentric loading

Eccentric loading tends to give larger bond values as concluded by multiple researches. Instead of applying a load exactly in the middle of the plug (like in Figure 6.1), the axial load is placed eccentric. This causes a wedging effect of the plug inside the pile which subsequently causes an increased capacity.

6.2.8 Cyclic loading

Cyclic loading lowers the bond by progressive loss of stiffness as found by Nezamian et al. (2006). Micro cracks appear at the interface, which increase with each load cycle. To account for this effect, a cyclic reduction factor is introduced. This factor is defined as the ratio between the cyclic loading

(Figure 6.9) strength and the static strength with a given slip. Slip is subsequently defined as the relative movement between the concrete core and the steel pile. The cyclic reduction factor is, according to Nezamian et al. (2006), based on the rate of load, the number of cycles, concrete characteristics, imperfections of the steel tube, plug length and the presence of reinforcement.
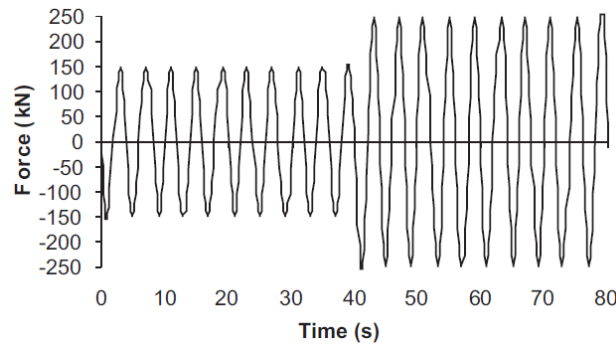
Figure 6.9: Cyclic loading regime by Nezamian et al. (2006).

Based on various tests on ten specimens, the cyclic reduction factor is determined to be 0.74 with a coefficient of variation of 0.25 for 10 cycles. The findings of each specimen are presented in Table 6.1. Specimen S1.0D-2 and S1.25D-3 show remarkable result since the reduction factor is above one meaning that with cyclic loading, the capacity increased. According to the writers, this is attributed to steel tube imperfections or concrete shrinkage.

Table 6.1: The cyclic reduction factor found by Nezamian et al. (2006).

Specimen No.	Failure regime	Ultimate strength (kN)	Cyclic ultimate strength (kN)	Cyclic reduction factor	Slip at peak load (mm)
S1.0D-2	Pull out with pre-cyclic loading	665	711	1.07	12.2
S1.0D-3	Pull out with pre-cyclic loading	665	410	0.62	11.7
S1.25D-2	Symmetric cycling loading	460	439	0.95	24.1
S1.25D-3	Pull out with pre-cyclic loading	460	540	1.17	20.9
S1.5D-2	Pull out with pre-cyclic loading	1000	500	0.50	1.8
S1.5D-3	Pull out with pre-cyclic loading	1000	404	0.40	9.2
S1.75D-2	Symmetric cycling loading	395	300	0.76	14.8
S1.75D-3	Cycling with pre-pull-out test	395	250	0.63	18.6
S2.0D-1	Cycling with pre-pull-out test	1000	600	0.60	16.0
S2.0D-3	Symmetric cycling loading	479	350	0.73	18.6

Similar results are found by Aly et al. (2009) which performed tests on seven test specimens. Results showed that the collapse limit for specimens subjected to cyclic loading is in between 0.7 and 0.789 of the static collapse load (at most 40 cycles per specimen). Therefore, when cyclic loading is to be expected, this should be taken into consideration for the strength determination.

The same behaviour is seen for the pile-sleeve systems as introduced in section 5.1.2. The large windmills at sea, the so-called monopiles, have been reported to settle due to the effect of cyclic loading (Lotsberg et al. (2012)). This results in a different force flow which causes fatigue cracking of the grout. The Det Norske Veritas (DNV) 2013 states that no axial force may be transferred when only bond covers the axial capacity. Other structural arrangements are required for this transfer. It must be added that the loading conditions of the monopiles is rather different than that of other grouted connections. Jacket structures for instance, are mainly subjected to axial loading in contrast to the monopiles which are mainly subjected to bending moments (Lotsberg et al. (2012)).

6.3   Improvement

Xu et al. (2007) tried to improve the strength with expansive cement. This expansive behaviour compensates for the shrinkage and also induces residual compressive forces in the concrete. Sulfoaluminate-type expansive cement is used for the performed experiment. Twenty specimens are tested with the same tube diameter of 150mm.

The load – slip curve (Figure 6.10) shows the difference between the ordinary Portland cement and the expansive concrete. The difference between the concrete mixes is given in the right of Figure 6.10. The SI-o is ordinary Portland cement.

Mix identification	Mix ratio (cement to aggregates)	Mix proportion by weight
		Cement:water:sand:gravel:additional high-range water reducer
a	0.40	1.00:0.40:1.40:1.68:0.02
b	0.42	1.00:0.42:1.10:1.20:0.02
c	0.45	1.00:0.45:0.80:0.98:0.02
d	0.45	1.00:0.45:1.10:1.30:0.02
e	0.42	1.00:0.42:1.40:1.65:0.02
f	0.38	1.00:0.38:1.15:1.26:0.02
o	0.45	1.00:0.40:1.51:2.55:0.015
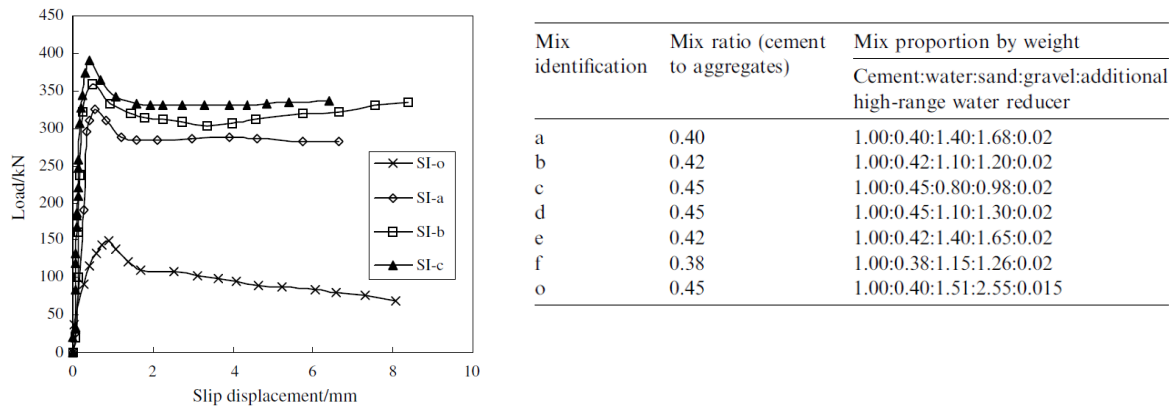
Figure 6.10: Load slip curve for the expansive concrete (Xu et al. (2007)).

Conclusions of Xu et al. (2007) are that the bond stress is 1.2 - 3.3 times the bond strength of the normal concrete and that the compressive strength of the expansive concrete makes a difference on the strength.

6.3.1   Fly ash

Further improvement of the bond stress has been done by Li et al. (2005) and Radhika et al. (2012). The former tried to improve on the bond stress with the use of fly-ash. Observed is that the bond strength is improved for low levels of fly ash at all tested ages (varied from 28 to 365 days). When the steel tube is coated on the inside with fly-ash, the increase in bond strength was even more severe. When the addition of fly-ash is over 40%, the strength in the early stages decreases in comparison to ordinary Portland cement. On the long term, the capacity actually increased with 39% after 365 days.

Radhika et al. (2012) improved on the bond stress characteristics using a mineral admixture metakaoline. The writers report that with an addition of 15% metakaoline, the strength is significantly increased.

6.4   Bond stress along the interface

The capacity of the connection is a function of both the plug and pile lateral contraction as discussed in Chapter 5. These radial displacements are not constant over the interface length. For the same reason is the bond strength dependent on the location along the plug. This effect is measured by Al-Mahaidi et al. (1999); multiple specimens have been tested and gauged. A typical result for the pull-out case is given in Figure 6.11. The large bond stresses are attributed to the presence of reinforcement. This causes an extra wedging effect which enhances the bond capacity.
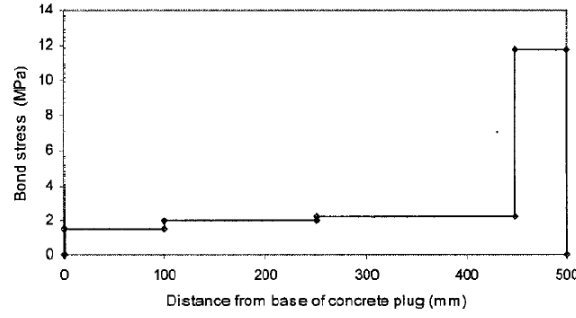
Figure 6.11: Bond stress along the interface in pull-out (Al-Mahaidi et al. (1999)).

6.5 Design expressions

Multiple expressions have been formulated over the years to calculate the bond capacity. Differences show when these expressions are examined in more detail.

6.5.1 Circular piles

In spite of all conducted research presented above, the Eurocode prescribes a constant value of 0.55N/mm^2 for bond in circular hollow sections (ECS (2011d)). So despite of the pile diameter, shrinkage properties, pile wall thickness, surface roughness, concrete strength, compaction levels, additives or plug length, this value could be used in design. The American Petroleum Institute (API) prescribes a value of 0.248MPa. This means a whopping 222% difference between the two design codes. The British Standard (BSI (1999)) adopts a value of 0.4N/mm^2 for concrete filled hollow steel sections.

6.5.2 Roeder et al. (1999).

Roeder et al. (1999) performed a linear regression based on the test results by Virdi et al (1980) and Shakir-Khalil (1993). According to this analysis, 97.5% of the test specimens should have a bond stress which is larger than

$$f_{b,2\sigma} = 2.109 - 0.026(D_p/t_p) \qquad \text{(Eq. 6.3)}$$

in which $f_{b,2\sigma}$ is two standard deviations above the mean value, D_p is the pile diameter and t_p the wall thickness. The mean average bond stress equals

$$f_{b,mean} = 2.314 - 0.0195(D_p/t_p). \qquad \text{(Eq. 6.4)}$$

6.5.3 Pile-sleeve systems

The pile-sleeve systems are already introduced in section 0. Four empirical expressions for the axial capacity (bond and shear keys), f_{axial}, are found for this pile-sleeve connection type. All four formulations adopt the same principle, namely an addition of the part by bond and the part by shear key. For the definition of all the parameters, reference is made to Figure 6.12 and the glossary on page 133. More background information regarding these expressions is given in Appendix D. A comparative study is included regarding the influences on the bond stress. The expressions presented in this section are the complete formulations (bond and shear key parts).

- Offshore Technology (OT (2002)):

$$f_{axial} = K_{OT} \cdot C_L \left(9C_s + 1100\frac{h}{s}\right)\sqrt{f_{ck}} \qquad \text{(Eq. 6.5)}$$

With: $$K_{OT} = \left[m\left(\frac{D_g}{t_g}\right)\right]^{-1} + \left[\left(\frac{D_p}{t_p}\right) + \left(\frac{D_s}{t_s}\right)\right]^{-1} \qquad \text{(Eq. 6.6)}$$

- American Petroleum Institute (API (2003)):

$$f_{axial} = 0.248 + 0.9 f_{ck} \frac{h}{s}$$ (Eq. 6.7)

- Det Norske Veritas (DNV (2010)):

$$f_{axial} = \frac{\mu_{DNV} \cdot E_s}{K_{DNV}} \left(\frac{\delta_{DNV}}{Rp} + \frac{h}{21 \cdot s} \cdot f_{ck}^{0.4} \sqrt{\frac{t_p}{R_p}} \cdot \frac{s}{L} N \right)$$ (Eq. 6.8)

With:

$$K_{DNV} = \frac{R_p}{t_p} + \frac{E_s t_g}{E_g R_p} + \frac{R_s}{t_s}$$ (Eq. 6.9)

In DNV (2013), solely the axial capacity changed to (only a part by shear keys):

$$f_{axial} = \frac{\mu_{DNV} \cdot E_s}{K_{DNV}} \left(\frac{h}{21 \cdot s} \cdot f_{ck}^{0.4} \sqrt{\frac{t_p}{R_p}} \cdot \frac{s}{L} N \right)$$ (Eq. 6.10)

- Norsok (2012):

$$f_{axial} = \frac{C_I \cdot E_s}{C_F \cdot D_p} + C_p \cdot 140 \left(\frac{h}{s} \right)^{0.8} \cdot C_S^{0.6} \cdot f_{ck}^{0.3}$$ (Eq. 6.11)

With:

$$C_s = \left[m \left(\frac{D_g}{t_g} \right) \right]^{-1} + \left[\left(\frac{D_p}{t_p} \right) + \left(\frac{D_s}{t_s} \right) \right]^{-1}$$ (Eq. 6.12)

$$C_F = \frac{D_p}{2 t_p} + 2m \frac{t_g}{D_p} + \frac{D_s}{2 t_s}$$ (Eq. 6.13)
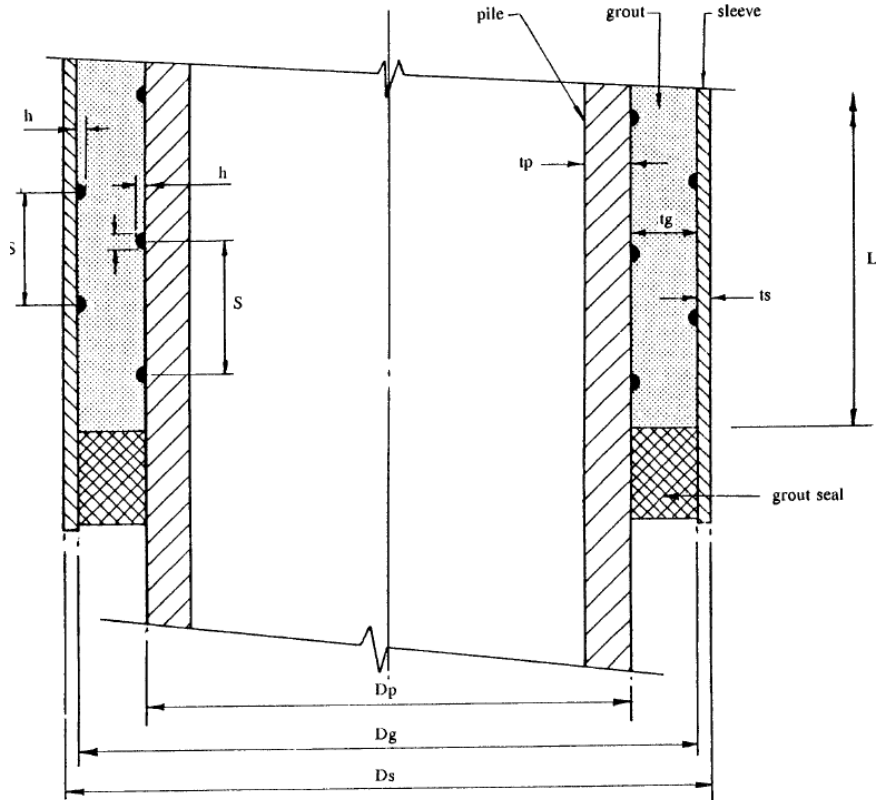
Figure 6.12: Definitions for the pile-sleeve expressions (OT (2002)).

6.5.3.1 Capacity

The presented pile-sleeve formulations give expressions for the axial capacity. Like (Eq. 6.1), the axial load (P_u) is divided over the interface as follows (Norsok (2012)).

$$\tau_A = \frac{P_u}{\pi D_p L}.$$

(Eq. 6.14)

Plug connections carry more than just axial force (in almost all cases). According to all four pile-sleeve expressions, bending moments ($M_{s,d}$) are transferred via bond (Figure 6.13). This seems a conservative approach since the plug will wrench in the pile and additional friction forces will arise. This enhances the capacity further but is not appointed by the design codes. The shear force along the interface introduced by the bending moment is equal to

$$\tau_M = \frac{M_{s,d}}{\pi D_p{}^2 L}.$$

(Eq. 6.15)
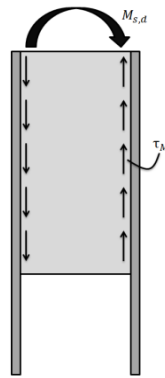
Figure 6.13: Bending moment transfer according to the four pile-sleeve design codes.

6.5.3.2 Usability

Three out of four of these pile-sleeve definitions make use of a stiffness factor (denoted as K or C_s in case of Norsok). This stiffness factor has been drafted by Billington et al. (1978) and compared with just six test specimens. Nezamian (2003) rewrote this stiffness factor to which, according to the writer of the publication, the presented formulations are applicable for plug connections.

$$K_{Nezamian} = \left[m\left(D_g/t_g\right)\right]^{-1} + \left(D_p/t_p\right)^{-1}$$

(Eq. 6.16)

in which, t_g is the thickness of the concrete between the longitudinal reinforcement bars and the pile and m is defined as E_s/E_c. The comparison between both systems seems however risky since expressions are based on experimental results concerning pile-sleeve systems. It remains a comparison between apples and oranges.

6.5.4 Comparison (example)

To illustrate the differences in outcome between the four introduced pile-sleeve formulations, the expression by Roeder et al. (1999), the Eurocode (EC) and the British standard (BS), an example is created for a plug connection (Figure 6.14). Assume a pile with a diameter of 1016mm and with a wall thickness of 16mm. The used concrete has a Young's modulus of 30.000MPa. The L/D_p ratio is chosen to be 2.0, resulting in an interface length of 2032mm. Finally, longitudinal reinforcement is adopted with a cover of 40mm.
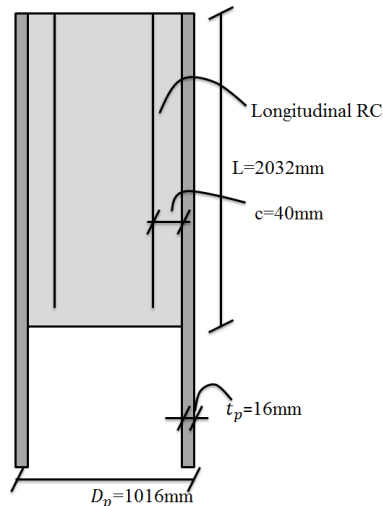
Figure 6.14: Example for the comparison analysis.

The result for this comparison is given in Figure 6.15. Differences between the various codes are quite large. The EC calculated the highest capacity for this example whereas the OT gives the lowest. The difference between the two is a huge discrepancy of 275%. The DNV (2013) states that no axial capacity is present when only bond is present.
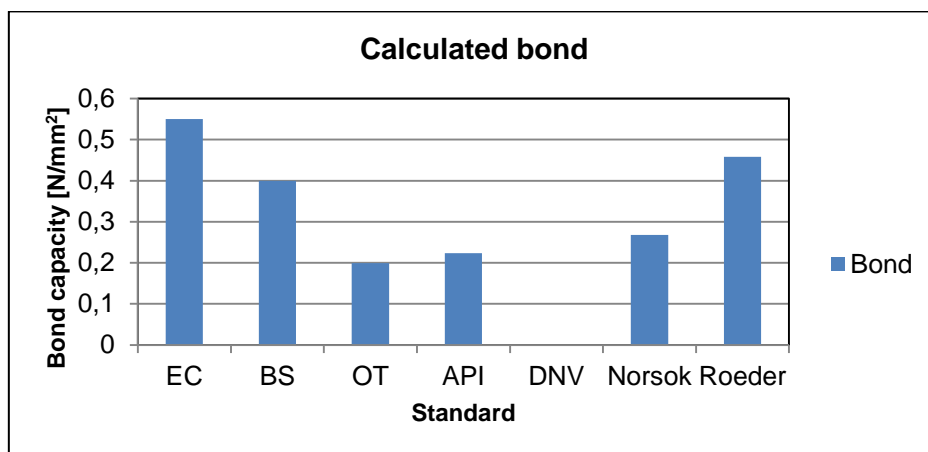
Figure 6.15: Differences between design code for the given example.

6.6 Conclusion

The main influences on the bond capacity are the pile diameter, shrinkage of the concrete, surface roughness and the diameter over thickness ratio. One effect which should not be underestimated is the effect of cyclic loading. A reduction of 30% of the capacity is found in two researches when only limited cycles are measured. The same is found with the pile-sleeve systems. Therefore, this fatigue behaviour should be included in design.

Multiple design expressions for the bond capacity are given. Several are related to pile-sleeve systems (to which the applicability is rather unknown) or constant values are advised. Looking at the conducted research, constant bond values are unrealistic due to the long list of influences on the bond capacity. The only formulation which is truly based on plug connections is the formulation by Roeder et al. (1999). This linear regression result gives the relation between bond and the diameter of thickness ratio. One similarity for all given standards remains, all are empirically determined and lack analytical background. Therefore, a new formulation for the bond stress will be derived in the next chapter.

New Axial Strength Model Without Shear Keys

Current available design expressions for bond strength are based on experimental results and lack analytical background. A new analytical model is required for the axial strength of the plug connection. In this chapter, a new model is proposed based on pressure vessels. The derivation is given for the <u>push-out case</u> since this will be the most common situation. This theory can naturally also be used for the pull-out case. The steel and concrete component are separated and considered independently. Expressions for the radial displacements are found to which the bond strength is linked. During the derivation, equations are solved with the help of computer software Maple, version 18.

The following steps are to be completed:
- The bond capacity is expressed as a function of the adhesion and micro-friction,
- The internal pressure is defined,
- Circumferential stresses and strains of both the steel and concrete are expressed,
- The displacements are calculated and the relative displacement between pile and core is solved,
- The bond capacity is solved out of the equation,
- The radial stiffness factor K is analytically determined and substituted into the expression for the bond capacity,
- The final formulation is formulated.

7.1 Definitions

The definition of the directions is given in Figure 7.1. In the formulation, the index 's' stands for steel and 'c' for concrete. A positive strain means enlargement of the diameter and a negative strain equals a reduction. The stresses and strains are defined as follows (Figure 7.1):
- σ_n and ε_n are respectively the stress and strain in radial direction,
- σ_θ and ε_θ are respectively the stress and strain in circumferential direction,
- σ_z and ε_z are respectively the stress and strain in longitudinal direction.
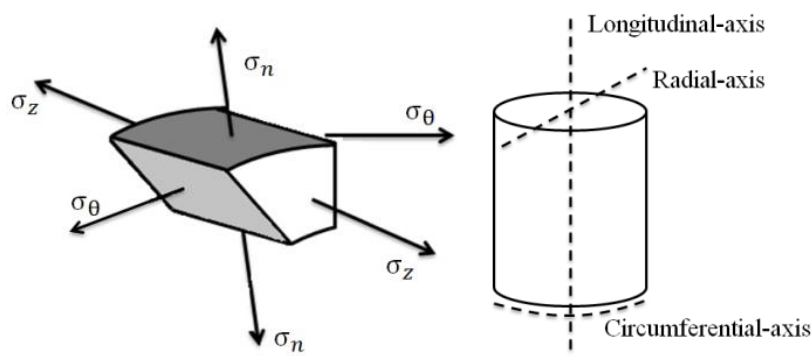
Figure 7.1: Stresses within the cylinder – definitions.

7.2 Friction

Roeder et al. (1999) found that bond is a function of both chemical adhesion and micro-friction. These two contributions are formulated as:

$$f_b = a + b_{fr}.$$ (Eq. 7.1)

In which 'a' is the cohesion and b_{fr} is the part due to friction. Friction is a function of pressure and roughness of the steel surface. The principle of friction is given in Figure 7.2 in which the block exerts a pressure on a slope. Gravity tends to move the box down the slope. However due to the gravity induced pressure, this motion is resisted by friction. This friction is the Coulomb friction coefficient (μ) multiplied with the force perpendicular (pressure) to the sliding surface.
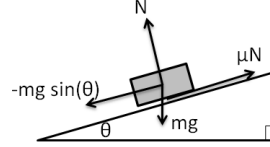
Figure 7.2: Principle of friction.

Translating this well-known principle to the plug connections, a pressure σ_n is introduced between the concrete core and steel tube since bond is a function of friction. This friction (Roeder et al (1999)) is a function of the difference in radial displacements (Δ) between inner core (Δ_c) and outer shell (Δ_s). The pile and the plug are in contact whenever Δ is smaller than the surface irregularities (μ_s) of the steel tube. In push-out, the plug exerts a pressure on the pile to which the pile will move outwards. The plug will laterally expand due to the Poison ratio. Therefore the following definition is used

$$\Delta = \Delta_s - \Delta_c.$$ (Eq. 7.2)

It must be noted that it is physically impossible that the factor Δ is lower than zero. This would mean that the concrete would have larger displacements than the confining steel tube. Therefore, the following constraint is added

$$\Delta \geq 0.$$ (Eq. 7.3)

Three different states can be obtained:
- A: $\mu_s - \Delta > 0$
- B: $\mu_s - \Delta = 0$
- C: $\mu_s - \Delta < 0$

In state A, the two surfaces are in contact and bond is present. In state B, de difference in radial deflection equals the roughness. In this state, there is no contact and therefore both the radial pressure and friction are zero. The two materials are separated in state C. Linking the friction term to the expression of μ_s-Δ, a stiffness parameter K is introduced. This parameter links a radial deflection (δ) to the associated pressure

$$\sigma_n = K \cdot \delta.$$ (Eq. 7.4)

The friction term of the bond formulation can now be expressed as (Chilvers (1984))

$$b_{fr} = \mu \cdot (\mu_s - \Delta) \cdot K,$$ (Eq. 7.5)

and subsequently, the pressure σ_n equals

$$\sigma_n = (\mu_s - \Delta) \cdot K.$$ (Eq. 7.6)

One assumption in this formulation is that the friction is linear related to the degree of contact. When Δ is zero, bond equals 100%, Δ= μ_s contact is zero and Δ= 0.5μ_s contact is 50%. Substituting (Eq. 7.5) in (Eq. 7.1) results in

$$f_b = a + \mu \cdot (\mu_s - \Delta) \cdot K.$$ (Eq. 7.7)

The frictional forces with the associated pressure are shown in Figure 7.3. In Chapter 6, it is found that bond stress is not constant along the interface. To deal with this phenomenon, stresses and strains are expressed as averages. This will result in a formulation for the average bond within a plug connection.
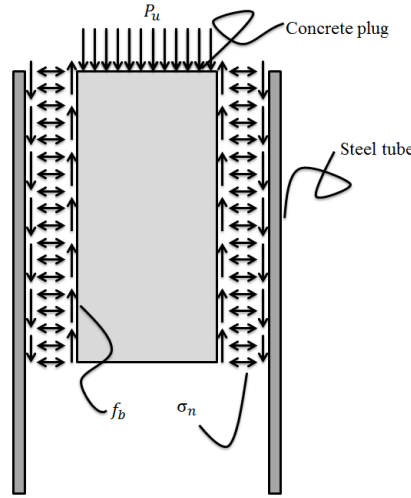
Figure 7.3: Force decomposition of the system.

7.3 Steel stresses and strain

7.3.1 Thin walled cylinders

The ratio between the diameter of the pile (D_p) and the associated thickness (t_p) is typically in the order of 30-80 in this field of application. This means that the pile should be regarded as a thin walled cylinder since the following definition holds (University of Colorado (2015))

$$t_p \leq \frac{1}{20} D_p.$$

(Eq. 7.8)

Regarding the pile as thin walled means that the internal radial stress in the section is zero. Furthermore, circumferential stresses are constant within one cross-section. With considerably small pile diameters, chances are that D_p/t_p ratios are less than 20 which would change the derivation in this chapter.

7.3.2 Circumferential stress

The average internal pressure on the pile is defined in (Eq. 7.6). Due to the thin walled assumption, the pressure vessel equation holds. This equation defines the circumferential stress based on equilibrium as a function of the internal pressure $\sigma_{s,n}$ on the pile (Figure 7.4).

$$\sigma_{s,\theta} = \sigma_{s,n} \frac{2R_p}{2t_p} = \sigma_{s,n} \frac{R_p}{t_p}$$

(Eq. 7.9)
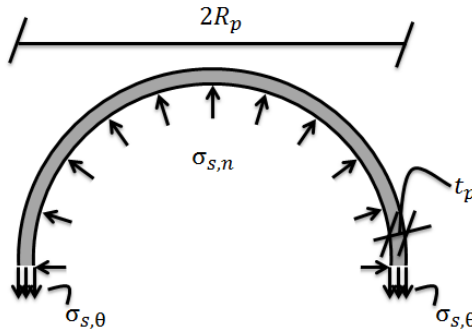
Figure 7.4: Definition of $\sigma_{s,\theta}$.

7.3.3 Longitudinal stress

The longitudinal stress within the pile is a function of the maximum force which can be exerted onto the plug. This maximum force (P_u) is defined as a function of bond along the circumference and past the interface length. This is illustrated in Figure 7.5 and expressed as

$$P_u = -f_b \cdot 2\pi \cdot R_c \cdot L. \tag{Eq. 7.10}$$
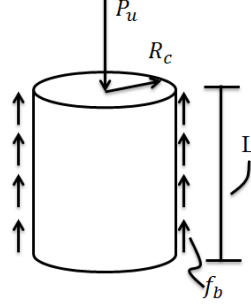
Figure 7.5: The ultimate capacity (P_u) of the plug connection.

In the expression for the maximum pressure force, the assumption is made that the total interface length contributes to the resistance. Roeder et al. (1999) proposed a different model in which the effective length is the minimum of the interface length or 3.5 times the diameter of the pipe. This model will be verified at the end of this chapter by comparing it with test results.

Since the maximum force is known, the average longitudinal stress can be defined. A stress distribution, like depicted in Figure 7.6, is adopted. The longitudinal stress in the pile at the top of the plug equals zero. At the bottom of the plug, due to the bond stress, the longitudinal stress equals the force divided by the steel area. The average along the plug can therefore be expressed as

$$\sigma_{s,z} = \frac{\left(\frac{P_u}{2}\right)}{2\pi \cdot R_p \cdot t_p} = -\frac{1}{2}\frac{f_b R_c L}{R_p t_p}. \tag{Eq. 7.11}$$
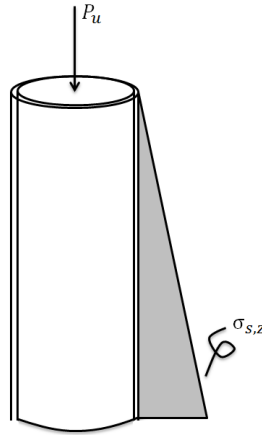
Figure 7.6: Assumed longitudinal stress distribution within the pile.

7.3.4 Radial stress

The internal radial stress within the pile is zero due to the thin walled cross-section.

$$\sigma_{s,n,internal} = 0. \tag{Eq. 7.12}$$

7.3.5 Circumferential strain

Stresses in all three principle directions have been derived as a function of the unknown bond stress. The circumferential strain is a function of these internal stresses

$$\varepsilon_{s,\theta} = \frac{1}{E_s}\Big(\sigma_{s,\theta} - \nu_s\big(\sigma_{s,z} + \sigma_{s,n,internal}\big)\Big). \tag{Eq. 7.13}$$

By substituting the expressions for $\sigma_{s,\theta}$, $\sigma_{s,z}$ and $\sigma_{s,n,internal}$ into (Eq. 7.13) results in the following expression for the circumferential steel strain

$$\varepsilon_{s,\theta} = \frac{1}{E_s}\left(\frac{K(\mu_s - \Delta)R_p}{t_p} + \frac{1}{2}\frac{\nu_s f_b R_c L}{R_p t_p}\right). \tag{Eq. 7.14}$$

7.4 Concrete stresses and strain

In contrast to the steel section, the concrete cylinder needs to be regarded as a thick walled cylinder. This results in a different approach for defining the radial and circumferential stresses. These stresses are defined by making use of Lame's equations (proof is given in Appendix E)

$$\sigma_n = a + \frac{b}{R^2} \tag{Eq. 7.15}$$

$$\sigma_\theta = a - \frac{b}{R^2}. \tag{Eq. 7.16}$$

The factors 'a' and 'b' are constants which should be solved with the boundary conditions of the system. For the plug, the following two boundary conditions can be defined:
- At the internal radius (R_i, which is actually zero), the radial stress on the plug is zero,
- At the outer radius (R_c), the radial stress is equal to the exerted pressure σ_n (Eq. 7.6).

Solving the first boundary condition, an expression for 'a' can be found

$$0 = a + \frac{b}{R_i{}^2} \rightarrow a = -\frac{b}{R_i{}^2}. \tag{Eq. 7.17}$$

The second boundary condition results in an expression for 'b' after which 'a' can be solved as well.

$$-K(\mu_s - \Delta) = -\frac{b}{R_i{}^2} + \frac{b}{R_c{}^2} \rightarrow b = K(\mu_s - \Delta)\frac{R_i{}^2 R_c^2}{R_c^2 - R_i^2} \tag{Eq. 7.18}$$

and subsequently 'a' is equal to

$$a = -K(\mu_s - \Delta)\frac{R_c^2}{R_c^2 - R_i^2}. \tag{Eq. 7.19}$$

7.4.1 Circumferential and radial stress

Substituting the expression for 'a' and 'b' into (Eq. 7.15) and (Eq. 7.16), results in the expressions for the circumferential and radial stress within the plug.

$$\sigma_{c,\theta} = -K(\mu_s - \Delta)\left(\frac{R_c^2}{R_c^2 - R_i^2} + \frac{R_i{}^2}{R_c^2 - R_i^2}\right) \tag{Eq. 7.20}$$

$$\sigma_{c,n,internal} = -K(\mu_s - \Delta)\left(\frac{R_c^2}{R_c^2 - R_i^2} - \frac{R_i{}^2}{R_c^2 - R_i^2}\right). \tag{Eq. 7.21}$$

The concrete part of the connection is casted as a solid cylinder. This means that the internal radius (R_i) is equal to zero. By doing so, the expressions for the stresses reduce to

$$\sigma_{c,\theta} = -K(\mu_s - \Delta) \tag{Eq. 7.22}$$

$$\sigma_{c,n,internal} = -K(\mu_s - \Delta). \tag{Eq. 7.23}$$

7.4.2 Longitudinal stress

The longitudinal stress can be defined as like the longitudinal stress in the pile. The opposite stress distribution is assumed, zero stress at the bottom and P_u divided by the area at the top of the plug. This results in

$$\sigma_{c,z} = \frac{\left(\frac{P_u}{2}\right)}{\pi R_c{}^2} = -\frac{f_b L}{R_c}. \tag{Eq. 7.24}$$

7.4.3 Concrete strain

Just like the steel part, the circumferential strain is a function of the three stress components.

$$\varepsilon_{c,\theta} = \frac{1}{E_c}\Big(\sigma_{s,\theta} - v_c\big(\sigma_{c,z} + \sigma_{c,n,internal}\big)\Big). \tag{Eq. 7.25}$$

By substituting (Eq. 7.22), (Eq. 7.23) and (Eq. 7.24) into the strain equation (Eq. 7.25), the following definition for the strain is found

$$\varepsilon_{c,\theta} = \frac{-K(\mu_s - \Delta) - v_c\left(\frac{-f_b L}{R_c} - K(\mu_s - \Delta)\right)}{E_c}. \tag{Eq. 7.26}$$

7.5 Relative displacement between pile and plug

The relative displacement between the pile and the plug can be defined since both expressions for the strains are known. A radial displacement (δ) is related to the circumferential strain as follows

$$\varepsilon_\theta = \frac{Increase\ in\ circumference}{Initial\ circumference} = \frac{2\pi(R + \delta) - 2\pi R}{2\pi R} = \frac{\delta}{R}. \tag{Eq. 7.27}$$

Since the pile is considered thin walled, the radial displacement is constant along the cross-section. The inner- and outer circumference are subjected to the same radial displacement. The strain of the concrete varies along the axis. Both displacements at the location of the interface are therefore equal to

$$\Delta_s = \varepsilon_{s,\theta} R_p = \left(\frac{\frac{K(\mu_s - \Delta)R_p}{t_p} + \frac{1}{2}\frac{v_s f_b R_c L}{R_p t_p}}{E_s}\right) R_p \tag{Eq. 7.28}$$

$$\Delta_c = \varepsilon_{s,\theta} R_c = \left(\frac{-K(\mu_s - \Delta) - v_c\left(\frac{-f_b L}{R_c} - K(\mu_s - \Delta)\right)}{E_c}\right) R_c. \tag{Eq. 7.29}$$

The relative displacement as defined in the beginning of this chapter equals

$$\Delta = \Delta_s - \Delta_c. \tag{Eq. 7.30}$$

Substituting (Eq. 7.28) and (Eq. 7.29) into (Eq. 7.30) gives the expression for the difference in radial displacement

$$\Delta = \left(\frac{\frac{K(\mu_s - \Delta)R_p}{t_p} + \frac{1}{2}\frac{v_s f_b R_c L}{R_p t_p}}{E_s}\right) R_p - \left(\frac{-K(\mu_s - \Delta) - v_c\left(\frac{-f_b L}{R_c} - K(\mu_s - \Delta)\right)}{E_c}\right) R_c. \tag{Eq. 7.31}$$

(Eq. 7.31) is a recursive equation with only one unknown parameter Δ. By making use of the solve function within computer software Maple, this equation can be solved with respect to Δ. This results in the following

$$\Delta = \frac{1}{2}\left(\frac{-2v_cE_sKR_ct_p\mu_s + Lv_sE_cf_bR_c - 2Lv_cE_sf_bt_p + 2E_cKR_p{}^2\mu_s + 2E_sKR_ct_p\mu_s}{-v_cE_sKR_ct_p + E_cKR_p{}^2 + E_sKR_ct_p + E_cE_st_p}\right). \tag{Eq. 7.32}$$

7.6 Bond expression

Recall that bond is a function of both chemical adhesion and friction. When there is a relative radial displacement between the two materials, it is likely that the chemical adhesion is broken. This part of the bond is therefore set to zero.

$$f_b = \mu \cdot \sigma_{s,n} = \mu \cdot K(\mu_s - \Delta). \tag{Eq. 7.33}$$

Substituting the expression for the difference in radial displacement (Δ) results in

$$f_b = \mu K\left(u_m - \frac{1}{2}\left(\frac{-2v_cE_sKR_ct_p\mu_s + Lv_sE_cf_bR_c - 2Lv_cE_sf_bt_p + 2E_cKR_p{}^2\mu_s + 2E_sKR_ct_p\mu_s}{-v_cE_sKR_ct_p + E_cKR_p{}^2 + E_sKR_ct_p + E_cE_st_p}\right)\right). \tag{Eq. 7.34}$$

By solving this equation with respect to the bond strength, the expression for bond is found.

$$f_b = \frac{2\mu K\mu_sE_cE_st_p}{L\mu v_sE_cKR_c - 2L\mu v_cE_sKt_p - 2v_cE_sKR_ct_p + 2E_cKR_p^2 + 2E_sKR_ct_p + 2E_cE_st_p}. \tag{Eq. 7.35}$$

7.7 Stiffness factor K

The radial stiffness factor K sets the relation between the radial traction (radial stress) and the associated displacement. This relation is determined in the same manner as before. Consider the situation in Figure 7.7. The internal stress σ causes a radial deflection δ. The radial deflection (again thin walled section) due to this σ can be expressed as:

$$\varepsilon_\theta = \frac{1}{E_s}\left(\sigma\frac{R_p}{t_p}\right) \tag{Eq. 7.36}$$

$$\delta = \varepsilon_\theta R_p = \frac{1}{E_s}\left(\sigma\frac{R_p}{t_p}\right)R_p. \tag{Eq. 7.37}$$

K is defined as the ratio between the applied stress and the displacement

$$K = \frac{\sigma}{\delta}. \tag{Eq. 7.38}$$

Rearranging (Eq. 7.37) gives

$$\sigma = \frac{E_st_p}{R_p^2}\cdot\delta \rightarrow K = \frac{E_st_p}{R_p^2}. \tag{Eq. 7.39}$$
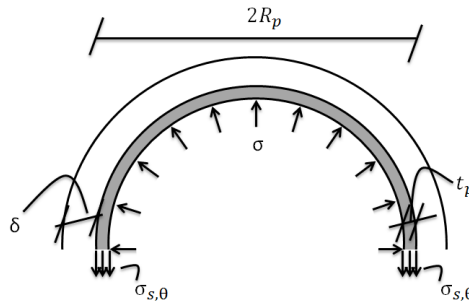
Figure 7.7: Determination of the stiffness factor K.

7.7.1   Comparing stiffness factors

Comparing the derived factor with the one from Billington et al. (1978), shows substantial differences. The one from Billington (Eq. 6.6) is related to the radius of the pile whilst in the derived formulation it is related to the radius squared. This means that the formulation is way more sensitive to scale effects, which is in line with test results from chapter 6. A comparison of the units gives

$$K_{analytically} = \frac{[N]}{[mm]^2} \frac{[mm]}{[mm]^2} = \left[\frac{N}{mm^3}\right] \tag{Eq. 7.40}$$

$$K_{Billington} = \frac{[N]}{[mm]^2} \frac{[mm]}{[mm]} = \left[\frac{N}{mm^2}\right]. \tag{Eq. 7.41}$$

When both formulations are checked, it seems that the formula, formulated by Billington et al. (1978) to which current design formulations are based, is incorrect. In the denoted paper, the stiffness factor is introduced as an approximation rather than an equality. This might be the reason that current formulations diverge with large pile diameters.

7.8   Bond formulation

The expression for the bond strength from section 7.6 can be shortened. The following properties are adopted:

- The friction coefficient between steel and concrete (μ) is examined by Rabbat et al. (1985). The purpose of their research was to examine the friction coefficient in containment vessels by testing. For a dry interface (meaning that the concrete has hardened), a value for μ of 0.57 is found. ECS (2011c) prescribes a value of 0.5 for steel without paint. This latter value is considered safe and will be used,
- The surface roughness of the steel (μ_s) can be taken as 0.05mm for steel sections (ECS (2005)),
- The Poisson ratio for steel is 0.3 and for concrete 0.2.

Applying the previous values for the friction, roughness and Poisson ratios together with the derived stiffness factor K (Eq. 7.39), the bond expression reduces to

$$f_{b,push-out} = \frac{E_s t_p}{R_c(3L + 32mt_p) - 4Lmt_p + 80R_p{}^2}. \tag{Eq. 7.42}$$

In which m is defined as the modular ratio (E_s/E_c). Note that this is the expression for the push-out mechanism of the plug. When the complete derivation is deduced again for pull-out, the following formulation is found

$$f_{b,pull-out} = \frac{E_s t_p}{R_c(3L - 32mt_p) - 4Lmt_p - 80R_p{}^2}. \tag{Eq. 7.43}$$

7.9   Final bond formulation including shrinkage

Shrinkage is denoted as one of the most influencing factors on the bond capacity and therefore it should be incorporated in the model. In the equation for the concrete strain (Eq. 7.26), an additional shrinkage term ($\varepsilon_{shrinkage}$) is included. This equation changes to

$$\varepsilon_{c,n} = \frac{1}{E_c}\left(-K(\mu_s - \Delta) - v_c\left(\frac{-f_b L}{R_c} - K(\mu_s - \Delta)\right)\right) - \varepsilon_{shrinkage}. \tag{Eq. 7.44}$$

By rerunning the analysis and resolving the equations, the bond formulations (including shrinkage) are found

$$f_{b,push-out} = \frac{-E_s t_p (20\varepsilon_{shrinkage} R_c - 1)}{R_c(3L + 32mt_p) - 4Lmt_p + 80R_p{}^2} \qquad \text{(Eq. 7.45)}$$

$$f_{b,pull-out} = \frac{-E_s t_p (20\varepsilon_{shrinkage} R_c - 1)}{R_c(3L - 32mt_p) - 4Lmt_p - 80R_p{}^2}. \qquad \text{(Eq. 7.46)}$$

7.10 Assumptions

The following assumptions have been made during the derivation:

- The longitudinal stress in the steel pile is assumed linear which implies zero at the top and maximum at the bottom of the plug. This assumption seems to be correct since Nezamian (2003) found the curve displayed in Figure 7.8.
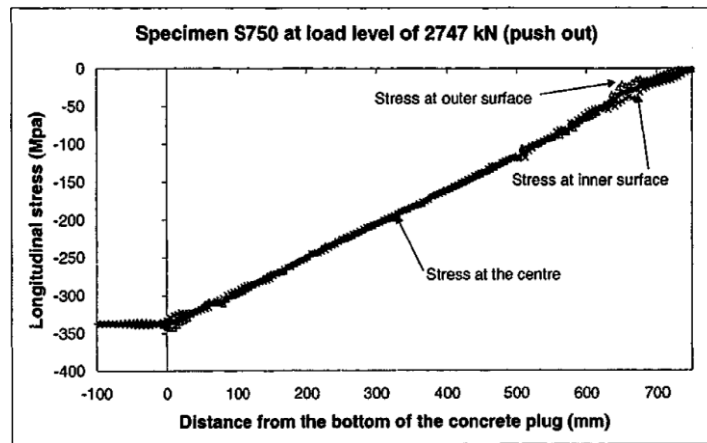
Figure 7.8: Longitudinal stress in the pile found by Nezamian (2003) for specimen S750.

- The stress in the concrete plug is also assumed linear. This assumption seems correct as well since the longitudinal stress in the pile is linear.
- During the derivation, it is assumed that the total interface length contributes for the capacity, as seen in Figure 7.5. Roeder et al. (1999) proposed a model in which the maximum contributing length is reduced. This length is the minimum of the interface length and three times the diameter of the tube as displayed in Figure 7.9. This additional model accounts for lowering of the average bond with increasing length. Figure 7.8 shows an almost perfect linear stress distribution for the longitudinal steel stresses. Based on this graph, it is revealed that the complete interface is active.
- For the plug connections, thin walled cross-sections are used.
- The radial stiffness of the pile is used as the stiffness factor for the connection, which is considered conservative. Actually, the plug will also contribute a little which enhances the stiffness and therefore also the bond capacity.
- Confinement of the concrete is neglected in this analysis. When this effect is included, it would only make a marginal difference on the bond capacity as is demonstrated in Figure 8.5.
- The chemical adhesion is assumed zero, which is deemed conservative since it will probably be broken when there is a difference in radial displacement between pile and plug.
- The roughness of the pile wall is assumed to be constant. Spiral weld beads of the pile may act as a shear connector and enhance the capacity.
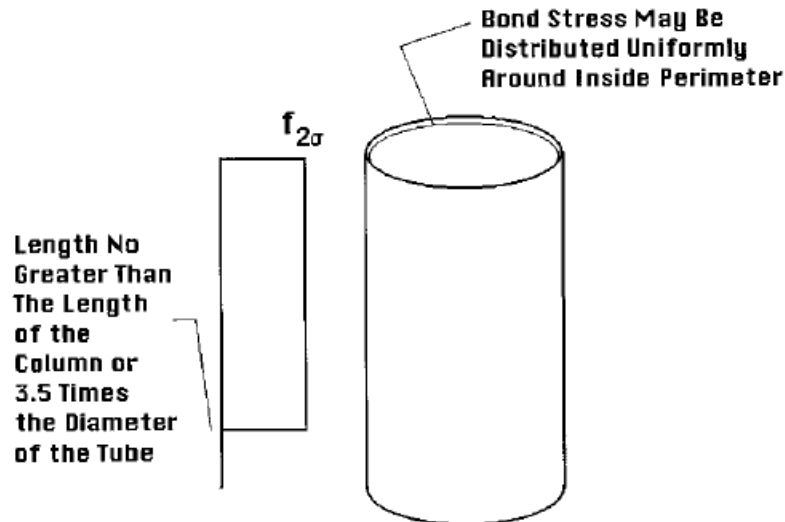
Figure 7.9: Distribution of the bond along the interface according to Roeder et al. (1999).

7.11 Conclusion

A new analytical model for the axial strength without shear keys is derived. This model is based on the stresses and strains of both the steel and the concrete to which the bond is related. The assumptions made in this derivation coincide well with the findings from testing. The new model is the first equation which is completely analytical for the bond stress in circular piles.

The new analytical model will be verified according to the statements and conclusions from Chapter 6. Whenever there is a lack of clarity, an explanation will be sought within the given equations. Furthermore, a large scatter in test results has been found. Specimens with supposedly the same strength can differ greatly in outcome. The new expression should account for these uncertainties by matching it to test data. By doing so, a comparison between all the presented standards can be made to check the accuracy and usability.

Comparison Bond Formulation to Test Results

To check the validity of the analytical model, a verification should be performed with representative test data. At first, a comparison is made to check whether the same influences are of importance as found in literature. Conclusions of previous research are inspected and explanations for these effects are given. Finally, a calibration of the model is performed and compared with the existing expressions.

8.1 Comparing trends

Multiple trends have been identified by previous research on the bond capacity and led to contradicting conclusions. The findings from literature are compared with the results from the derived formulation. To be able to analyse the effect of different parameters, an example is created. The dimensions for the pile diameter and wall thickness are given in Figure 8.1. The used concrete has a compressive strength of 44.9N/mm^2 to which the modulus of elasticity equals 36262N/mm^2. Shrinkage is not incorporated in this example since the appropriate shrinkage model is yet to be determined.
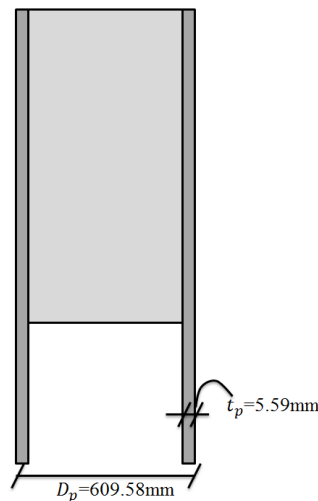
Figure 8.1: Dimensions for the example.

8.1.1 Interface length

Nezamian et al. (2006) and Roeder et al. (1999) both found lowering of the average bond capacity with increasing plug length. However, no clear reason was found for this effect. By adopting the given example in combination with the derived formulation, the relation between bond and interface length is examined in Figure 8.2. The interface length is varied from $1D_p$=609.58mm to $8D_p$=4876.64mm (this is possible since no pile-to-cap reinforcement is present). The same trend is denoted as in literature; the average capacity lowers with increasing interface length.
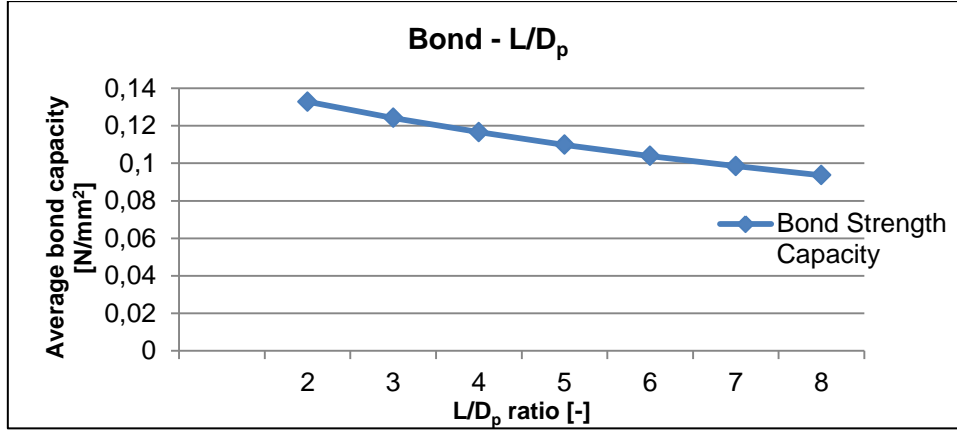
Figure 8.2: Effect of the interface length on the bond capacity.

A decrease of the capacity can be explained by looking at the formulations for the longitudinal stress in both the steel and concrete (Eq. 7.11 and (Eq. 7.24)).

$$\sigma_{s,z} = \frac{\left(\frac{P_u}{2}\right)}{2\pi \cdot R_p \cdot t_p} = -\frac{1}{2}\frac{f_b R_c L}{R_p t_p}$$ (Eq. 8.1)

$$\sigma_{c,z} = -\frac{f_b L}{R_c}$$ (Eq. 8.2)

An estimation is made for the radius of the concrete core over the radius of the pile like

$$\frac{R_c}{R_p} \approx 1.$$ (Eq. 8.3)

Substituting (Eq. 8.3) into the expression for the longitudinal steel stress (Eq. 8.1) results in

$$\sigma_{s,z} = -\frac{f_b L}{2t_p}.$$ (Eq. 8.4)

Comparing (Eq. 8.2) and (Eq. 8.4) results in the explanation for the decrease in bond for the push-out case. At increasing length (L), the longitudinal stress of the concrete increases with $1/(R_c)$ whilst the steel stress with $1/(2t_p)$. Since $R_c >> 2t_p$, the compressive stress in the steel increases faster in comparison to the concrete stress. This results in more radial displacement (increase in diameter) of the tube in relation to the plug to which the bond capacity lowers.

8.1.2 Diameter

In section 6.2.3, the effect of the pile diameter is discussed in detail. A significant lowering of the capacity is seen with increasing pile diameter. This effect is analysed in Figure 8.3 with constant interface length chosen at a value of 500mm. The thickness of the pile is linearly increased with the diameter to keep the D_p/t_p ratio constant at a chosen value of 40, which is a likely ratio for a foundation pile.

The lowering of the bond can be attributed to multiple causes. At first, the stiffness of the pile is reduced by a factor of R_p^2 as seen in (Eq. 7.39). Furthermore, the longitudinal stress difference between steel and concrete increases. This will cause an increase of Δ as seen in (Eq. 7.2). The last reason which is actually not adapted in this example is concrete shrinkage. This effect is verified in a later stage in this chapter.
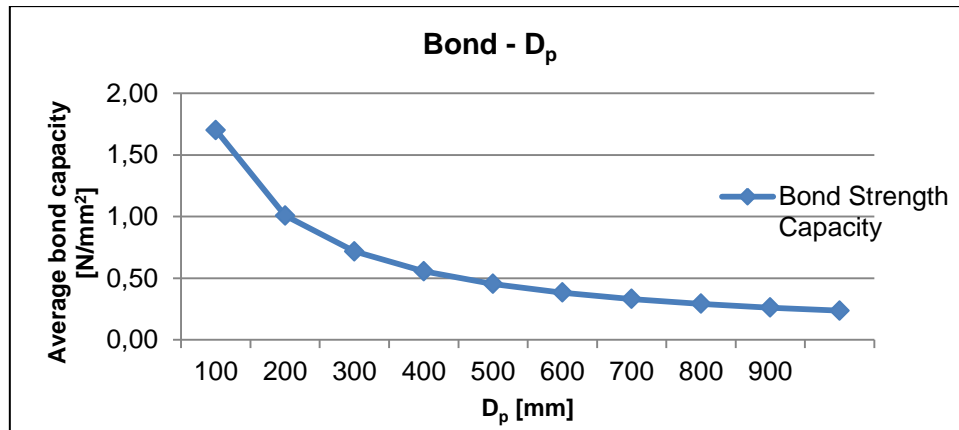
Figure 8.3: Effect of the pile diameter (D_p) on bond.

8.1.3 Thickness

Just like the pile diameter (D_p), the D_p over t_p ratio is denoted as a major influence on bond by Roeder et al. (1999). However, it is not possible to change the D_p/t_p ratio since either the diameter or the thickness should be changed or both. For the given example, the thickness is varied to show the effect in Figure 8.4. The lowest adopted value is D_p/t_p equal to 20, due to the thin walled assumption in the derivation. Other influences are according to the example displayed in Figure 8.1, with an interface length of 500mm.

The same trend is observed by lowering the thickness of the pile as with the increase in pile diameter. The stiffness of the pile is linearly reduced with a decreasing thickness. Subsequently, the longitudinal stress (Eq. 7.9) and circumferential stress (Eq. 7.11) in the pile are decreased. This causes an increase of pile diameter to which the capacity reduces fast.
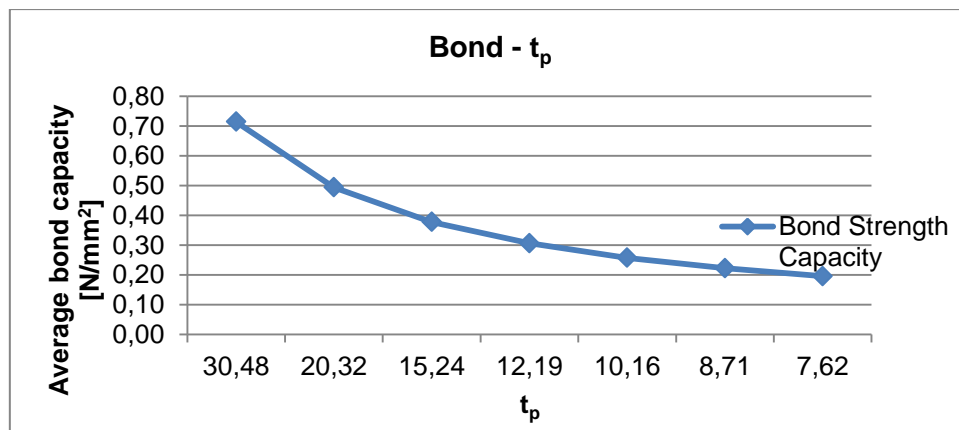
Figure 8.4: Effect of the pile thickness (t_p) on bond.

8.1.4 Concrete compressive strength

According to Virdi et al. (1980) and Roeder et al. (1999), the bond strength is independent from the concrete compressive strength. Aly et al. (2009) disagree and conclude that a decrease of the bond with increasing f_{ck} occurs.

The effect of the concrete compressive strength is displayed in Figure 8.5. Only a very small increase (1.7% difference between the highest and lowest value) is seen when increasing f_{ck}. However, it should be noted that shrinkage is not taken into account in this example. Higher strength concretes tend to shrink more in comparison to lower strength concretes. Therefore, Aly et al. (2009) is most certainly right about this parameter.
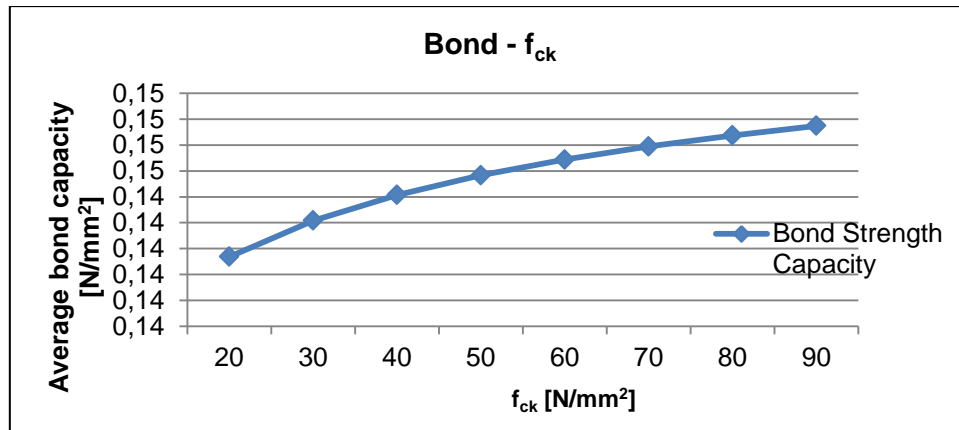
Figure 8.5: Effect of the concrete compressive strength on bond.

8.1.5   Difference pull- and push-out

Nezamian et al. (2006) state that the pull-out strength is larger than the push-out capacity. This has been verified with (Eq. 7.42) and (Eq. 7.43). For the same case as Figure 8.3, the pull-out strength is calculated as shown in Figure 8.6. It shows that for small diameters, the pull-out strength is considerably higher than the push-out strength. With larger diameters, this reduces to less than 10% difference between the two cases. All tests by Nezamian are conducted on small diameter piles (D_p of 237mm), so the found results are in line with the test results.
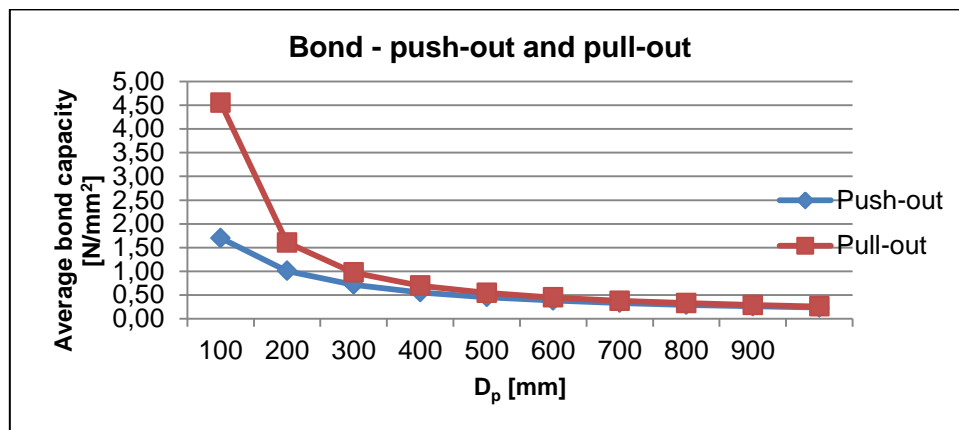
Figure 8.6: Comparison pull- and push-out in relation to the diameter.

8.2   Shrinkage models

The shrinkage of the concrete core is often denoted as one of the most important influences. Therefore, it is important to adopt the correct shrinkage behaviour into the formulation. Enclosed concrete shows different shrinkage behaviour than exposed concrete. Shrinkage values of 10-20% of exposed concrete are detected during testing for concrete confined by steel tubes (Vincent et al. (2014)). They conducted tests and conclude that 85% of the total shrinkage occurs during the first two months after casting. After approximately four months, the shrinkage comes to a halt and almost no recordable differences can be found anymore (Figure 8.7).
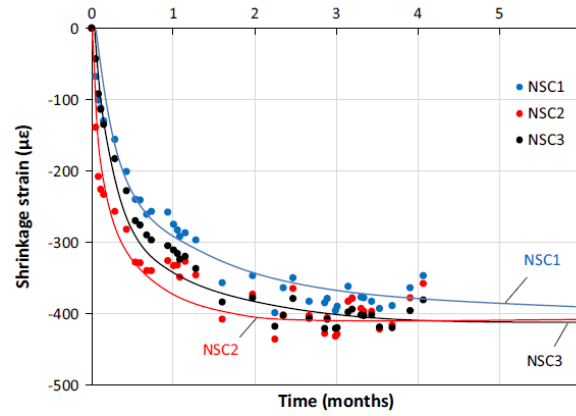
Figure 8.7: Shrinkage over time during testing for normal strength concrete (Vincent et al. (2014)).

8.2.1 Models

Two different models are considered for this behaviour, the shrinkage model from the Eurocode and the Kelvin shrinkage model (Ichinose et al. (2000)). The Eurocode shrinkage model contains two contributions (ECS (2011b))

$$\varepsilon_{cs} = \varepsilon_{cd} + \varepsilon_{ca}. \tag{Eq. 8.5}$$

The first contribution (ε_{cd}) is equal to the chemical shrinkage and account for the loss of water. The second part (ε_{ca}) is the autogenous shrinkage of the concrete. The latter is highly related to the concrete compressive strength like follows

$$\varepsilon_{ca}(t) = \beta_{as}(t)\varepsilon_{ca}(\infty) \tag{Eq. 8.6}$$
$$\beta_{as}(t) = 1 - \exp(-0.2t^{0.5}) \tag{Eq. 8.7}$$
$$\varepsilon_{ca}(\infty) = 2.5(f_{ck} - 10) \cdot 10^{-6} \tag{Eq. 8.8}$$

in which t is the time in days. Chemical shrinkage is a function of the relative humidity, the concrete class and the height of the element. The following is provided by Eurocode 2

$$\varepsilon_{cd}(t) = \beta_{ds}(t, t_s) \cdot k_h \varepsilon_{cd,0} \tag{Eq. 8.9}$$
$$\beta_{ds}(t, t_s) = \frac{(t - t_s)}{(t - t_s) + 0.04\sqrt{h_0^3}} \tag{Eq. 8.10}$$
$$h_0 = \frac{2A_c}{u}. \tag{Eq. 8.11}$$

In which $\varepsilon_{cd}(0)$ and k_h are determined via tables provided by the Eurocode. The second model is the Kelvin shrinkage model which is based on Figure 8.8. The formulation for the shrinkage behaviour has been solved by Ichinose et al. (2000) to which the following expression is found

$$\varepsilon(t) = \frac{\sigma_0}{E_c}\left\{\alpha(1 - e^{-\kappa t}) + \frac{1 - \alpha}{1 - \kappa/\beta}\left(e^{-\kappa t} - e^{-\beta t}\right)\right\}. \tag{Eq. 8.12}$$
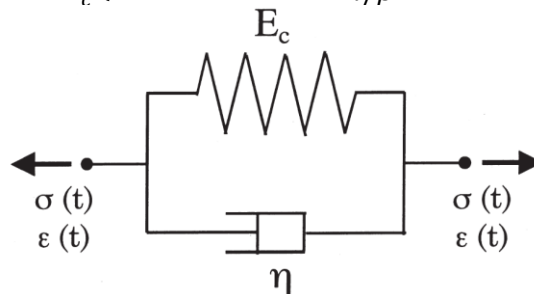
Figure 8.8: Kelvin model (Ichinose et al.(2000)).

In the formulation, σ_o is the initial applied stress at the top of the plug, t is the time in days and the α, β and κ factors are parameters which should be determined experimentally. For the normal strength concrete (NSC) from Figure 8.7, the following values give a good approximation for the shrinkage behaviour (Figure 8.9).

- $\alpha = 0.38$,
- $\kappa = 0.0001$,
- $\beta = 0.03$.

A major disadvantage of this model is that for every concrete mix, the three parameters should be determined with a least-squares method based on experiments. Since this will lead to impracticalities in usage, the Eurocode shrinkage model is adopted into the model. Only little data is required to obtain the shrinkage of each specimen. Since, the concrete shrinkage is just a fraction of exposed concrete, the following model is proposed for usage.

$$\varepsilon_{cs} = 0.2\varepsilon_{cd} + \varepsilon_{ca}. \tag{Eq. 8.13}$$

The upper bound of 20% is assumed to be conservative. The autogenous shrinkage will occur by any means and is therefore not lowered by 80%. The relative humidity is chosen at a value of 40% to determine $\varepsilon_{cd}(0)$. This is a little more conservative than Nezamian (2003) proposed which used a value of 60%. The term h_0 (as defined in (Eq. 8.11)) equal two times the plug length as set by Nezamian (2003).

Plotting the shrinkage behaviour results in Figure 8.9. Both the Kelvin- and the Eurocode shrinkage models are plotted for a test case. This is done to show that the adopted model and the Kelvin model give very similar shrinkage values. To be able to compare the results, the same data is used as the specimens of Vincent et al. (2014). A pile with diameter of 152mm and a length of 305mm are used during testing. Concrete used is normal strength concrete with a compressive strength of 44.8N/mm². The shrinkage strain measured in Figure 8.7 is the strain at the top of the specimen where there is an open contact surface with the environment. Taking 20% of this value results in the shrinkage behaviour in time as depicted with the green line. The adopted model based on the Eurocode shrinkage model seems to give similar results to the Kelvin model.
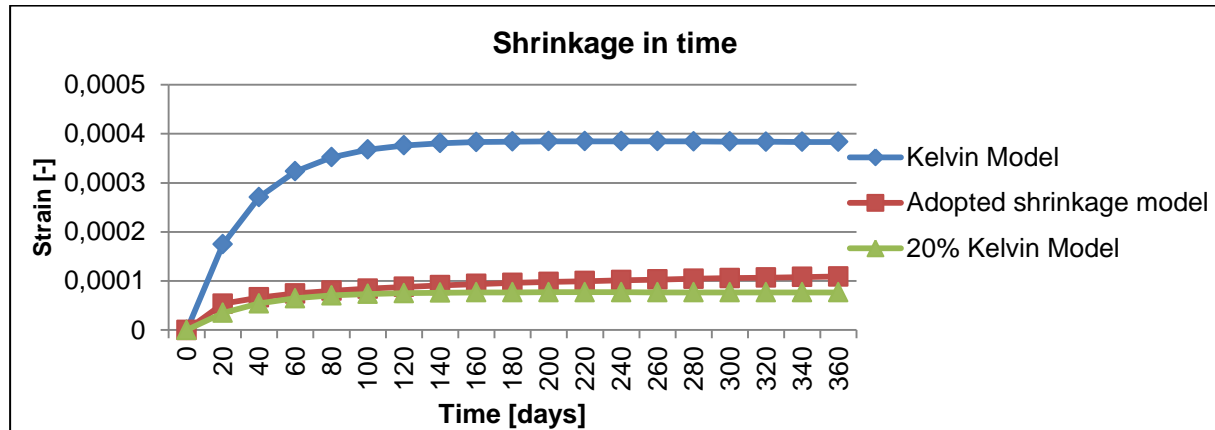
Figure 8.9: Shrinkage in time.

8.3 Matching to test results

To check whether (Eq. 7.45) gives accurate results in combination with the adopted shrinkage model, the theoretical values should be verified to the available test data. Representative test data from Virdi et al. (1980), Shakir-Khalil (1993), Roeder et al. (1999), Nezamian et al. (2002) and Aly et al. (2009) are selected. This selection is based on the appropriate failure mechanism to which the formulation is derived. The test specimens are tested for the push-out case, so (Eq. 7.45) is used in this analysis. The list of data with the associated test set-up is given in Appendix F. The two largest cases are denoted as

outliers and are therefore remover from the test data, such that the number of specimens is reduced from 63 to 61.

8.3.1 Validation

A validation procedure for the resistance model (Eq. 7.45) is given in Eurocode 0 (ECS (2011a)) and will be completed in this section. This procedure calculates a correction factor in order to match the test results with the derived formulation. Five assumptions are made for adaptation of this method.
1. The resistance model is a function of independent variables,
2. Sufficient test data is available,
3. All independent variables are measured during testing,
4. The variables are independent of each other,
5. All variables are normally- or log-normally distributed.

8.3.2 Comparison of theoretical and experimental values

The resistance value (bond strength) is calculated for each single test specimen. The calculated and the experimentally found values are illustrated (Figure 8.10). The X-axis represents the theoretical values (r_t) and the Y-axis, the experimental (r_e). Per test specimen, a dot is given in the graph with coordinates of (r_{ti}, r_{ei}). The 'i' indicates the test specimen number.

The orange line represents a line under an angle of 45 degrees. Al values above this line are approximated safely (the theoretical value is lower than the measures value). The opposite holds for the points below this line, the theoretical value is larger than the measured one. The larger the distance to this orange line, the larger the difference between theoretical and experimental values.

The dispersion between the points is considered to be large. As seen in Chapter 6, the scatter in experimental values is very large. Differences of 200% between two identical specimens occur in which no logical explanation is given in the denoted literature. This rather extreme example indicates the reason for the scatter found in Figure 8.10. To match test results, it is definitely necessary to apply a correction factor.
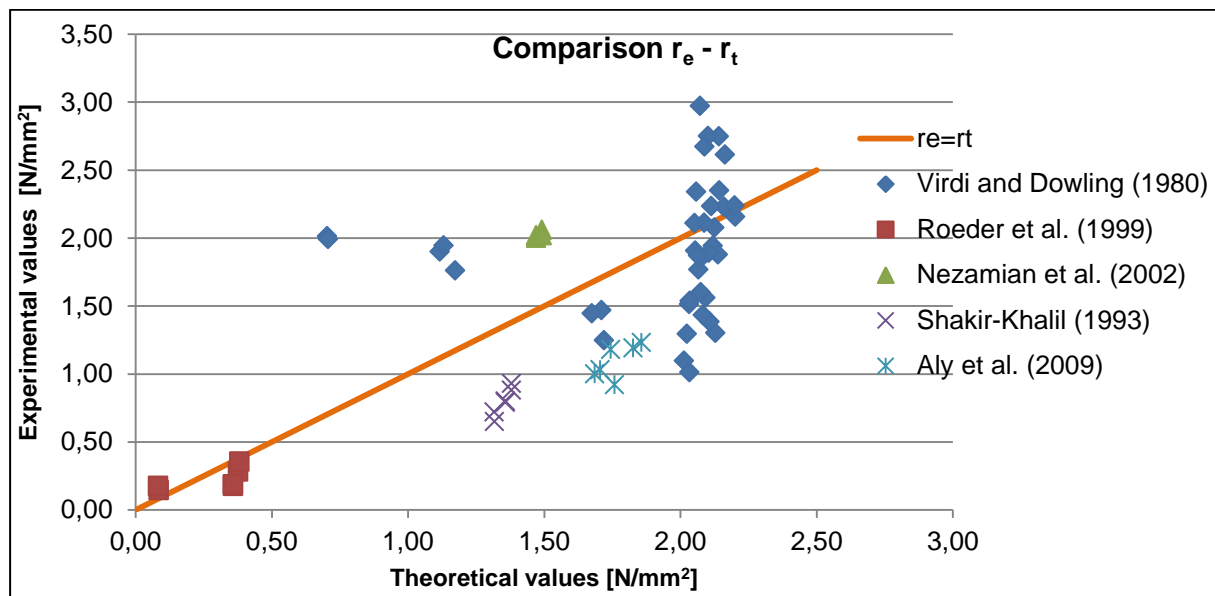
Figure 8.10: Comparison between the experimental and theoretical values.

8.3.3   Correction

An estimation of the correction factor b can be made with the least squares method (ECS (2011a)). This correction factor changes the slope of the orange line. The following estimation is used

$$b = \frac{\sum r_e r_t}{\sum r_t^2}.$$

<div align="right">(Eq. 8.14)</div>

Applying this to the test data from Appendix F, the factor b is equal to 0.90. In order to estimate the standard deviation, the dispersion per specimen should be obtained with

$$\delta_i = \frac{r_{ei}}{b r_{ti}}.$$

<div align="right">(Eq. 8.15)</div>

Taking the natural logarithm of each of these term like

$$\Delta_i = \ln(\delta_i)$$

<div align="right">(Eq. 8.16)</div>

and averaging this per specimen gives

$$\Delta^- = \frac{1}{n} \sum_{i=1}^{n} \Delta_i = -0.009.$$

<div align="right">(Eq. 8.17)</div>

The standard deviation is a measure for the spreading around the average bond value. The lower this spread is, the better the experimental results are approximated by the formulation. Since samples are considered, the following formulation is applicable

$$s_\Delta = \sqrt{\frac{1}{(n-1)} \sum_{i=1}^{n} (\Delta_i - \Delta^-)^2}.$$

<div align="right">(Eq. 8.18)</div>

For the newly derived formulation, the standard deviation is equal to 0.416N/mm^2 which is considered quite large with respect to the found bond values during testing. The average calculated strength is 98.92% of the measured average for all 61 specimens. The standard deviation on the other hand, is regarded large. This was to be expected considering the huge scatter which is found in Chapter 6. The relative deviation (called the variance) is denoted as

$$V_\delta = \sqrt{\exp(s_\Delta^2) - 1}$$

<div align="right">(Eq. 8.19)</div>

and is equal to 0.435N/mm^2. By making a validation for the parameters used in the resistance function, a variance coefficient can be obtained. It is chosen that geometry parameters, like the thickness, diameter and length are obtained with a precision of 1%, the modulus of elasticity (MOE) of the concrete 20% and the MOE of the steel of 7%. With these values approximated, the following holds

$$V_r^2 = (V_\delta^2 + 1)\left[\prod_{i=1}^{n}(v_{Xi}^2 + 1)\right] - 1$$

<div align="right">(Eq. 8.20)</div>

$$V_{rt}^2 = \sum_{i=1}^{j} V_{Xi}^2.$$

<div align="right">(Eq. 8.21)</div>

This function for V_r^2 is the variance function including the product function. The final formulation for the characteristic resistance model (r_k) is formulated in (Eq. 8.22). This formulation is used since the number of test specimens is less than 100. Statistical uncertainties are incorporated in this manner. The factor k_n is chosen according to ECS (2011a) and is equal to 1.64.

$$r_k = b g_{rt}(X) \cdot \exp(-k_\infty \alpha_{rt} Q_{rt} - k_n \alpha_\delta Q_\delta - 0.5Q^2)$$

<div align="right">(Eq. 8.22)</div>

In which:

$$Q_{rt} = \sqrt{ln(V_{rt}^2 + 1)} = 0.058 \qquad \text{(Eq. 8.23)}$$

$$Q_{\delta} = \sqrt{ln(V_{\delta}^2 + 1)} = 0.417 \qquad \text{(Eq. 8.24)}$$

$$Q = \sqrt{ln(V_r^2 + 1)} = 0.421 \qquad \text{(Eq. 8.25)}$$

$$\alpha_{rt} = \frac{Q_{rt}}{Q} = 0.139 \qquad \text{(Eq. 8.26)}$$

$$\alpha_{\delta} = \frac{Q_{\delta}}{Q} = 0.990 \qquad \text{(Eq. 8.27)}$$

With k_{∞} equal to 1.64, the factor to calibrate the derived formulation to the test results is equal to 0.40. The resistance function therefore changes to

$$f_{b,push-out} = 0.40 \cdot \frac{-E_s t_p \left(20\varepsilon_{shrinkage} R_c - 1\right)}{R_c \left(3L + 32mt_p\right) - 4Lmt_p + 80R_p^2}. \qquad \text{(Eq. 8.28)}$$

8.3.4 Comparison with correction factor

The effect of this correction factor can be seen in the r_e-r_t graph. When the graph of Figure 8.10 is redrawn including the correction factor, Figure 8.11 is obtained. All data points are now above the orange line which indicates that the calculated numbers are below the measured values. The average calculated bond (including correction factor) for the 61 specimens is 0.67N/mm^2.
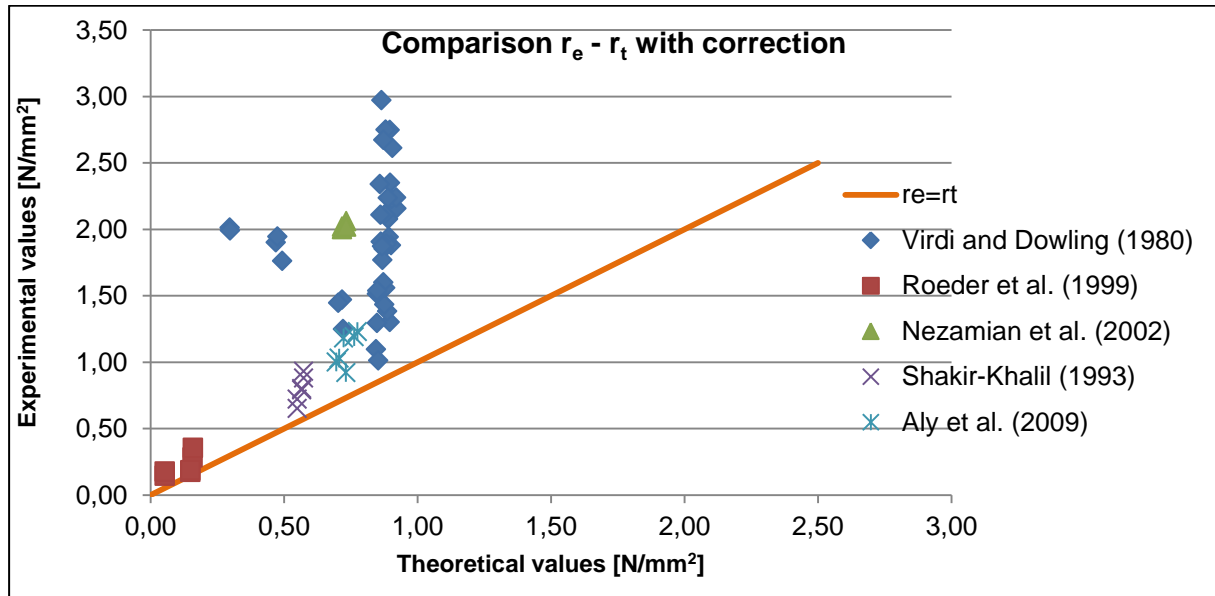
Figure 8.11: Comparison between the experimental and theoretical values with the correction factor.

8.4 Comparison with other expressions

To put the obtained numbers from the previous section into perspective, the same analysis is performed using the bond formulation of Roeder et al. (1999)

$$f_b = 2.109 - 0.026\left(D_p/t_p\right). \qquad \text{(Eq. 8.29)}$$

The expression is obtained with a regression analysis based on experimental data, partly similar to the data used in this report. The bond expression is derived in order that only 2.5% of the measurements exceed the predicted strength.

The sample standard deviation for the formulation from (Eq. 8.29) is 0.46N/mm^2 which is 18.5% larger in comparison to the standard deviation of the derived formula. The final correction factor is 0.46, which is 15% higher than before. This is attributed to the conservative nature of the regression analysis. The factor b (Eq. 8.14) is relative large to which the correction factor is relative high regarding the large standard deviation. When the correction factor of 0.46 is applied and verified against the test data, an average of 0.64N/mm^2 is found. This is 5% lower in comparison to the new formula. A remarkable detail is that of all data, the own test results by Roeder et al. (1999) are approximated the worst. Even with the applied correction factor, the measured data is still lower than the calculated ones.

The results of this analysis for all design expressions (without design factors) are given in Table 8.1. The expressions are used in combination with the proposed stiffness factor by Nezamian et al. (2003). (Eq. 7.39) has also been tried as stiffness factor but performed much worse. The derived formula (DF) has the lowest standard deviation (SD) and when applying the correction factor, it has the largest average for all 61 specimens within a safe margin. This implies that the most accurate and the highest bond stresses are obtained for the derived formulation within a safe margin. The most right column indicates the percentage of the average in relation to the derived formulation. The API, the British Standard (BS) and the Eurocode (EC) which prescribe constant bond values, all result in similar results. The average to be used according to these standards is 0.38N/mm^2. Based on the selection of test specimens used in this report, the British Standard seems to use the most appropriate value of 0.4N/mm^2. The Eurocode value of 0.55N/mm^2 is, based on this analysis, regarded not safe. This value will hold for small diameter pipe piles. It must be noted that when more test data on large pile is available, the average of all three codes will drop drastically.

Table 8.1: Comparison of all design expressions.

Formulation	SD [N/mm^2]	Correction factor	Average [N/mm^2]	Percentage of av. [%]
DF	0.42	0.40	0.67	100%
Roeder (1999)	0.46	0.46	0.64	95%
Norsok (2012)	0.47	0.16	0.61	91%
EC (2011)	0.72	0.69	0.38	57%
BS (1999)	0.73	0.95	0.38	57%
API (2003)	0.75	1.53	0.38	57%
OT (2002)	0.78	0.05	0.29	43%

8.4.1 Design factors

The design factors (including safety factors, material factors etc.) of each expression can be verified with the correction factor. The American Petroleum Institute (API) seems to be too conservative to which the factor is well above one. The correction factors in the OT and Norsok standard are much lower in relation to the design factors. The statement by Nezamian (2003) that these pile-sleeve expressions should be used for the plug connection is doubtful since the expression by Roeder et al. (1999) and the newly derived formulations perform better.

8.4.2 Comparison of the different shrinkage models

A comparison is made to review the difference between the introduced shrinkage models. The Eurocode model, the Kelvin model and the formulation introduced in (Eq. 8.13) are compared in Table 8.2. Noticeable is the average value found using the Kelvin model, which is considerably larger than the other two. The correction factor, which is relative high, is originated from the average of the predictions at first glance. Without correction factor, the average is estimated with 119.62% for the Kelvin model. This results in a large b factor as defined in (Eq. 8.14) of 1.32. However, as pointed out before, the Kelvin model depends on the compressive strength of the concrete via the three empirical parameters α, κ and β. The values found in section 8.2.1 are adopted for this analysis which is not

completely correct. For every mix, these parameters should be determined individually via experimental results.

Table 8.2: Comparison of shrinkage models.

Model	SD [N/mm^2]	Correction factor	Average [N/mm^2]	Percentage of av. [%]
(Eq. 8.13)	0.42	0.40	0.67	100%
Eurocode	0.42	0.40	0.67	100%
Kelvin	0.43	0.60	0.80	120%

8.5   Conclusion

The derived formulation has been verified against 61 selected test specimens. At first, an influence study is performed to check if the same behaviour is found as in Chapter 6. The trends and conclusions are in very close agreement to the findings from the new derived model. With a reformulation of the Eurocode shrinkage model, the new formula performs better than all other currently available formulations. The largest average is obtained for the 61 specimens with the smallest standard deviation. This shows that the new formulation in combination with the adopted shrinkage model is the most accurate model in comparison to the current expressions. Generally speaking, the pile-sleeve expressions do not give very satisfying results and therefore it is not recommended to use these for the plug connection. Using a constant bond value such as the EC, BS and API, gives mixed results. These constant values are conservative for small diameters, but unsafe when large diameters are used.

Based on this analysis, it is strongly advised to use the newly derived formulation in design.

Design:
Furthermore, it is advised to use low shrinkage or even expanding concrete for the plug connections without shear keys. In the latter case, the shrinkage can be taken negative which will enhance the bond capacity. Whenever possible, the wall thickness should be chosen large whilst the diameter should be as small as possible. Furthermore, it is important that the concrete is forced into the surface irregularities of the steel pile, which can be achieved with sufficient vibrating. In this way, the largest bond capacity can be achieved when a new structure is designed.

Chapter 9

Axial Capacity With Shear Keys

The axial capacity without shear keys is examined in more detail in previous chapters and a new model is proposed. The second method of transferring the loads is via shear keys. The analytical model will be expanded to allow for shear keys. Some assumptions need to be made due to the lack of data concerning plug connections with shear keys.

9.1 Ratio between bond and shear keys

First of all, the usefulness of shear keys is demonstrated with an example from Chapter 6 (section 6.5.4). When shear keys are adopted for the same example (Figure 9.1), the ratio between bond and shear keys can be found.

Rectangular shear keys are welded onto the inside of the pile. To maximise the capacity of this example, the maximum h/s ratio is used for each design expression. This means 0.04 for the OT and 0.10 for the API, DNV and Norsok standard. The pile diameter is again 1016mm with a wall thickness of 16mm. The used concrete has a compressive strength of 35N/mm^2.
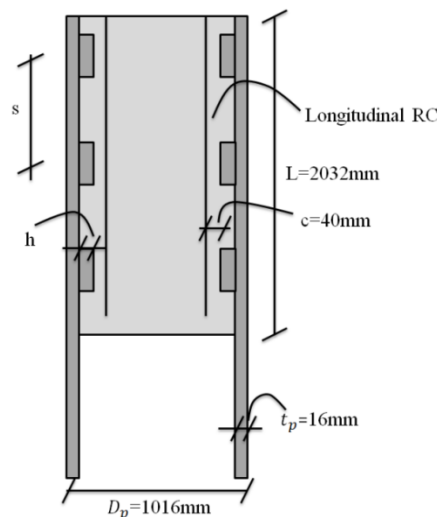
Figure 9.1: Fictitious example with shear keys.

The results from this comparison are given in Figure 9.2. The Norsok code results in the largest design value (green bars) for the combined case of shear keys and bond. The OT gives the lowest value due to the large design factor which is used. On the other hand, solely bond (without factor) is predicted the highest. The DNV prescribes no axial capacity for bond, only for shear keys. The part which is associated with bond and the part associated with the shear keys are depicted in Figure 9.3. The part by bond is apparently in between 7 to 17% of the total capacity for this example. The shear keys account for 80-95% of the total axial strength. Just like for the case with bond, a comparison study to determine the influences is conducted in Appendix G.
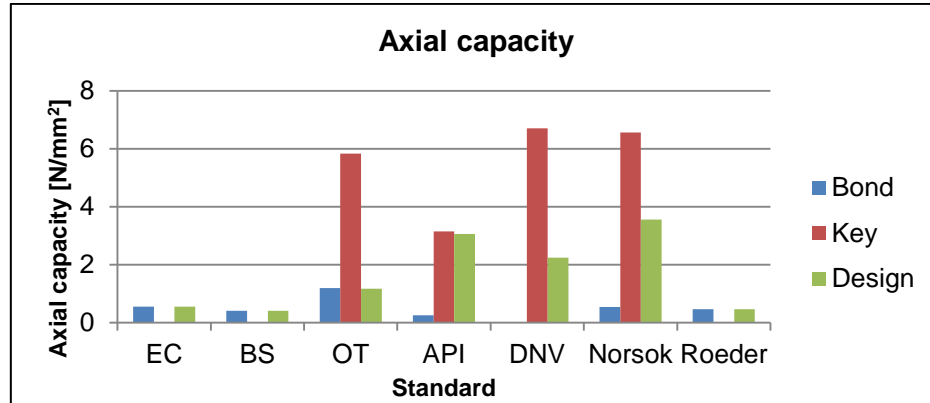
Figure 9.2: Results for the axial capacity according to the various codes.
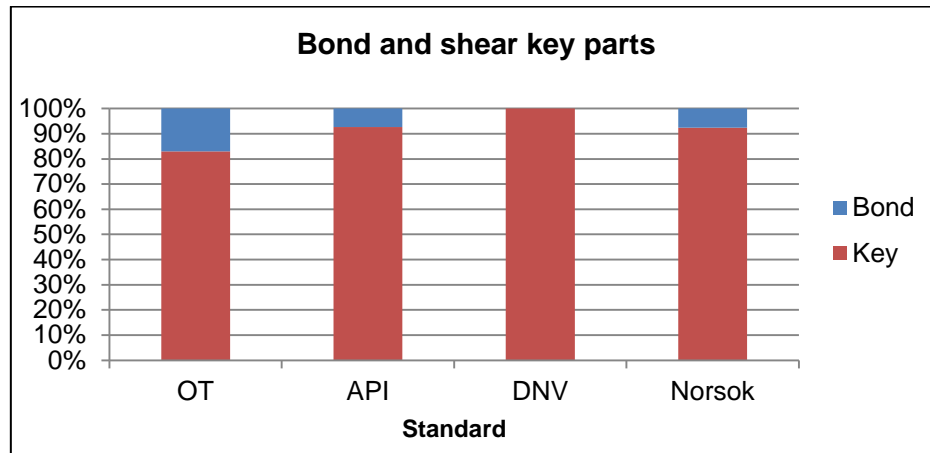
Figure 9.3: Bond- and shear key parts of the total capacity of the four pile-sleeve models.

9.2 Shear key capacity

All four expressions adopt the factor h/s to indicate the shear key axial strength. This ratio (the shear key height to the spacing ratio) indicates an area which is used to define the axial capacity. To clarify the previous, the principle is drawn in Figure 9.4. The area of the shear keys is averaged over the total interface length.
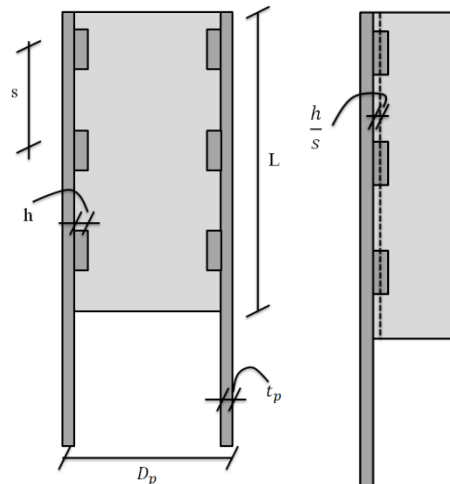
Figure 9.4: Average shear key axial strength according to the design codes.

The failure mechanism which is adopted in the expressions is crushing of the concrete either above or below the shear keys (depending on the loading). This mechanism is displayed in Figure 9.5 which is proposed by Krahl et al. (1985). To be on the safe side, the shear key capacity is related to the concrete compressive strength rather than the crushing strength as follows

$$f_{sk} = \frac{h}{s} f_{ck}.$$
(Eq. 9.1)
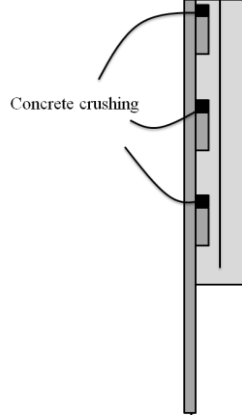
Figure 9.5: Concrete crushing above the shear keys in push-out (Krahl et al. (1985)).

This formulation assumes that the keys are positioned at a constant spacing s, otherwise the h/s ratio cannot be used. Secondly, the shear keys do not fail prior to the concrete crushing failure mechanism and the concrete/grout has sufficient shear capacity. This means that the shear capacity must be proportionate and weld sizes adequate. Two expressions for this shear strength of the grout (τ_{kg}) in the pile-sleeve models are given by DNV and Norsok

$$\tau_{kg,DNV} = \kappa f_{ck}^{0.7}\left(1 - e^{-2L/R_p}\right)$$
(Eq. 9.2)

$$\tau_{kg,Norsok} = \left[0.75 - 1.4\frac{h}{s}\right] f_{ck}^{0.5}.$$
(Eq. 9.3)

In which κ is an early age reduction factor. Since there is a lack of experimental data of the plug connection in combination with shear keys, the failure mechanism is <u>unknown</u>. This is an important limitation of the research concerning this connection. Only two issues are examined, namely the seismic usage (without testing the actual bending moment capacity) and the bond stress. From now on, the failure mechanism displayed in Figure 9.5 is assumed. This could be verified by means of testing of finite element modelling.

9.3 Expanding the analytical model with shear keys

The reasoning of the derived bond model from Chapter 7 can be used to derive an axial strength model including shear keys. The bond capacity of the connection is defined as (Eq. 7.7)

$$f_b = a + \mu \cdot \sigma_n.$$
(Eq. 9.4)

Since the situation has changed, the capacity increases with a shear key component. The shear key capacity is related to the h/s ratio and the concrete compressive strength as seen in the beginning of this chapter. However, the derived model from Chapter 7 makes use of an interface gap between the steel and the concrete. This gap is a result of concrete shrinkage and differences in radial displacement from the tube and the plug. The contact length of the shear keys is lowered by this gap (Δ) (Figure 9.6). This results in the following

$$f_{sk} = \frac{h - \Delta}{s} f_{ck}.$$
(Eq. 9.5)
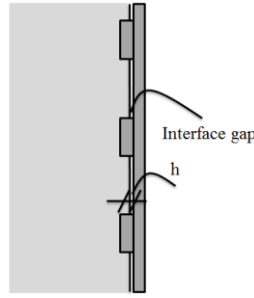
Figure 9.6: Shear keys with interface gap.

As seen with some pile-sleeve expressions, both contributions (bond and shear keys) are added to form the axial capacity. DNV changed this in the 2013 standard (in the 2010 edition, both capacities are added as well). When the same idea is implemented in the model, the interface strength (f_{axial}) is equal to

$$f_{axial} = a + \mu \cdot \sigma_n + \frac{h - \Delta}{s} f_{ck}. \tag{Eq. 9.6}$$

Naturally, the question arises whether this assumption is correct or not. This assumption will be checked in a later stage.

9.3.1 Stresses and strains

The same stress and strain analysis, as in Chapter 7, can be performed with the new defined axial strength definition (Eq. 9.6). Since bond is still present (assumption), the radial pressure on the steel tube is still defined as (Eq. 7.6) to which the circumferential stress in the tube is defined the same as before, see (Eq. 7.9). The ultimate axial capacity (Eq. 7.10) for the connection is redefined to

$$P_u = -f_{axial} \cdot 2\pi \cdot R_c \cdot L. \tag{Eq. 9.7}$$

The bond capacity (f_b) has now been changed for the axial capacity (f_{axial}). Since the shear key strength is averaged along the interface length, it can still be multiplied with the inner perimeter of the tube. Hence the same reasoning behind the stresses and strains is used as before. The results are given in Table 9.1.

9.3.2 Difference in radial displacement

The difference in radial displacement (Δ) is defined as the difference between the steel radial displacement (Δ_s) and the concrete radial displacement (Δ_c). Using the definition of (Eq. 7.2), the axial strength formulation is again solved with computer software Maple. This results in the following formulation

$$\Delta = \frac{1}{2}\left(\frac{-2v_c E_s KR_c t_p \mu_s + Lv_s E_c f_{axial} R_c - 2Lv_c E_s f_{axial} t_p + 2E_s E_c \varepsilon_{shrinkage} R_c t_p + 2E_c KR_p^2 \mu_s + 2E_s KR_c t_p \mu_s}{-v_c E_s KR_c t_p + E_c KR_p^2 + E_s KR_c t_p + E_c E_s t_p}\right). \tag{Eq. 9.8}$$

9.3.3 Stiffness factor

The same stiffness factor is used as for the pile (without shear keys) as defined in (Eq. 7.39). The welded shear keys will slightly enhance the radial stiffness. When the shear keys are averaged over the interface length, the thickness of the pile increases with h/s. The stiffness factor would change to

$$K = \frac{E_s\left(t_p + \dfrac{h}{s}\right)}{R_p^2}. \tag{Eq. 9.9}$$

Shear keys are used when the diameter is around 900mm. Pile wall thicknesses for this diameter are around 14.2mm (RUUKKI (2014)). Since h/s ratios are in the range of 0.01-0.1 according to the limitations of the pile-sleeve expressions, it can be stated that $t_p \gg h/s$. The increase in stiffness would be less than 1%. Therefore, this enhancement is neglected.

Table 9.1: Stresses and strains for both the steel and the concrete including shear keys.

Stresses & strains	Expressions
Steel stresses	
$\sigma_{s,\theta}$	$$\sigma_{s,\theta} = \sigma_{s,n}\frac{R_p}{t_p}$$
$\sigma_{s,z}$	$$\sigma_{s,z} = -\frac{1}{2}\frac{f_{axial}R_cL}{R_pt_p}$$
$\sigma_{s,n,internal}$	$\sigma_{s,n,internal} = 0$
Concrete Stresses	
$\sigma_{c,\theta}$	$\sigma_{c,\theta} = -K(\mu_s - \Delta)$
$\sigma_{c,z}$	$$\sigma_{c,z} = -\frac{f_{axial}L}{R_c}.$$
$\sigma_{c,n}$	$\sigma_{c,\theta} = -K(\mu_s - \Delta)$
Steel strain	
$\varepsilon_{s,\theta}$	$$\varepsilon_{s,\theta} = \frac{\dfrac{K(\mu_s - \Delta)R_p}{t_p} + \dfrac{1}{2}\dfrac{v_sf_{axial}R_cL}{R_pt_p}}{E_s}$$
Concrete strain	
$\varepsilon_{c,n}$	$$\varepsilon_{c,n} = \frac{-K(\mu_s - \Delta) - v_c\left(\dfrac{-f_{axial}L}{R_c} - K(\mu_s - \Delta)\right)}{E_c} - \varepsilon_{shrinkage}$$

9.3.4 Axial capacity

All parameter of the capacity are known and the equation can be solved. By substituting (Eq. 9.8) into (Eq. 9.6) and by adopting the following characteristics

- Coulomb friction μ=0.5,
- Steel roughness μs=0.05,
- vs=0.3,
- vc=0.2.

The equations can be solved with the use of computer software. This results in

$$f_{axial} = -\frac{\varepsilon_{shrinkage}(2RE_sst_p + 4R_cf_{ck}) + f_{ck}(-8h - 3.2mhRt_p + 0.16mR + 0.2) - \dfrac{E_sst_p}{10R_p^2}}{L\left(0.3Rs - \dfrac{0.4mst_p}{R_p^2} - \dfrac{0.8f_{ck}mt_p + 0.6R_cf_{ck}}{E_cmt_p}\right) + s(9 + 3.2mRt_p)}$$ (Eq. 9.10)

in which εshrinkage is equal to the proposed model in (Eq. 8.13).

9.3.5 Assumptions

The following assumptions have been made during the derivation of (Eq. 9.10)

- The failure mechanism is assumed to be concrete crushing around the shear keys. The shear keys are supposed not to fail prior to crushing of the concrete. This is one of the assumptions which cannot be verified by test data at the moment. Testing is required for this verification.
- The same stiffness factor is used as for the plain pile case (bond formulation).
- The friction between the concrete and the shear keys is neglected in the derivation of the gap.
- The shear keys do not exert a horizontal force on the pile wall. This means that there is no radial component of the shear keys. This is related to the shear key shape. When weld beads are used as in Figure 5.6 a, there is a horizontal component which should be taken into account. The configuration of Figure 5.6 b is adopted in this analysis.

- The axial capacity is an addition of the bond- and shear key capacities. Indirectly, this means that the same load-slip curve is valid for the bond- and shear key capacity. This assumption is questionable and will therefore be inspected.

9.3.6 Verification assumption

For the verification of the last assumption, an example is used as guidance. Since the bond lowers dramatically with large diameters, the smallest D_p in which shear keys are available is adopted in this example. Bond is directly related to the interface gap $(\Delta_s-\Delta_c)$; the gap will be less with small diameters. Hence in this example, a pile with diameter of 914mm and wall thickness 20mm is assumed (RUUKKI (2014)). The maximum wall thickness is chosen in order to achieve the largest pile stiffness. This equals the largest bond capacity (as seen in (Eq. 7.7)) and therefore the smallest gap.

To limit the gap size, a normal strength concrete is chosen with an $f_{ck} = 35\text{N/mm}^2$ and the assumption is made that the shear capacity of the concrete is sufficient (Figure 9.7). Not all shear keys are drawn in the figure for illustrative reasons. With respect to the limitations of the pile-sleeve expressions, the h/s ratio is chosen at 0.1 with h=25mm and s=250mm. The concrete age is 120 days after which shrinkage stops (as seen in section 8.2).
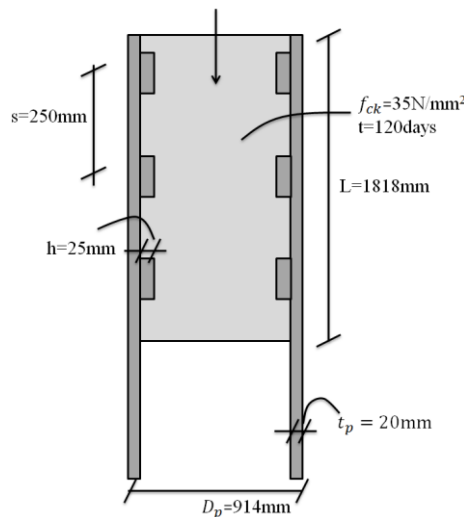
Figure 9.7: Dimensions of the example.

Substituting all parameters in the equation for the difference in radial displacement (Eq. 9.8) results in a gap of 0.065mm. This value exceeds the roughness of the steel surface which is 0.05mm.

This example is chosen to give a low value for the interface gap. Therefore, increasing the pile diameter, lowering the stiffness, increasing f_{ck} or increasing the plug length all result in lowering of the bond stress. So according to this model, the bond and the shear key capacity <u>cannot be summed</u> to form the axial capacity.

9.4 Reformulating shear key expression

With this finding, the axial capacity (Eq. 9.6) is reformulated to

$$f_{axial} = \frac{h - \Delta}{s} f_{ck}.$$

(Eq. 9.11)

The difference in radial displacement, like in (Eq. 9.8), does not change. Only now, the new definition of f_{axial} is used as in (Eq. 9.11). Substituting the expression for Δ into the expression for f_{axial} and solving it with Maple gives

$$f_{axial} = -\frac{1 + 20\varepsilon_{shrinkage}R_c - h(40 + 16mRt_p) + 0.8mRt_p}{\left(L\left(\frac{3R_c}{mt_pE_c} - \frac{4}{E_c}\right) + \frac{16mRst_p + 40s}{f_{ck}}\right)}. \qquad \text{(Eq. 9.12)}$$

In which m and R are defined as

$$m = \frac{E_s}{E_c} \qquad \text{(Eq. 9.13)}$$

$$R = \frac{R_c}{R_p^2}. \qquad \text{(Eq. 9.14)}$$

Because the part by bond is neglected, the axial capacity as defined in (Eq. 9.12) is the same for both the push-out and pull-out case. The height over the spacing ratio of the shear keys cannot be chosen completely free. When the spacing s is minimized, the shear keys would practically be touching each other. In the most extreme case, the capacity would rely solely on bond again. For this reason, the limitation (h/s≤0.10) adopted by DNV, Norsok and API is respected for (Eq. 9.12).

9.5 Verification

Unfortunately, the shear key model cannot be verified, likewise the bond expression. Since the same reasoning is used as in Chapter 7, no large disorders are to be expected. Expectations are that when sufficient data is available, the scatter would be a lot smaller in comparison to the bond capacity test data. The influence of for instance shrinkage will be a lot less.

For the example of section 9.1, the calculated capacity is equal to 3.49N/mm², which is only slightly lower than the design value of 3.55N/mm² for the Norsok standard (Figure 9.2, green bar). The most important influences on the axial capacity are the concrete compressive strength and the h/s ratio.

9.6 Consideration shear keys or bond

Both axial load transfer methods are modelled specifically for the plug connection. Now the question arises whether shear keys should be used when possible (D_p≥900mm). A consideration can be made regarding the aspects which are found during this research.

- The bond capacity shows a large scatter in experimental testing. There are significant differences in outcome between researches and a number of parameters seem to drastically influence the capacity. The unpredictable character is demonstrated in section 8.3.1 where a correction factor for each expression is obtained (only 0.40 for the derived formulation). For the shear keys, this scatter is expected to be considerably less based on experimental data of the pile-sleeve systems. This should however be verified with testing.
- The axial capacity without shear keys is naturally a lot less than when shear keys are used. The ratios for the part by bond and the part by shear key are given at the beginning of this chapter for the pile-sleeve equations. When the capacity is calculated with (Eq. 7.42) for the situation <u>without shear keys,</u> the capacity is 0.08N/mm² against 3.49N/mm² for the situation <u>with shear keys</u> (Eq. 9.12).
- Bond is considerably lowered when cyclic loading is an issue. This effect is seen in the pile-sleeve connections as in the case of the monopiles. Shear keys must always be used to carry the axial load in these monopile connections. As seen in section 6.2.8, the capacity is reduced with almost 30% after just 40 cycles for the plug connections. Shear keys improve on the reliability of the connection according to the OT.
- It is of course possible to increase the plug length to make the axial capacity equal to the one with shear keys. However, this means increasing the plug length and using more material which will increase the cost.

The last bullet implies that a cost comparison should be made for the situation with and without shear keys. For this analysis (Figure 9.8), the same pile as in the example of section 9.3.6 is used. For the cost analysis, it is assumed that this connection is made at a location with relative high wages (west European wages). The distance to suppliers is considered reasonable and all required labour and materials are present within reasonable distances.

The smallest possible diameter of 914mm is adopted with a large wall thickness of 20mm (RUUKKI (2014)). These values are chosen because the bond capacity will be the highest for this situation since it drops dramatically with increasing diameters. The used plug length is equal to the minimal length of 1200mm. With the limitations in mind, the shear key height is 25mm and the width (w) equal to 40mm. The latter is chosen according to the API limitation. In total two shear keys are used which result in an h/s ratio of 0.06. The used concrete is C35/45 at an age of 120 days.

For this example, an axial force (P) of 3000kN is assumed, which needs to be transferred from the plug to the pile. For the plain plug connection (without shear keys), the interface length can be determined with the given axial force. The bond multiplied with the area, should equal the exerted axial force

$$f_b \cdot 2\pi R_c L = P. \tag{Eq. 9.15}$$

Substituting the expression for f_b (Eq. 7.45) and solving (Eq. 9.15) with respect to L gives

$$L = \frac{16P(5E_c R_p^2 + 2E_s R_c t_p}{40\pi E_c E_s \varepsilon_{shrinkage} R_c^2 t_p - 2\pi E_c E_s R_c t_p + 3PE_c R_c - 4PE_s t_p}. \tag{Eq. 9.16}$$

Substituting all parameters gives the required plug length, which is equal to 6050mm.
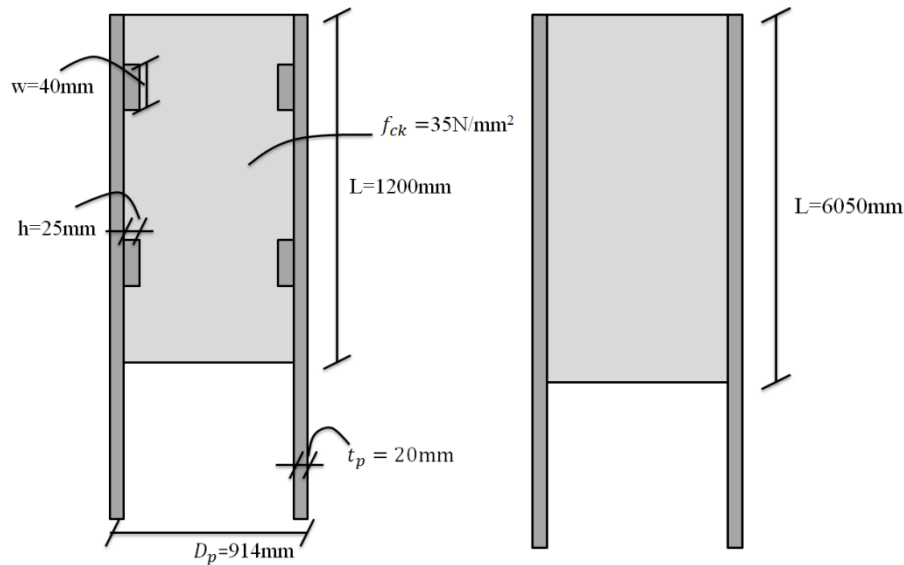
Figure 9.8: Example with the given dimensions, on the left the option with shear keys and on the right the option without shear keys.

9.6.1 Costs comparison

The main differences in costs between the two options arise due to two reasons:
- Welding of the shear keys and the required steel,
- The amount of concrete which is used with the associated reinforcement and transportation costs.

Assumptions for this comparison are
- Formwork for casting the plug for both cases is equally expensive,
- 20 plugs a day can be casted for the one with shear keys and 15 plugs for the plain connection,
- 200kg reinforcement is used per m^3 concrete.
- Labour costs €35/hr except for welders, which cost €50/hr.
- Concrete costs €150/m^3 (including additional pumping charges of €10/m^3) and steel €1500/m^3.
- Transportation is done with a pontoon propelled by a tug boat.

With the given assumptions, the costs per plug connection are estimated in Appendix H. When the costs for the plug with shear keys are set to 100%, the costs for the plug without (plain connection) are approximately 104% for the axial load of 3000kN. With an axial load of 2500kN, the plain plug is only 91% of the costs of the one with shear keys, since the plug length is less.

Like seen in section 4.4.4, the costs are closely related to the situation at hand. Distance to suppliers, availability of certified welders, available equipment, labour costs etc. are aspects which should be taken into account. <u>A statement regarding which solution to adopt in general based on the costs, cannot be made</u>. A cost comparison should be made for every project to determine the most favourable option of the two. Furthermore, it is noted that the costs which are presented are only the direct material and labour costs. The profit margin, costs for potential risks, and general company costs are not included.

Since the difference in costs is rather limited, it is advised to use shear keys whenever possible. The problem of deterioration of the bond capacity due to cyclic loading is excluded from happening in this manner. The long term behaviour of the connection will be secured.

9.7   Conclusion

In this chapter, a new equation is proposed for the plug connection with shear keys. Due to the lack of test data, this formulation cannot be verified in the same way as with the bond model. When sufficient data is present, the formulation will most probably give satisfactory results because the same reasoning is used as with bond. One of the most important conclusions is that the bond and shear key part cannot be summed according to the used methodology. The gap exceeds the surface roughness and therefore the bond is broken.

A cost analysis should be made for each project to determine the cheapest solution. Shear keys are advantageous over bond when cyclic loading is considered. Since the difference in costs between the two options is rather limited, it is advised to use shear keys when possible to exclude the cyclic loading effect.

Design:
For the design of the plug with shear keys, it is advised to use an adequate dimensioned reinforcement net to provide the required shear capacity for the plug itself. The concrete compressive strength has a large influence on the shear key capacity, so usage of high strength concrete is advised. Furthermore, the keys should be placed with a constant distance and with an appropriate spacing. The maximum h/s ratio of 0.10 is therefore respected.

Bending Moment Capacity

New formulations have been proposed for the axial capacity of the plain plug connection (without shear keys) and the plug connection with shear keys. Bending moments are almost always present in combination with these axial forces. The moments are induced by e.g. horizontal traffic forces in case of a bridge construction. In this chapter, considerations will be given regarding the pile-sleeve connections.

10.1 Contributions

Three contributions can be distinguished for the bending moment capacity of the plug connection (Lotsberg et al. (2012)). These include horizontal contact pressure due to wrenching of the plug within the pile (blue arrows), vertical friction forces due to this horizontal pressure (red arrows) and the axial capacity part (black arrows). These three contributions combined (Figure 10.1), give the bending moment capacity of the connection.
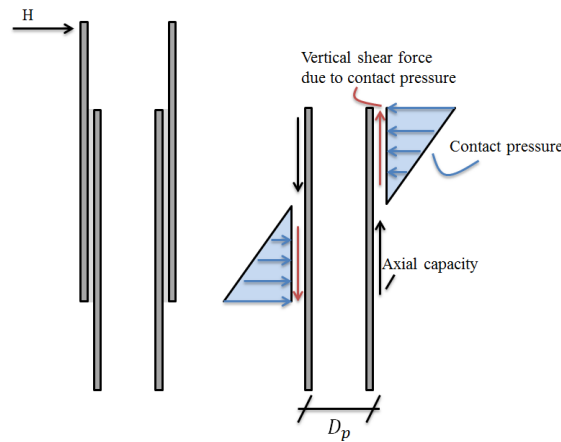
Figure 10.1: Bending moment contributions according to Lotsberg et al. (2012).

10.1.1 Shear key component

The shear keys provide resistance in the longitudinal direction of the plug. When a bending moment is exerted on the plug, the keys will form resistance by developing a force couple. The maximum stress (f_{key}) on the shear keys can be calculated with the derived formulation for the axial capacity. By multiplying the axial strength with the interface length and dividing by the number of shear keys (N), the strength per key is obtained

$$f_{key} = f_{axial} \cdot L/N. \qquad \text{(Eq. 10.1)}$$

The bending moment capacity per shear key can be obtained with a model (Figure 10.2) proposed by Lotsberg et al. (2012). The stress distribution in the radial direction is showed in the lower part of this figure. At the ends (furthest from the centre line), the stress equals the maximum stress which can be carried by the shear keys. Along the interface, this force lowers to zero in the centre line. The integral

to which the bending moment capacity per shear key is obtained can be composed by (based on Figure 10.2)

$$M_{Shear\ key} = 4 \int_0^{\pi/2} R_c \sin \varphi \cdot R_c d\varphi \cdot f_{key} \sin \varphi. \qquad \text{(Eq. 10.2)}$$

Solving (Eq. 10.2) and multiplying with the number of adopted shear keys (N), gives the capacity for all the shear keys

$$M_{SK} = \pi R_c^2 f_{key} N. \qquad \text{(Eq. 10.3)}$$
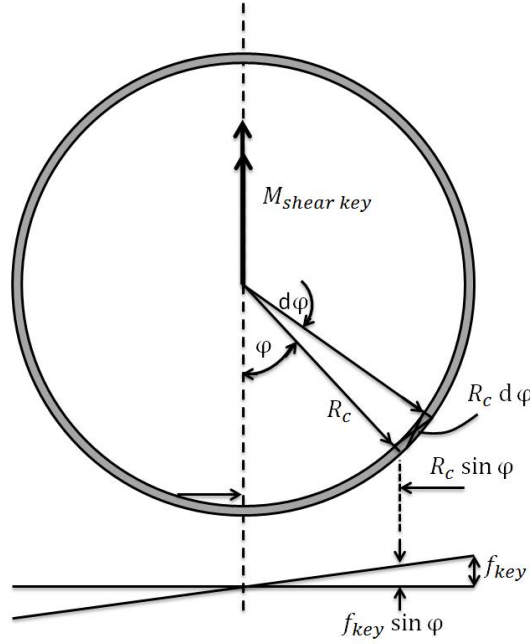
Figure 10.2: Analysis model for the shear key bending moment capacity (Lotsberg et al. (2012)).

10.1.2 Wrenching component

When a bending moment is exerted on the connection, the plug will tend to move a little within the pile. This so-called wrenching causes horizontal pressures between the pile and the plug. The contact stress distribution of Figure 10.3 is assumed, where the maximum is found at the top and the bottom of the plug. This distribution has also been used in the analysis for the monopile foundation (Lotsberg et al. (2012)). It should be added that the movement of the plug is restricted by the capping beam. A section of the plug is cast together with a part of the capping beam. This part of the connection should have sufficient ductility.
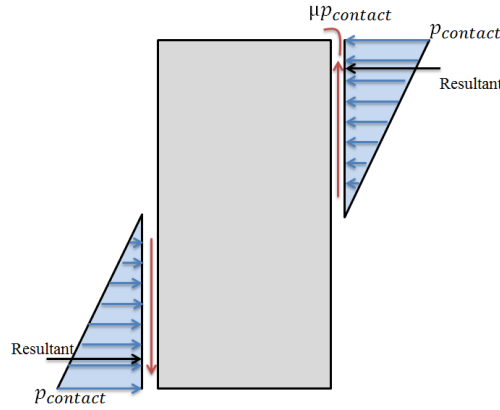
Figure 10.3: Horizontal pressures on the plug and the associated friction (Lotsberg et al. (2012)).

The top view of the stress distribution for this effect is shown in Figure 10.4. The compressive stress will be greatest in the middle of the cross-section and zero at the sides. The maximum pressure in the middle is denoted as the nominal pressure (p_{nom}) by Lotsberg et al. (2012). This pressure should be limited in order to avoid cracking of the concrete due to repetitive loading. One effect that is not considered is the ovalisation of the pile due to wrenching. This would increase the compressive stress at the sides. This stress distribution is depicted in Figure 10.5.
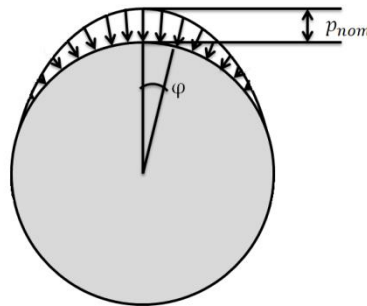
Figure 10.4: Stress induced by wrenching, top view of the plug (CIE5305 (2014)).
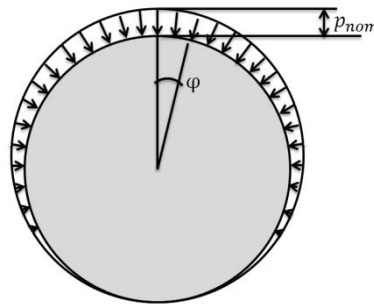
Figure 10.5: Stress distribution when ovalisation is included, top view.

The stress distribution of Figure 10.4 can be approximated with either a cosine or sine function. When a cosine function is adopted, the following integral is found ((CIE5305 (2014)).

$$p_{contact} = 2 \int_0^{\frac{\pi}{2}} p_{nom} (\cos \varphi)^2 R_c d\varphi. \qquad \text{(Eq. 10.4)}$$

The contact pressure at the top and bottom of the plug is obtained by integrating (Eq. 10.4). This results in

$$p_{contact} = \frac{1}{2}\pi p_{nom} R_c. \tag{Eq. 10.5}$$

The bending moment capacity (see Figure 10.3) due to the wrenching of the plug is then equal to

$$M_{wr} = \frac{\frac{1}{2}\pi p_{nom} R_c * \frac{1}{2}L}{2} \cdot \frac{2}{3}L = \frac{1}{12}\pi p_{nom} R_c L^2. \tag{Eq. 10.6}$$

10.1.3 Friction component

Due to the contact pressure, which is exerted between the pile and the plug, a friction force causes an additional component for the bending moment capacity (denoted with the red arrows in Figure 10.3). The integral can be composed in the same manner as in the case of the shear keys based on Figure 10.2. The bending moment capacity of the friction component is equal to

$$M_{\mu,wr} = \frac{1}{4}\pi R_c^2 \mu p_{nom} L. \tag{Eq. 10.7}$$

10.2 Bending moment capacity

The total bending moment capacity is an addition of the three components. The capacity is therefore defined as

$$M_{tot,plug} = M_{SK} + M_{wr} + M_{\mu,wr}. \tag{Eq. 10.8}$$

Substituting (Eq. 10.3), (Eq. 10.6) and (Eq. 10.7) into (Eq. 10.8) results in

$$M_{tot,plug} = \pi R_c^2 f_{key} N + \frac{1}{4}\pi R_c^2 \mu p_{nom} L + \frac{1}{12}\pi p_{nom} R_c L^2. \tag{Eq. 10.9}$$

By looking at all three contributions, the part by shear keys is considered relative small. The wrenching and the associated friction are related to $R_c L^2$ and $R_c^2 L$ respectively whilst the shear key part only to R_c^2. Normal values of the interface length are in the order of $4R_c$, this means a difference of a factor 16. This ratio depends on the geometry at hand. A small plug length in combination with a large pile diameter results in a much higher shear key contribution. This result corresponds with an additional requirement of the Norsok and DNV standard. When a pile-sleeve system is designed for both axial force and bending moment, the following holds

$$\tau_a \leq \frac{f_{axial}}{\gamma_m}. \tag{Eq. 10.10}$$

In which τ_a is defined as the shear stress along the interface exerted by only an axial force and γ_m is a material factor (3 for DNV (2010) and 2 for Norsok). This means that only the axial force is resisted by shear keys and that this component is not used for the bending moment capacity. The main contribution for the bending moment capacity of the pile-sleeve systems is believed to be the horizontal wrenching force (Lotsberg et al. (2012)). The effectiveness of the shear keys is a lot higher in combination with axial force than with bending moments as is found in Chapter 9 and in (Eq. 10.9). Depending on the flexibility of the connection, shear keys which are used for transferring axial loads will also apply part of the applied bending moment. For the bending moment capacity the shear key part may be neglected, however for the design of the shear keys it should be taken into account. When dismissing the shear key contribution, (Eq. 10.9) changes to

$$M_{tot,plug} = \frac{1}{4}\pi R_c^2 \mu p_{nom} L + \frac{1}{12}\pi p_{nom} R_c L^2. \tag{Eq. 10.11}$$

10.3 Assumptions

A number of assumptions have been made during the derivation of (Eq. 10.11):

- The shear keys are not used for the bending moment capacity since the effectiveness is considerably higher for the axial capacity.
- Ovalisation of the pile is not taken into account. When a pressure is exerted as in Figure 10.4, the pile will change shape. The pressure at the sides will not be equal to zero anymore. The capacity is therefore approximated conservative by not considering this change in shape.
- The stress distribution of Figure 10.3 is assumed. This should be verified by testing.
- Not only in longitudinal but also in circumferential direction, a horizontal shear force is present (Figure 10.6). This frictional force is not taken into account.
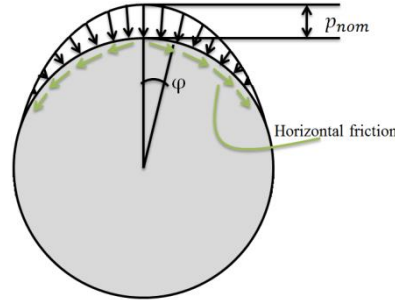
Figure 10.6: Horizontal friction.

10.4 Contact pressure

When there is a bending moment applied to the plug equal to $M_{s,d}$ and (Eq. 10.11) is solved with respect to the contact pressure, the following can be found

$$p_{nom} = \frac{12M_{s,d}}{L\pi R_c(3\mu R_c + L)}.$$ (Eq. 10.12)

According to the DNV, the nominal stress is related to the local stress (p_{local}) at the top and bottom of the concrete. This increased stress is caused by discontinuities at the end of the concrete section. The concrete should be able to resist this local contact pressure taking into account dynamic loading. The stress equals, according to DNV (2013), the pressure multiplied with a stress concentration factor (SCF)

$$p_{local} = SCF \cdot p_{nom}.$$ (Eq. 10.13)

The SCF is defined as

$$SCF = 1 + 0.025 \left(\frac{R_c}{t_p}\right)^{\frac{3}{2}}.$$ (Eq. 10.14)

This SCF is determined for the pile-sleeve systems, so again the usability for the plug connections is questionable. Furthermore the limits, to which (Eq. 10.14) is applicable, are outside the range of the considered topic in this research. The nominal pressure is limited to 1.2N/mm² according to the DNV, unless higher values can be documented for the pile-sleeve connections. This value is adopted to prevent abrasive wear of the contact surfaces.

Abrasive wear is considered less of an issue in case of the plug connection compared to the pile-sleeve systems. The loading in pile-sleeve systems is rather different, since they are mostly loaded by bending moments due to wind with an alternating character. Connections in jacket structures or pile caps are mainly subjected to constant axial loading and constant bending moments (Lotsberg et al. (2012)). Since the fatigue will be less (but can definitely <u>not</u> be neglected), the contact pressure is most likely higher than the 1.2MPa the DNV prescribes. Furthermore, the concrete is enclosed in the

pile. This will enhance the concrete compressive strength due to the confining pressure. This maximum value for the contact pressure should be found by testing or modelling.

10.5 Bending plug

Each cross-section should be able to transfer the bending moment. Therefore, the cross section needs to be checked. This can be done with computer software or by hand, using the plastic stress distribution method (PSDM). Usage of this method (Figure 10.7) is simple to use and gives accurate results according to Lehman et al. (2012). With this method, the required reinforcement can be calculated.

The following definitions are used:

- A_{cc} = area concrete in compression,
- A_{sc} = steel area in compression,
- A_{st} = steel area in tension,
- C_c = compressive force concrete,
- C_s = compressive force steel,
- T_s = tensile force steel,
- P = compressive force.
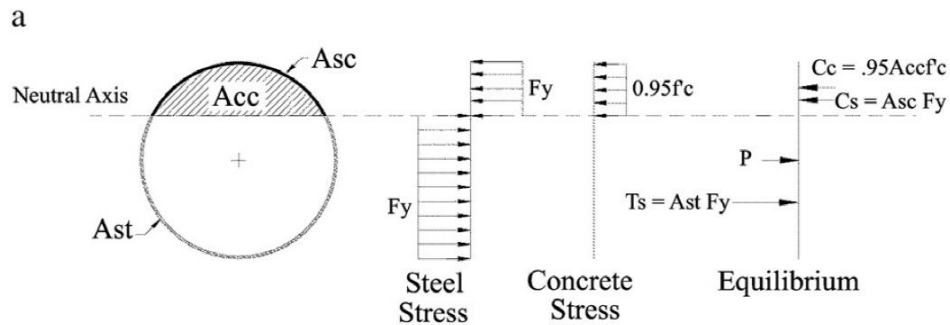
Figure 10.7: PSDM to determine the CFT behaviour.

10.6 Conclusion

The bending moment capacity of the connection has been evaluated in more detail in this part of the report. The capacity contains of two contributions because the shear key part is assumed little depending on the geometry. The main conclusion is that more research is required, especially regarding the maximum contact pressure and the assumed stress distribution (Figure 10.3). This should be verified with testing or finite element modelling. The contact pressure proposed by the DNV is considered very conservative, since the loading regime is different. When this contact pressure is known, also the shear force capacity can be obtained.

Chapter 11

Conclusions & Recommendations

The most important conclusions of this research are drawn in this chapter. The main research question will be answered and recommendations for future research are formulated.

11.1 Conclusions

Various possible solutions for the steel pile to concrete element connection are developed over the years. The embedded alternatives result in capping beam reinforcement problems and large concrete elements due to punching shear. This is associated with constructability issues on site and an increase of the costs due to the very dense reinforcement lay-out. The encased-fixed based detail suffers from the same issues as the embedded connection types. Additionally, a lot of welding is required which need to be performed on site.

Concluding from a trade-off analysis, the plug connection is less expensive, equally fast to make and more durable in relation to the plate connection and the reinforcement welded to steel shell option. The latter solution is dismissed, due to the many steps during production and the amount of required welding on site. Furthermore, the plug connection is adopted in almost 90% of the cases. This latter finding is based on experience and a proposed decision scheme. This decision scheme is subsequently based on a list of possible influences on the connection design.

The plug connection can either be axially loaded in tension (pull-out) or compression (push-out). In pull-out, the plug breaks at the tip of the longitudinal reinforcement bars. The push-out case is purely a bond failure. Two axial transfer methods are possible, namely by bond or by shear keys. The most influential parameters for bond are the geometry of the pile, concrete shrinkage and cyclic loading. The latter gives a reduction up to 30% with only limited cycles.

Bond
Various bond formulations are available today based on pile sleeve-systems, constant values or linear regression. All lack an empirical background. A new formulation is proposed based on the stresses and strains of both the plug and the pile. Bond is defined as micro-friction, the adhesion part is assumed zero. This new formulation coincides well with the found trends from literature. The main disadvantage of the Kelvin shrinkage model is the required testing for each concrete mixture. The shrinkage behaviour within the tubular piles is different than that of exposed concrete. Therefore, it is concluded that a reformulation of the Eurocode shrinkage model is preferred.

This new formulation together with the chosen shrinkage model is verified with 61 test specimens. The standard deviation equals 0.42N/mm^2 which is regarded as large. The main reason is the large scatter in the test data. With the correction factor of 0.40, the average bond for the 61 specimens is equal to 0.67N/mm^2. These numbers are put into perspective by testing the six currently available formulations. All resulted in higher standard deviations and average values which are lower. Therefore, it is concluded that the new formulation predicts best. Low shrinkage or even expanding concrete should be used. Furthermore, it is not recommended to use the pile-sleeve expressions.

Shear keys
The bond and shear key capacities cannot be summed in the new shear key formulation. Furthermore, there is a lack of experimental data of the plug connection in combination with shear keys. The new formulation cannot be verified as is done with the new bond expression. Shear keys should be used whenever possible due to the deterioration effect of cyclic loading on the bond capacity. The difference in costs between the two options is rather limited depending on the specific situation.

The bending moment capacity contains two contributions, namely the wrenching effect and the associated friction. The third possible contribution, shear keys, is only limited when common geometry values are used. The maximum contact pressure is set to a maximum value based on cyclic loading effects in pile-sleeve connections. This effect is expected to be less for the plug connections and therefore this value can most probably be increased.

11.2 Research question

The findings of this research are used to answer the main research question, formulated at the beginning of this report:

What is the best strategy of connecting a steel pipe pile to a concrete element in different near-shore situations dealing with unknown/inconsistent factors and with respect to trade-off aspects such as economy, durability and manufacturability?

The best strategy of connecting the pipe pile to a concrete element is by using the concrete plug connection. This connection type can be used in all kinds of situations, can transfer high loads and is relatively easy to construct. The costs of this connection are rather low and the durability of the connection is good.

The main issues concerning the plug connection are the inconsistent design formulations for the bond capacity and the lack of formulations for the axial capacity. These matters are addressed by formulating new design expressions. The formulation for the bond capacity agrees better with test data than any other currently available formulation. It is therefore highly recommended to use this new equation in design.

Currently, formulations including shear keys are only available for pile-sleeve applications. Therefore, there is a large need for shear key formulations for the plug connection. The analytical model is expanded such that shear keys are adopted in the formulation. It is expected that as with the bond, these values will coincide well with reality. This should however be verified. Finally, an expression for the bending moment capacity is formulated. Before using this for design, certain assumptions need to be checked.

11.3 Recommendations

Based on this research, the following recommendations for future research are formulated:

- This research is focused on the load transfer from the plug to the pile. The top part of the connection, namely the dowels connecting the plug to the concrete element, can be further optimized.
- Reinforcement in the plug can change the failure mode due to wedging effects. It is believed that this effect increases the bond capacity of the connection. This should be determined in more detail.
- The effect of cyclic loading can be determined in more detail.
- The plug connection should be tested in combination with shear keys. The assumed failure mechanism should be checked. Subsequently, the proposed formulation of Chapter 9 can be verified as done with the formulation for bond.
- The maximum contact pressure should be verified with either testing or modelling.
- The assumed stress distribution used to calculate the bending moment capacity should be verified with experiments.

References

AASHTO (2012). '*AASHTO LRFD Bridge, Design Specifications.*' American Association of State Highway and Transportation Officials (AASHTO), 2012, ISBN 978-1-56051-523-4.

Al-Mahaidi, R., Grundy, P. and Bean, W. (1999). '*Pullout Strength of Concrete Plugs in Tubular Piles.*' Proceedings of the Ninth International Offshore and Polar Engineering Conference, Brest France, May 1999, pp. 24-29.

Aly, T., Elchalakani, M., Thayalan, P. and Patnuikuni, I. (2009). '*Incremental Collapse Treshold for Pushout Resistance of Circular Concrete Filled Steel Tubular Columns.*' Journal of Constructional Steel Research 66, Elsevier, 2010, pp. 11-18.

API (2003). '*API Recommended Practice2A-LRFD.*' American Petroleum Institute (API), Chapter 4: Grouted Pile-to-Structure Connections, pp. 79-80.

Arcelor Mittal (2010). '*Spirally Welded Steel Pipes.*' Product Range, 2010.

BN (2015). Ballast Nedam (BN), Personal Communication.

Berg, L.M. (2014). '*CFT Column-to-Cap Beam Connections for Accelerated Bridge Construction in Seismic Regions.*' Master Thesis, Civil and Environmental Engineering, University of Washington.

Billington, C.J. and Lewis, H.G. (1978). '*The Strength of Large Diameter Grouted Connections.*' Offshore Technology Conference, 10th Annual OTC 3083, Houston Texas.

Billington, C.J. and Tebbett, I.E. (1980). '*The Basis for New Design Formulae for Grouted Jacket to Pile Connections.*' Offshore Technology Conference, 12th Annual OTC, OTC 3788, Houston, Texas.

BSI (1999). '*Steel, Concrete and Composite Bridges: Code of Practice for Design of Composite Bridges.*' British Standard Institution (BSI), British Standard BS5400, London UK, pp. 29.

CIE5305 (2014). '*Bored and Immersed Tunnels.*' Chapter 4: Bored Tunnels.

Chilvers, G.A. (1984). '*Analysis of the Structural Behaviour of Grouted Pile/Sleeve Connections for Offshore Structures.*' Thesis Submitted to the City University for the Degree of Doctor of Philosophy in the Department of Civil Engineering.

DNV (2013). '*Design of Offshore Wind Turbine Structures.*' Det Norske Veritas (DNV), Offshore Standard, DNV-OS-J101.

ECS (2001). '*NEN-EN12699: Adopted European Prestandard, Execution of Special Geotechnical Work – Displacement Piles.*' NEN-EN12699, European Committee for Standardization (ECS), Brussels Belgium.

ECS (2005). '*Eurocode 1: Adopted European Prestandard.*' NEN-EN1991-1-4 European Committee for Standardization (ECS), Brussels Belgium.

ECS (2007). *'NEN-EN12944: Adopted European Prestandard.*' NEN-EN12944, European Committee for Standardization (ECS), Brussels Belgium.

ECS (2008). '*Eurocode 3: Adopted European Prestandard.*' NEN-EN1993-5 (en), European Committee for Standardization (ECS), Brussels Belgium.

ECS (2011a). '*Eurocode 0: Adopted European Prestandard.*' NEN-EN1990+A1+A1/C1, European Committee for Standardization (ECS), Brussels, Belgium.

ECS (2011b). '*Eurocode 2: Adopted European Prestandard.*' NEN-EN1992-1-1+C2, European Committee for Standardization (ECS), Brussels Belgium.

ECS (2011c). '*Eurocode 4: Adopted European Prestandard.*' NEN-EN1994-1-1+C1, European Committee for Standardization (ECS), Brussels Belgium.

ECS (2011d). '*Eurocode 4: Adopted European Prestandard.*' NEN-EN1994-2+C1, European Committee for Standardization (ECS), Brussels Belgium.

ECS (2011e). '*NEN-EN1536: Adopted European Prestandard, Execution of Special Geotechnical Work - Bored Piles.*' NEN-EN1536, European Committee for Standardization (ECS), Brussels Belgium.

Ferritto, J., Dickenson, S., Priestley, N., Werner, S. and Taylor, C. (1999). '*Seismic Criteria for California Marine Oil Terminals Volume 1.*' Naval Facilities Engineering Service Centre, California, Technical Report TR-2103-SHR.

FinnRa (2000), '*Steel Pipe Piles.*' Finnish National Road Administration (FinnRa) Bridge Engineering, Helsinki, 2000, ISBN 951-726-617-0.

Harn, R., Mays, T.W. and Johnson, G.S. (2010). '*Proposed Seismic Detailing Criteria for Piers and Wharves.*' Twelfth Triannual International Conference on Ports, ASCE, Jacksonville Florida USA, April 2010, pp. 460-469.

Hosseini, R. and Amini, A. (2015). *'Scour Depth Methods around Pile Groups.*' Korean Society of Civil Engineers (KSCE), Journal of Civil Engineering, 2015, pp. 1-13.

Hsiao, J.K. (2012). '*Statical Analysis of Pile Groups Containing Batter Piles.*' Electronic Journal of Structural Engineering 12, 2012, pp. 74-81.

Ichinose, L.H., Watanabe, E. and Nakai, H. (2000). '*An Experimental Study on Creep of Concrete Filled Steel Pipes.*' Journal of Constructional Steel Research 57, Elsevier, 2001, pp. 453-466.

Jensen, U.F. and Hoang, L.C. (2012). '*Collapse Mechanisms and Strength Prediction of Reinforced Concrete Pile Caps.*' Engineering Structures 35, Elsevier, 2012, pp. 203-214.

Kappes, L., Berry, M. and Stephens, J. (2013). '*Performance of Steel Pipe Pile-to-Concrete Cap Connections Subject to Seismic or High Transverse Loading: Phase III Confirmation of Connection Performance.*' The State of Montana Department of Transportation (MDT), Report No. FHWA/MT-13-001/8203.

Kingsley, A.M. (2005). '*Experimental and Analytical Investigation of Embedded Column Base Connections for Concrete Filled High Strength Steel Tubes.*' Master Thesis, Civil and Environmental Engineering, University of Washington.

Kraft, L.M. (1991). '*Performance of Axially Loaded Pipe Piles in Sand.*' Journal of Geotechnical Engineering 117-2, ASCE, February 1991, pp. 272-296.

Krahl, N.W. and Karsan, D.I. (1985). '*Axial Strength of Grouted Pile-to-Sleeve Connections.*' Journal of Structural Engineering 111-4, ASCE, April 1985, pp. 889-905.

Lamport, W.B., Jirsa, J.O. and Yura, J.A. (1991). '*Strength and Behaviour of Grouted Pile-to-Sleeve Connections.*' Journal of Structural Engineering 117-8, ASCE, August 1991, pp. 2477-2498.

Lehman, D.E. and Roeder C.W. (2012). '*Foundation Connections for Circular Concrete-Filled Tubes.*' Journal of Constructional Steel Research 78, Elsevier, 2012, pp. 212-225.

Li, G., Zhao, X., Wang, P. and Liu, X. (2005). '*Behaviour of Concrete-Filled Steel Tubular Columns Incorporating Fly Ash.*' Cement & Concrete Composites 28, Elsevier, 2006, pp. 189-196.

Lotsberg, I., Serednicki, A., Bertnes, H. and Lervik, A. (2012). '*Design of Grouted Connections for Monopile Offshore Structures.*' Stahlbau 81, Ernst & Sohn, Berlin Germany, 2012, pp. 695-704.

Marson, J. and Bruneau, M. (2004). '*Cyclic Testing of Concrete-Filled Circular Steel Bridge Piers Having Encased Fixed-Based Detail.*' Journal of Bridge Engineering 9-1, ASCE, January 2004, pp. 14-23.

Moon, J., Lehman, D.E., Roeder, C.W. and Lee, H. (2013). '*Evaluation of Embedded Concrete-Filled Tube (CFT) Column-to-Foundation Connections.*' Engineering Structures 56, Elsevier, 2013, pp. 22-35.

Morley, J. and Bruce, D.W. (1983). '*Survey of Steel Piling Performance in Marine Environments, Final Report.*' Commission of the European Communities, 1983, EUR8492 EN.

NCHRP (2011). '*Application of Accelerate Bridge Construction Connections in Moderate-to-High Seismic Regions.*' National Cooperative Highway Research Program (NCHRP), 2011, Report 698.

Nezamian, A. (2003). '*Bond Strength of Concrete Plugs Embedded in Tubular Steel Piles.*' Thesis in Fulfilment of the Requirements for the Degree of Doctor of Philosophy in Civil Engineering, Monash University.

Nezamian, A., Al-Mahaidi, R. and Grundy, P. (2006). '*Bond Strength of Concrete Plugs Embedded in Tubular Piles Under Cyclic Loading.*' Canadian Journal of Civil Engineering 33, NRC, 2006, pp. 111-125.

Nezamian, A., Al-Mahaidi, R., Grundy, P. and O'Loughlin, B. (2002). '*Push-Out Strength of Concrete Plugs in Tubular Steel Piles.*' Proceedings of the Twelfth International Offshore and Polar Engineering Conference, Kitakyushu Japan, May 2002, pp. 60-64.

Nori, V.V. and Tharval, M.S. (2007). '*Design of Pile Caps – Strut and Tie Model Method.*' The Indian Concrete Journal, April 2007, pp. 13-19.

Norsok standard (2012). 'Design of *Steel Structures.*' Annex K, Special Design Provisions for Jackets.

OT (2002). '*Pile/Sleeve Connections.*' Offshore Technology (OT), Edited by HSE, Report No. 2001/016, ISBN 0717623904.

Rabbat, B.G. and Russell, H.G. (1985). '*Friction coefficient of Steel on Concrete or Grout.*' Journal of Structural Engineering 111-3, ASCE, March 1985, pp. 505-515.

Radhika, K.S. and Baskar, K. (2012). '*Bond Stress Characteristics on Circular Concrete Filled Steel Tubular Columns Using Mineral Admixture Metakaoline.*' International Journal of Civil and Structural Engineering 3-1, July 2012, pp. 1-8.

Raj, A. and Airin, M.G. (2008). '*Experimental and Analytical Investigation of Strut and Tie Model Method of Pile Cap.*' IOSR, Journal of Mechanical and Civil Engineering, 2008, pp. 30-35.

Richards, P.W., Rollins, K.M. and Stenlund, T.E. (2011) '*Experimental Testing of Pile-to-Cap Connections for Embedded Pipe Piles.*' Journal of Bridge Engineering 16-2, ASCE, March-April 2011, pp. 286-294.

Roeder, C.W. and Lehman, D.E. (2008). '*An Economical and Efficient Foundation Connection for Concrete Filled Steel Tube Piers and Columns.*' International Conference on Composite Construction in Steel and Concrete, Tabernash Colorado, USA, July 2008, pp. 351-363.

Roeder, C.W., Cameron, B. and Brown, B. (1999). '*Composite Action in Concrete Filled Tubes.*' Journal of Structural Engineering 125-5, ASCE, May 1999, pp. 477-484.

Roeder, C.W., Graff, R., Soderstrom, J. and Yoo, J.H. (2005). '*Seismic Performance of Pile-Wharf Connections.*' Journal of Structural Engineering 131-3, ASCE, March 2005, pp. 428-437.

Rollins, K.M. and Stenlund, T.E. (2010). '*Laterally Loaded Pile Cap Connections.*' Utah Department of Transportation Research Division, August 2010, Report No. UT-10.16.

RUUKKI (2014). '*Large Diameter Steel Pipe Piles in Foundation Construction.*' RUUKKI, Energy Efficient Steel Solution for Better Living. Working. Moving.

Shakir-Khalil, H. (1993). '*Pushout Strength of Concrete-Filled Steel Hollow Sections.*' The Structural Engineer 71-13. 6 July 1993, Civil Engineering Department, University of Manchester.

Shritharan, S. (2005). '*Improved Design Procedure for Concrete Bridge Joints.*' Journal of Structural Engineering 131-9, ASCE, September 2005, pp. 1334-1344.

Skyline (2013). '*Pipe.*' Skyline Steel I, A Nucor Company.

Souza, R., Kuchma, D., Park, J. and Bittencourt, T. (2009). '*Adaptable Strut-and-Tie Model for Design and Verification of Four-Pile Caps.*' ACI Structural Journal 106-2, March-April 2009, pp. 142-150.

Stephens, J.E. and McKittrick, L.R. (2005). '*Performance of Steel Pipe Pile-to-Concrete Bent Cap Connections Subject to Seismic or High Transverse Loading: Phase II.*' The State of Montana Department of Transportation (MDT), Report No. FHWA/MT-05-001/8144.

Bibliography

Stephens, M.T., Roeder, C.W., Lehman, D.E. and Moon, J. (2014). '*Seismic Design of Concrete Filled Tube Columns and Their Connections.*' University of Washington, Department of Civil and Environmental Engineering.

Steunenberg (1996). '*A Contribution to the Study of the Performance of Steel Pipe Piles Welded to Concrete Pier Cap Beams Under Seismic Loading.*' Master Thesis, Department of Civil Engineering, University of British Columbia.

Steunenberg, M., Sexsmith, R.G. and Stiemer, S.F. (1998). '*Seismic Behaviour of Steel Pile to Precast Concrete Cap Beam Connections.*' Journal of Bridge Engineering 3-4, ASCE, November 1998, pp. 177-185.

Tomlinson, M. and Woodward, J. (2008). '*Pile Design and Construction Practice, Fifth Edition.*' Taylor & Francis: London and New York, 2008, ISBN 0-203-96429-2.

University of Colorado (2015). '*Thin Walled Pressure Vessels.*' Lecture 3.

University of Washington (2015). '*Thick Walled Cylinders.*' ME354A.

Vincent, T. and Ozbakkaloglu, T. (2014). '*Influence of Shrinkage on Compressive Behaviour of Concrete-Filled FRP Tubes: An Experimental Study on Interface Gap Effect.*' Construction and Building Materials 75, Elsevier, 2015, pp. 144-156.

Virdi, K.S. and Dowling, P.J. (1980). '*Bond Strength in Concrete Filled Tubes.*' IABSE Proceedings p-33/80, pp. 125-139.

Xu, C., Chengkui, H., Decheng, J. and Yuancheng, S. (2007). '*Push-Out Test of Prestressing Concrete Filled Circular Steel Tube Columns By Means of Expansive Cement.*' Construction and Building Materials 23, Elsevier, 2009, pp. 491-497.

Yap, W.T. (2012). '*Strut and Tie Modelling of Reinforced Concrete Short Span Beams.*' First Civil and Environmental Engineering Student Conference, Imperial College, London, June 2012, pp. 1-6.

Appendices

Formulations Embedded Connections

Following from testing and experimental research, several design expressions have been formulated for both the monolithic and isolated connection. A short overview of the main findings is given in this appendix.

A.1 Design expressions

A.1.1 Annular ring

The dimensions of the annular ring are based on research by Kingsley (2005). Different annular ring sizes are tested in order to establish the highest resistance against cone pull-out (right of Figure A.1). The pile is pulled-out of the concrete which cracks under an angle of approximately 45 degrees. The recommended dimensions for the annular ring are 16 times the pile wall thickness (t_p) on the outside and 8 times on the inside (Stephens et al. (2014)) like seen in the left of Figure A.1.
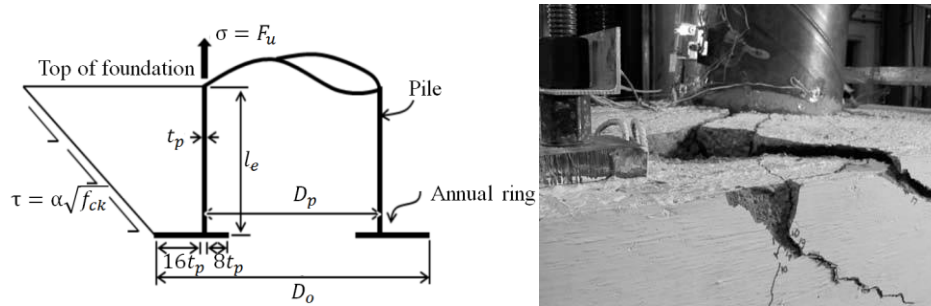
Figure A.1: Cone pull-out model and the failure mode found in testing (Stephens et al. (2014)).

A.1.2 Weld size

The weld (complete joint penetration weld or two fillet welds), connecting the annular ring to the pile, should have the following size (W) (Roeder et al. (2012))

$$W \geq 1.31 \, F_u t_p / F_{EXX}. \tag{Eq. A.1}$$

In which F_{EXX} is the minimum tensile strength of the weld metal, F_u the ultimate tensile strength of the tube and t_p the tube thickness.

A.1.3 Embedment depth

The embedment depth is denoted as the most important parameter for the behaviour of the embedded connection and is evaluated by Stephens et al. (2014). Based on the cone pull-out model depicted in Figure A.1, the following expression is derived

$$l_e = \sqrt{\frac{D_0^2}{4} + \frac{D_p t_p F_y}{0.5\sqrt{f_{ck}}}} - \frac{D_0}{2}. \tag{Eq. A.2}$$

In which D_0 is equal to the outside diameter of the annual ring (in case of a monolithic connection) or the corrugated pipe (in case of an isolated connection), D_p is the diameter of the steel tube, t_p is the thickness of the tube, F_y is the yield stress of the tube and f_{ck} is the compressive stress of the foundation concrete.

A.1.4 Punching shear

An adequate level of concrete needs to be present above the pile to avoid punching shear. The failure mode (Figure A.2) is a combination of downward punch of the central part and a horizontal translation of the remaining outer parts (Jensen et al. (2012)). This can only occur when the reinforcement is yielding. Stephens et al. (2014), proposed a minimal amount of concrete on top of the pile (d_{punch}) as follows

$$d_{punch} \geq \sqrt{\frac{D_p^{\,2}}{4} + \frac{C_C + C_S}{0.33\sqrt{f_{ck}}}} - \frac{D_p}{2}.$$

(Eq. A.3)

In which C_c is the compressive force in the concrete. C_s is the compressive force in the steel, due to combined axial load and bending moment.
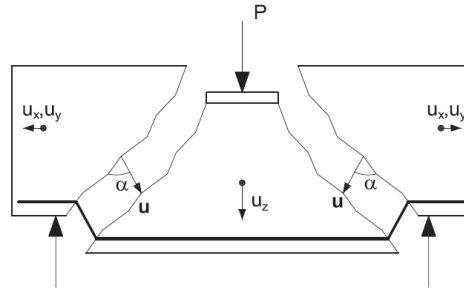
Figure A.2: Punching shear failure of the capping beam (Jensen et al. (2012)).

A.2   FE modelling

Modelling of the embedded connections is done by Moon et al. (2013) to verify the results by Lehman et al. (2012) and to perform a parameter study. Different embedment lengths are tested varying from $0.6D_p$ to $0.9D_p$. In contrast to the experimental research, the modelling is not just limited to seismic design only, which makes it an interesting addition to this report.

A.2.1 Findings

The shear strength of the concrete (τ) as displayed in Figure A.1, is defined as

$$\tau = \frac{D_p t_p f_y}{(l_e^2 + D_0 l_e)}.$$

(Eq. A.4)

With a linear regression, based on 56 models, two different expressions for the shear strength are obtained

$$\tau \leq \alpha\sqrt{f_{ck}} = 0.6\sqrt{f_{ck}}$$

(Eq. A.5.A)

$$\tau \leq \alpha\sqrt{f_{ck}} = 0.55\sqrt{f_{ck}}.$$

(Eq. A.5.B)

(Eq. A.5.A) gives the result for areas with no or little seismic activity whilst (Eq. A.5.B) should be adopted for areas with high activity. With the help of a regression analysis on the test data, the embedment length (l_e) should be obtained from

$$\frac{D_p t_p f_u}{(l_e^2 + D_0 l_e)} \leq \alpha\sqrt{f_{ck}} = 0.55(1 + \rho_v)^{0.46}(1 + P/P_0)^{0.51}\sqrt{f_{ck}}$$

(Eq. A.6.A)

$$\frac{D_p t_p f_u}{(l_e^2 + D_0 l_e)} \leq \alpha\sqrt{f_{ck}} = 0.47(1 + \rho_v)^{0.46}(1 + P/P_0)^{0.51}\sqrt{f_{ck}}.$$

(Eq. A.6.B)

In which ρ_v is the amount of shear reinforcement in % in the footing, P_o the maximal longitudinal force on the pile and P the applied force like depicted in Figure A.3. As in the previous, (Eq. A.6.A) is for design in low-seismic area and (Eq. A.6.B) for large-seismic activity.
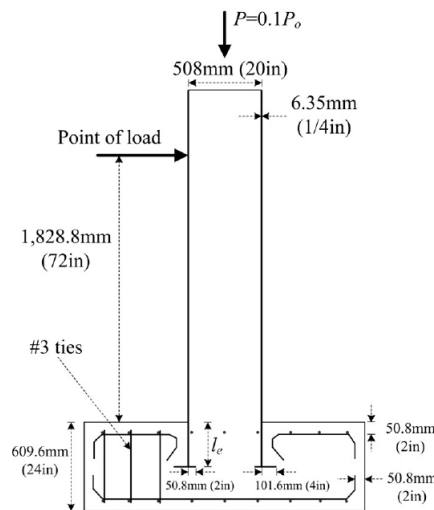
Figure A.3: Test set-up for the FEM (Moon et al. (2013)).

A.3   Capping beam reinforcement

A major concern is the reinforcement layout in the concrete element. Research is conducted and started in 2005 and was continued in 2013. Stephens et al. (2005) proposed three different solutions to this problem. The three options rely on the idea to deviate the longitudinal reinforcement around the embedded pile. The first two alternatives are almost similar to each other. Spiral reinforcement is applied around the pile which is connected with the remainder. In the punching shear depth (as in A.1.4), the longitudinal bars are continuous, as can be seen in the left of Figure A.4. The second option adopts the same spiral reinforcement as the previous, however in this case vertical reinforcement bars are added (right of Figure A.4).
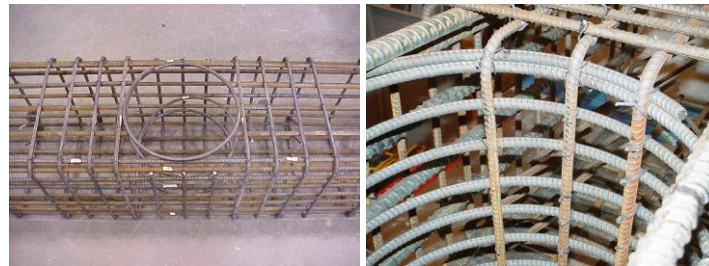
Figure A.4: Spiral reinforcement embracing the pile (Stephens et al. (2005)).

The last model is based on the idea to maximise the amount of steel which is limited by the constructability. A U-Shaped bar is placed right under the surface where the pile enters the footing (Figure A.5). These bars loop around the pile to provide for sufficient bending moment resistance.

Figure A.5: Third option with at the top the U-shaped bars (Stephens et al. (2005)).

Stephens et al. (2005) formulated a design guide (for seismic design) for the lay-out according to the U-shaped bar option. Reference is made to the denoted report to acquaint this guide. Kappes et al. (2013) continued testing the U-shaped reinforcement model. The reinforcement lay-out was constructed according to the proposed guide. Testing showed the usefulness of the guide, however with a few pitfalls. Concrete crushing appeared before it was accounted for. To resolve these issues, an analytical model is required to improve the system behaviour.

A.4   Conclusion

The development is at an advanced stage for the embedded connections with a high technological readiness. Multiple proposed formulations are listed in this section. The research is conducted for pile-footing details. The suggestion of Stephens et al. (2014) that the embedded pile-footing details provide valuable data for pile-to-cap usage is highly doubted. Piles will deviate from the intended position with a maximum of 150mm for which sufficient capacity is required. Capping beams contain higher reinforcement levels (up to 5%) than the tested footings (approximately 2%) which embrace new impracticalities. Furthermore, the constructability is of major concern and the occurrence of the punching shear phenomenon results in larger beam dimensions.

Influential Aspects

Subsequent to the example in section 4.1, potential design influences are listed and subdivided. This section gives an <u>indication</u> of the aspects involved and the decisions that are to be taken during the design process. This information is obtained, based on available project data, interviews and literature.

B.1 Influences

The composed list is given in Figure B.1. This figure illustrates the most important parameters which are of influence. It is pointed out that during new projects, new aspects or conditions can arise which are not included in the list.

Possible influencing aspects are clustered to keep a better overview of all the involved parameters. Each group of aspects is elaborated in more detail in the following sections.

B.1.1 Construction aspects

The considered connection is adopted in several different construction types and situations. Even within one construction, multiple solutions are adopted. Within a jetty, the piles may have considerably shorter lengths near the shore compared to the ones positioned further away from shore. Buckling lengths change and so will the capacity. This can be accommodated by filling the piles with concrete for instance. To remain with the location, the outer piles need to resist most of the loads induced by waves, berthing forces etc. This whilst the effect on the inner piles will remain limited. Construction size and quantities determine the most economic lifting equipment. With small batches, in-situ casting is preferred over prefabrication.

B.1.2 Function

It is already seen how the function can influence the design with the LNG jetty example (section 4.1). If this same structure is a cargo jetty, it is necessary to deal with loads from handling equipment, storage of containers, movements due to wind, berthing loads etc. One special consideration is made regarding situations where fire ignition is possible. This results in totally different situations in comparison to the earlier mentioned principles.

B.1.3 Loading

Loading conditions follow from the function of the structure, the type of construction and the local conditions in which it is adopted. A distinction can be made between piles which need to transfer axial- and shear force and piles which transfer bending moments as well.

B.1.4 Availability

The next issue is the availability of materials, labour and equipment. In some regions experienced/classified labour is hard or impossible to get. In some extreme cases, labour from other countries is flown in for specific jobs. The same applies to equipment. The design should be adapted to the available cranes, vessels etc.

B.1.5 Possible lifting weight

Following from the accessibility of the site, the availability of equipment, the local conditions and the construction size, the most cost effective equipment is chosen. The magnitude of the possible lifting capacity will determine the installation method of the piles and therefore the capacity, the construction method of the concrete element and thus the connection design.

B.1.6 Local conditions

Local conditions include wave-, water-, wind-, scour-, soil-, marine and climate conditions. Wave height sets the construction height, which subsequently influences the pile lengths. Water conditions like tidal data are already discussed with the jetty example. Climate conditions change material behaviour, the curing conditions for the concrete or ice loads might be present. Local soil conditions affect the construction- and installation method of the pipe piles. In soft soil, the herniation point is low down which results in long buckling lengths of the pipe piles, hard soil conditions result in a high herniation point.

B.1.7 Capacity and installation method piles

The required capacity is defined by the loading conditions following from the function and the type of construction. The possible capacity is subsequently determined by the local soil conditions, which influence the bearing capacity and the buckling capacity. External loading on the piles is induced by wave, wind and ice actions which is dependent on the local conditions. Furthermore, marine life might have an impact on the installation method, since it might affect animal behaviour during some time of the year due to noise and vibrations.

B.1.8 Practical experience

Common practice within an engineering department plays an important role in design. When a previous adopted alternative works properly, it is likely that this alternative is reused in new projects. Switching from alternative means investing in obtaining new knowledge, new design rules and laboratory testing.

B.2 Decisions

To get a grip on the design issue, the matter is subdivided into several decisions prior to the decision for the connection. These decisions follow from the influence groups from the previous section. Design decisions include the production method of the capping beam, the installation method of the piles, construction speed etc. To illustrate the basic design idea, the scheme in Figure B.2 is compiled.

The process starts at the basic principles which are known, namely local conditions and the type of structure. Subsequently, more detailed data is gathered concerning soil- and water properties, availability of equipment and materials etc. This contextual information is used for establishing the proper hoist equipment, the design loads and the required location-bound information.

The scheme is composed as follows: the bold printed texts are the groups as defined in section B.1. The round boxes indicate that properties need to be determined. A normal line stands for a link and an arrow for a design decision. The small boxes are the possible outcomes. When for instance the lifting weights are known, a decision can be made for the production method of the capping beam. This can be an in-situ solution, prefab or box option.

Local Conditions

Corrosion rates

Temperature
Salt or fresh water
Marine life
Etc.

Water conditions

Water depth   Scour
Wave heights   Tides
Etc.

Climate

Wind conditions
Wave conditions
Water density
Current
Ice
Collision impact
Etc.

Soil conditions

Modulus of subgrade reaction
Ground pressure coefficients
Hardness soil
Presence of boulders
Soil structure
Depth bearing layer
Etc.

Seismic activities

Capacity Piles

Buckling capacity

Restrainment connection
Diameter and wall thickness
Steel quality
Penetration depth
Young's modulus
Effective depth
Height concrete element
Etc.

Concrete class
Diameter and wall thickness
Natural frequency
Mass
Pile shape
Rock shoe
Etc.

Practical Experience

Common practice
Design rules
Schedules
Investments
Etc.

Construction Aspects

Type of pile

Installation method
Batter- or vertical pile
Method of constructing
Structure of the piles
Etc.

Type of construction
Location within construction
Number of piles
Number of piles within group
Construction tolerances
Pile sizes
Prefab or in situ capping beam
Deviation and settlement piles
Etc.

Function

LNG terminal
Fire protection
Etc.

Loading

Compression   Uniformly distributed
Tension   Magnitudes
Bending moment   Fatigue
Shear   Execution loads
Cyclic loading   Wave conditions
Distribution of forces   C.T.C. distances
Etc.

Availability

Availability equipment   Distance to workshop
Availability materials   Distance to material suppliers
Availability workers   Distance to rental
Local dimensions materials Dimensions
Speed of construction
Etc.

Possible Lifting Weights

Construction type
Size and weight of concrete element
Size of structure
Most cost-effective equipment
Availability
Etc.

Figure B.1: Design influences.

Figure B.2: Decisions during the design process.

Costs Comparison Plug and Plate

For the given example of section 4.4.3, the costs are estimated. It is noted that the used numbers are a general representation of the actual costs. These numbers will change for each project. A number of assumptions have been made during this analysis.

For the plate connection, the plate is 1500·1500mm with a thickness of 40mm. These are common values for a plate in a jetty construction. This plate is connected with 25 studs. An interface length of 5000mm is assumed for the plug connection without shear keys. Transport costs are not included.

The costs of the embedded plate connection are given in Table C.1. The total costs for such a connection is around €2500 depending on the location. The costs for the plug connection are around €2100 (Table C.2), so around 20% cheaper. In general, the plug will be 25-30% less expensive than the embedded plate (BN (2015)).

Table C.1: Costs for the embedded plate connection.

Element	Unit	Costs
Steel:		
Steel plate (1500·1500·40mm)	€/pile	527
Studs (Ø.25 nr 25. L=0.9m)	€/pile	60
Total:	**€/pile**	**587**
Welding plate:		
Drilling holes (25·€15)	€/pile	375
Welding studs (25 pieces)	€/pile	156
Inspection welding	€/pile	50
Ultra sonic testing	€/pile	100
Total:	**€/pile**	**681**
Welding pile:		
Welding	€/pile	750
Welding generator set and material	€/pile	100
Ultra sonic testing	€/pile	100
Total:	**€/pile**	**950**
Repair:		
Possible repair welding	€/pile	150
Total:	**€/pile**	**150**
Coating:		
Coating	€/pile	50
Total:	**€/pile**	**50**
Total:	**€/pile**	**2418**

Table C.2: Costs for the plug connection.

Element	Unit	Costs
Concrete:		
Formwork outside	€/pile	50
Formwork inside	€/pile	300
Material	€/pile	1080
Special equipment	€/pile	250
Total:	**€/pile**	**1680**
Reinforcement:		
Steel	€/pile	263
Bending & cutting	€/pile	132
Total:	**€/pile**	**395**
Total:	**€/pile**	**2075**

Background & Comparative Study Bond: Pile-Sleeve Standards

The pile-sleeve expressions are introduced in Chapter 6, since they provide formulations for bond in combinations with circular piles. To provide a better understanding of these design codes, the backgrounds are considered and a comparative study is performed in this section. Specifications of the codes will be considered in more detail.

D.1   Background

With the exception of the API, all codes are completely based on experimental results. This means that the most influential parameters are determined (following from variation studies) and that additional factors are obtained using test data. A major drawback of these compositions is that when an influential parameter is overlooked, formulations tend to deviate from test data to which new parameters have to be introduced.

D.1.1   American Petroleum Institute (API)

The API formulation is partly based on test data and partly on analytical grounds. The derivation for this expression is performed by Krahl et al. (1985) and will be discussed shortly.

The axial capacity is an addition of the bond- and shear key contribution as follows

$$P_u = f_b \pi D_p L + N f_{cu}^* \pi (D_p + h) h. \tag{Eq. D.1}$$
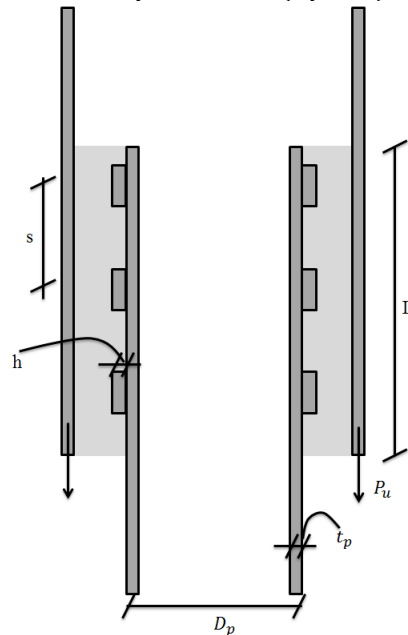
Figure D.1: Definitions for the shear keys used by the API (Krahl et al. (1985)).

In which h is defined as the shear key height, D_p as the diameter of the pile, f_{ck}^* the crushing strength of the concrete and N the number of shear keys used along the interface length (L/s). These definitions are illustrated in Figure D.1. The presupposed failure mechanism is concrete crushing above the shear keys and breaking of the bond. The axial strength of the interface (f_{axial}) is defined as the total capacity of the interface (both bond- and shear key capacity). By dividing the ultimate axial capacity (P_u) by the contact surface, the following definition is found for f_{axial}

$$f_{axial} = \frac{P_u}{\pi D_p L}.$$ (Eq. D.2)

Substituting (Eq. D.2) into (Eq. D.1) gives the following

$$f_{axial} = f_b + \left(1 + \frac{h}{D_p}\right) f_{cu}^* \frac{h}{s}.$$ (Eq. D.3)

A new parameter (k_{API}) is introduced by Krahl et al. (1985), which gives the ratio between the crushing strength of the concrete (f_{ck}^*) and the elastic compressive strength (f_{ck}). Furthermore, an approximation for the geometry is done as follows.

$$k_{API} = \frac{f_{ck}^*}{f_{ck}}$$ (Eq. D.4)

$$\left(1 + \frac{h}{D_p}\right) \approx 1.$$ (Eq. D.5)

Substituting (Eq. D.4) and (Eq. D.5) into (Eq. D.3), results in the final API formulation

$$f_{axial} = f_b + k f_{ck} \frac{h}{s}.$$ (Eq. D.6)

The presented k_{API} value represents the empirical part and is set to 0.9 in the final expression. This conservatism is physically impossible since the crushing strength of the concrete is lower than the elastic compressive strength. The bond part (f_b) is equal to 0.248N/mm^2 and independent from geometry, type of concrete etc.

D.2 Limitations

The empirical character forces to give restrictions to which the expressions are applicable. Since different test data is used, different limitations are formulated which are presented in Table D.1. The DNV standard uses by far the least amount of limitations. A second noticeable detail is the h/s limitation. The OT only allows a ratio of 0.04 whereas the API, DNV and Norsok allow 0.10. This is a remarkable difference. Lastly, the allowed D_p/t_p ratios are small considering that a plug connection can reach values over 80.

Table D.1: Ranges to which the codes are applicable.

Limitations	OT (2002)	API (2003)	DNV (2013)	Norsok (2012)
f_{ck}	-	$110 \geq f_{ck} \geq 17$	-	$80 \geq f_{ck} \geq 20$
h/s	$0.04 \geq h/s \geq 0$	$0.10 \geq h/s$	$0.10 > h/s$	$0.10 \geq h/s \geq 0$
D_p/t_p	$40 \geq D_p/t_p \geq 24$	$40 \geq D_p/t_p$	$60 \geq D_p/t_p \geq 10$	$40 \geq D_p/t_p \geq 20$
D_s/t_s	$140 \geq D_s/t_s \geq 50$	$80 \geq D_s/t_s$	$140 \geq D_s/t_s \geq 18$	$140 \geq D_s/t_s \geq 30$
D_g/t_g	$45 \geq D_g/t_g \geq 10$	$45 \geq D_g/t_g \geq 7$	-	$45 \geq D_g/t_g \geq 10$
C_S	-	-	-	$0.02 \geq C_S$
h/D_p	$0.006 \geq h/D_p$	-	-	$0.012 \geq h/D_p$
D_p/s	$8 \geq D_p/s$	$8 \geq D_p/s \geq 2.5$	-	$16 \geq D_p/s$
L/D_p	$L/D_p \geq 2$	$10 \geq L/D_p \geq 1$	-	$10 \geq L/D_p \geq 1$
$f_{ck} \cdot h/s$	-	$5.5 \geq f_{ck} \cdot h/s$	-	-
s	-	-	$s > \sqrt{(R_p \cdot t_p)}$	-

D.3   Design factors

In each standard, different design factors are assigned. Design factors include safety-, material- and/or load factors. The Offshore Technology (OT) uses a design factor of 6.0 during normal conditions which is lowered to 4.5 in extreme conditions. This includes a load factor of 1.5, a material factor of 1.5 and a behaviour factor accounting for grouting conditions, cyclic loading effects, incomplete grouting and differences in compressive strength between on- and offshore (Billington et al. (1980)). DNV (2010) and Norsok both apply material factors which are respectively 3.0 and 2.0 during normal operating conditions. DNV (2013) prescribes a material factor around 1.5 till 1.75 depending on the thickness of the grout layer. This values can only be used when small grout thicknesses are adopted which does not hold for the plug connections. Therefore, the material factor of 3.0 is applied which counts for offshore grouting operations. Lastly, the American design code applies a resistance factor for the axial load transfer stress equal to 0.9. The API factor seems low in relation to the other standards, however the k_{API} value which is adopted in their formulation is chosen very conservatively. Appropriate safety is arranged in this manner instead of applying higher factors.

D.4   Comparison between pile-sleeve codes

Comparing formulations of all four pile-sleeve systems result in the following findings. Agreements between codes are:
- Three formulations are completely empirical meaning they are fitted to test results,
- All four codes add up the bond- and the shear key part (implying the same load deflection curves),
- The shear key transfer strength is dependent on the ratio of the outstand divided by the spacing h/s, see Figure D.1,
- The interface strength of the connection is a function of the concrete compressive strength,
- OT and Norsok apply the same stiffness parameter. DNV uses a similar which gives slightly different results.

Differences between codes are:
- The API uses one single independent value for bond whereas the OT and Norsok involve a stiffness factor (based on Billington's findings),
- Norsok incorporates surface irregularities,
- Norsok includes a flexibility factor.

Further remarks which can be made are:
- The API does not involve the geometry of the connecting elements. This seems unreasonable since experimental results show lowering of strength with increasing diameters (also in the pile-sleeve format),
- The stiffness parameters in the OT, DNV and Norsok account for the D_p/t_p ratio of the pile, the sleeve and the grout. However, like noted in Table D.1, no limitation for the maximum pile thickness and diameter are given. This means when the thickness is increased linearly with the diameter of the pile, the diameter over thickness ratio keeps constant and the capacity remains constant. This is contrary to the conclusions from Chapter 6 in which shrinkage is depicted as one of the major influences,
- Again, it is pointed out that the plug- and the pile-sleeve are two different systems. Mutual differences are present.

D.5   Comparative study bond

From literature (Chapter 6), a number of parameters show large influences on the bond capacity in plug connections. To check whether the formulations follow these trends and show corresponding results, a parameter study is performed. All expressions for the bond capacity are included in this analysis. The design example from section 6.5.4 is used as guidance during this analysis unless stated

otherwise. The proposed stiffness factor (Eq. 6.16), as defined by Nezamian (2003), is used. The given outcomes include the design factors from section D.3 and the limits from section D.2 are respected.

D.5.1 Bond: concrete compressive strength

The effect of the concrete compressive strength is illustrated in Figure D.2. The bond capacity is only dependent on the compressive strength in the Offshore Technology (OT) formulation. The difference between C50/60 and C12/15 is over 200% for this standard. In experimental testing, a number of researchers concluded that the bond is not related to the concrete class, which most formulations agree on. The most important effect related to the compressive strength, concrete shrinkage, is not included by any of the standards.
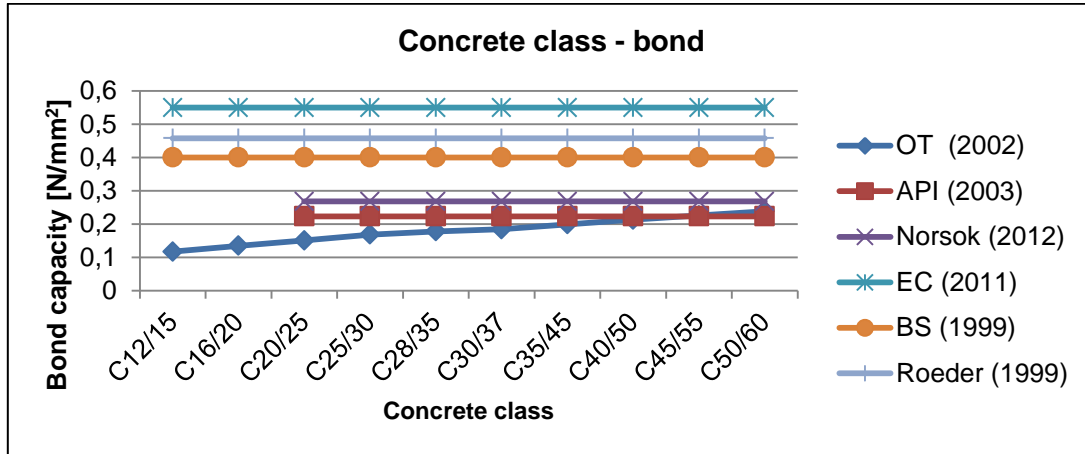
Figure D.2: Effect of the concrete compressive strength.

D.5.2 Bond: interface length

The only standard including the interface length is again the OT with a length parameter (C_L). This factor changes from 1.0 for $L/D_p<2$ to 0.7 for $L/D_p>12$. It is hard to make unambiguous statements based on Figure 6.5 in which the influence of the interface length is shown. Conclusions, based on testing, differ. Some researchers state that the strength is lowered with increasing length while others state no recordable differences.

The result for this analysis is presented in Figure D.3. Roeder's expression does not adopt a factor related to the interface length in the expression itself but uses an additional model (Figure 7.9) for the bond distribution. This addition does not affect the calculated bond stress but does influence the area on which it can be used. The total capacity (bond times surface) is lowered.
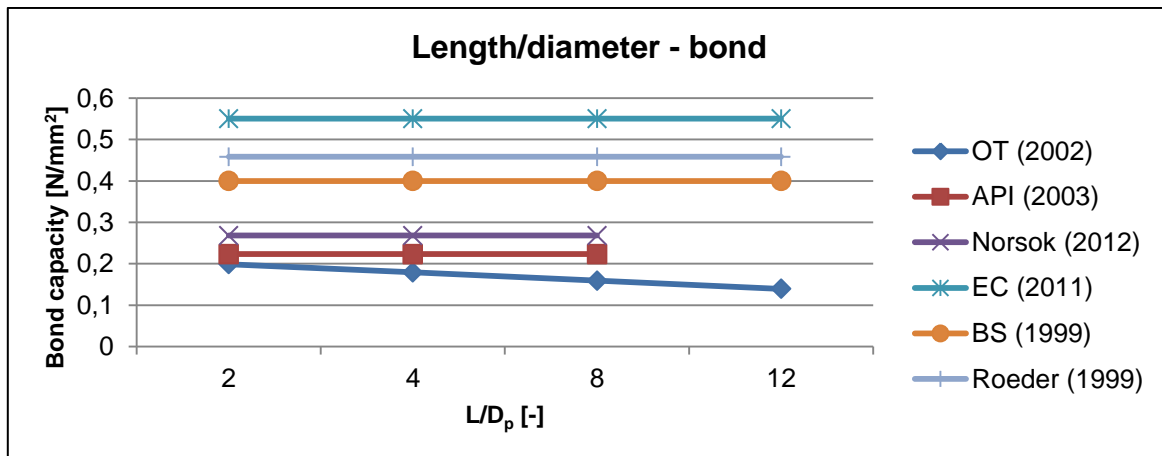
Figure D.3: Effect of the plug length on the bond capacity.

D.5.3   Bond: D_p/t_p

The stiffness factor depends on the diameter over thickness ratio of the pile as defined by Nezamian (2003). For the making of Figure D.4, the D_p/t_p has been varied. Two out of three pile sleeve-formulations show a lowering of the bond with increasing D_p/t_p. This seems in agreement with the result found in Figure 6.7. Roeder's expression gives a linear relation. At a ratio of approximately 80, the bond according to Roeder et al. (1999) is equal to zero. The constant values adopted by the EC, the BS, and the API seem conservative in comparison to Norsok and OT for small D_p/t_p ratios (in the order of 10). For large ratios (in the range of 60), the constant values are considerably higher than the non-constant equivalents.
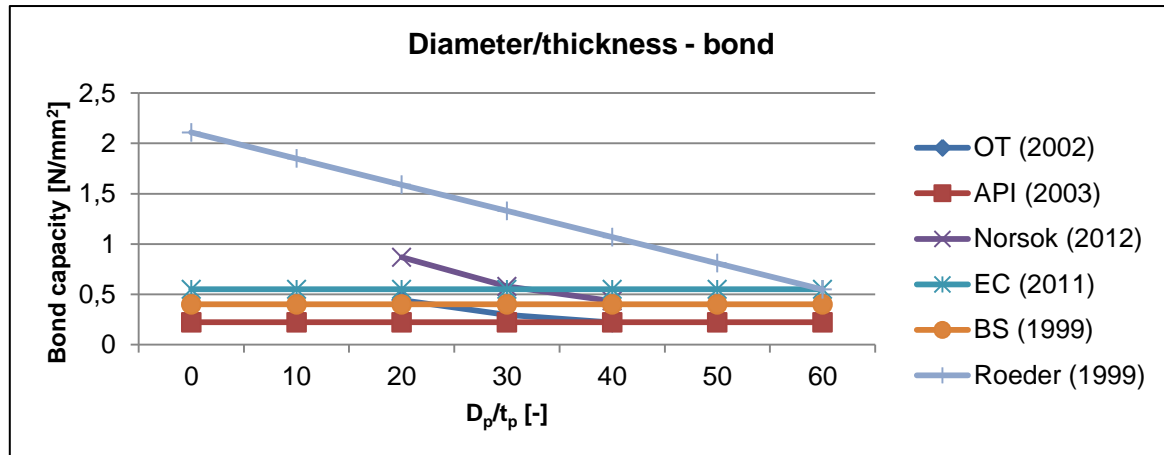
Figure D.4: D_p/t_p influence on the bond capacity.

D.6   Conclusion

Two out of three pile sleeve expressions are totally based on an experimental basis. Only the API expression has an analytical background in combination with an empirical determined parameter.

Some major differences between the expressions are pointed out by examining the design factors and the limitations to which the expressions are applicable. The OT expression agrees on an increase of the bond capacity with increasing compressive strength and a lowering of the capacity with raising interface length. These two influences are not acknowledged by the other formulations. The D_p/t_p ratio is adopted by the models of OT, Norsok and Roeder. This influence is also denoted as one of the major impacts on the capacity. The API on the other hand does not include any of the geometry dimensions. Although most standards give the same trends, the mutual differences are enormous. Furthermore, the constant design values are rather low for small D_p/t_p ratios but relatively high for larger ratios. So these values are either very conservative or probably unsafe. Lastly, none of the expressions state anything about concrete shrinkage which is denoted as a significant influence. Based on these findings, the usability of the pile-sleeve formulations for the plug connection is highly doubtable and needs to be verified.

Proof of Lame's Equations

The derivation for Lame's equations is given in this appendix (University of Washington (2015)). The used definitions are given in Figure E.1 (the same definitions as used in Chapter 7).
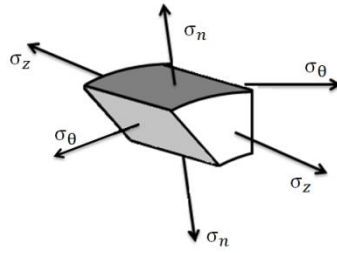
Figure E.1: Definitions for the derivation of Lame's equations.

For a Hookean material, the constitutive relations for the strains are given by

$$\varepsilon_z = \frac{1}{E}\left(\sigma_z - v(\sigma_n + \sigma_\theta)\right) \tag{Eq. E.1}$$

$$\varepsilon_\theta = \frac{1}{E}\left(\sigma_\theta - v(\sigma_z + \sigma_n)\right) \tag{Eq. E.2}$$

$$\varepsilon_n = \frac{1}{E}\left(\sigma_n - v(\sigma_\theta + \sigma_z)\right). \tag{Eq. E.3}$$
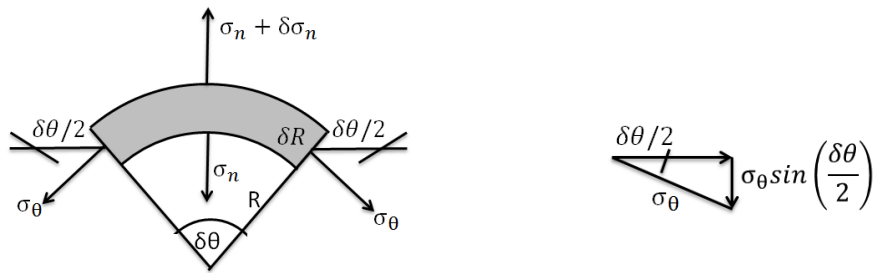
Figure E.2: Wall section of the cylinder.

When assuming a one meter long section, the area at the top is equal to the length times the angle (left of Figure E.2)

$$(R + \delta R)\delta\theta \cdot 1. \tag{Eq. E.4}$$

And at the bottom of the cylinder, this same surface is

$$R\delta\theta \cdot 1. \tag{Eq. E.5}$$

The force is defined as the stress times the area (as in (Eq. E.4) and (Eq. E.5)). The vertical force upwards (σ_n) and the vertical force down are given by (as seen in Figure E.2)

$$(\sigma_n + \delta\sigma_n)(R + \delta R)\delta\theta \tag{Eq. E.6}$$

$$\tag{Eq. E.7}$$

$$\sigma_n R \delta\theta + 2\sigma_\theta \delta R \cdot \sin\left(\frac{\delta\theta}{2}\right).$$

For small angles, the following holds

$$\sin\left(\frac{\delta\theta}{2}\right) = \frac{\delta\theta}{2}. \tag{Eq. E.8}$$

It is now possible to obtain the equilibrium in vertical direction. By setting the upwards facing force (Eq. E.6) equal to the downward force (Eq. 6.7), the following is obtained

$$(\sigma_n + \delta\sigma_n)(R + \delta R)\delta\theta = \sigma_n R \delta\theta + 2\sigma_\theta \delta R \frac{\delta\theta}{2}. \tag{Eq. E.9}$$

By solving this differential equation, one limits is derived

$$\frac{d\sigma_n}{dR} + \sigma_n = \sigma_\theta. \tag{Eq. E.10}$$

The longitudinal stress and strain is constant in the entire cross-section. With the expression for the longitudinal strain, a conclusion can be made regarding σ_θ and σ_n like

$$\varepsilon_z = \frac{1}{E}\left(\sigma_z - \nu(\sigma_n + \sigma_\theta)\right) \tag{Eq. E.11}$$

$$(\sigma_\theta + \sigma_n) = constant. \tag{Eq. E.12}$$

By introducing a constant (2a), the following can be stated

$$(\sigma_\theta + \sigma_n) = 2a \tag{Eq. E.13}$$

$$\sigma_\theta = 2a - \sigma_n. \tag{Eq. E.14}$$

Substituting (Eq. E.14) in the (Eq. E.10) gives

$$\frac{R d\sigma_n}{dR} + \sigma_n = 2a - \sigma_n. \tag{Eq. E.15}$$

(Eq. E.15) is equal to

$$2a = \left(\frac{1}{R}\right)\frac{d(R^2\sigma_n)}{dR}. \tag{Eq. E.16}$$

Rewriting (Eq. E.16) gives

$$2aR = \frac{d(R^2\sigma_n)}{dR}. \tag{Eq. E.17}$$

Integrating this equations results in

$$R^2\sigma_n = aR^2 + b. \tag{Eq. E.18}$$

In which b is an integration constant. The Lame equations are now derived and formulated as follows

$$\sigma_n = a + \frac{b}{R^2} \tag{Eq. E.19}$$

$$\sigma_\theta = a - \frac{b}{R^2}. \tag{Eq. E.20}$$

Representative Test Data

The list of representative test data adopted in the comparison analysis is listed in this appendix. Test data by Virdi et al. (1980), Shakir-Khalil (1993), Roeder et al. (1999), Nezamian et al. (2002) and Aly et al. (2009) have been selected for the appropriate failure mechanism. The test set-up and the results are given for each research.

F.1 Virdi et al. (1980)

The test set-up by Virdi et al. (1980) is given in Figure E.1. The numbering represents the following.
1. Air gap,
2. Deflection transduces,
3. Testing machine,
4. Loading plates,
5. Circular loading path.
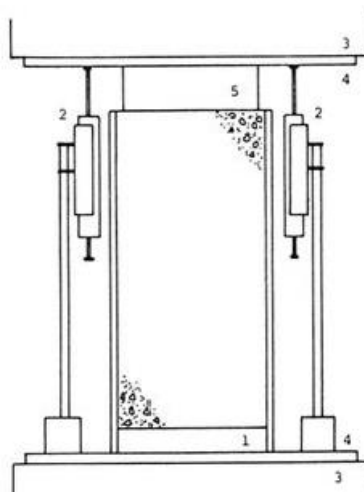
Figure F.1: Test set-up by Virdi et al. (1980).

Table F.1: Representative test results by Virdi et al. (1980).

Test Specimen	D_p [mm]	t_p [mm]	L [mm]	F_{ck} [N/mm²]	E_c [N/mm²]	E_s [N/mm²]	Age [days]	D_p/t_p [-]	L/D_p [-]	f_b [N/mm²]
MA 1	154.58	6.35	342.90	25.84	31715.43	2.10E+05	7	24.34	2.22	2.16
MA 4	155.27	6.35	342.90	36.05	34324.87	2.10E+05	7	24.45	2.21	2.23
MA 5	154.66	6.35	342.90	25.87	31721.29	2.10E+05	7	24.36	2.22	2.24
MA 9	155.04	6.35	342.90	30.69	33015.41	2.10E+05	10	24.42	2.21	2.61
MA 2	155.30	6.35	342.90	36.05	34324.87	2.10E+05	14	24.46	2.21	2.08
MA 7	154.71	6.35	342.90	36.05	34324.87	2.10E+05	14	24.36	2.22	2.75
MA 8	154.66	6.35	342.90	36.05	34324.87	2.10E+05	14	24.36	2.22	2.35
MA 10	155.04	6.35	342.90	37.52	34663.63	2.10E+05	21	24.42	2.21	2.75
MA 3	155.17	6.35	342.90	40.64	35359.86	2.10E+05	28	24.44	2.21	2.97
MA 6	154.58	6.35	342.90	40.64	35359.86	2.10E+05	28	24.34	2.22	2.67
CS14	155.68	6.35	342.90	22.16	30638.23	2.10E+05	28	24.52	2.20	1.94
CS21	154.97	6.35	342.90	22.16	30638.23	2.10E+05	28	24.40	2.21	1.88
CS28	155.32	6.35	342.90	22.16	30638.23	2.10E+05	28	24.46	2.21	1.30
CS19	155.19	6.35	342.90	27.56	32189.53	2.10E+05	28	24.44	2.21	2.24
CS22	155.40	6.35	342.90	27.56	32189.53	2.10E+05	28	24.47	2.21	1.38
CS25	156.16	6.35	342.90	27.56	32189.53	2.10E+05	28	24.59	2.20	2.11
CS13	156.24	6.35	342.90	28.31	32391.80	2.10E+05	28	24.60	2.19	1.43
CS24	155.88	6.35	342.90	28.31	32391.80	2.10E+05	28	24.55	2.20	1.56
CS27	156.49	6.35	342.90	28.31	32391.80	2.10E+05	28	24.64	2.19	1.85
CS12	156.57	6.35	342.90	30.29	32911.88	2.10E+05	28	24.66	2.19	1.77
CS18	155.17	6.35	342.90	30.29	32911.88	2.10E+05	28	24.44	2.21	1.89
CS26	156.26	6.35	342.90	30.29	32911.88	2.10E+05	28	24.61	2.19	1.60
CS11	156.08	6.35	342.90	36.86	34512.07	2.10E+05	28	24.58	2.20	1.91
CS16	155.68	6.35	342.90	36.86	34512.07	2.10E+05	28	24.52	2.20	1.87
CS20	156.16	6.35	342.90	36.86	34512.07	2.10E+05	28	24.59	2.20	2.11
CS15	155.50	6.35	342.90	42.05	35664.40	2.10E+05	28	24.49	2.21	2.34
CS17	156.46	6.35	342.90	42.05	35664.40	2.10E+05	28	24.64	2.19	1.51
CS23	156.36	6.35	342.90	42.05	35664.40	2.10E+05	28	24.62	2.19	1.54
SZ50	149.23	9.68	463.55	46.69	36625.97	2.10E+05	47	15.42	3.11	2.42
SZ51	150.06	9.73	463.55	46.69	36625.97	2.10E+05	47	15.43	3.09	1.79
SZ52	149.28	9.63	463.55	46.69	36625.97	2.10E+05	47	15.51	3.11	2.38
SZ53	156.39	6.53	463.55	46.69	36625.97	2.10E+05	47	23.96	2.96	1.10
SZ54	156.29	6.55	463.55	46.69	36625.97	2.10E+05	47	23.85	2.97	1.30
SZ55	156.79	6.63	463.55	46.69	36625.97	2.10E+05	47	23.65	2.96	1.01
SZ56	158.90	5.74	463.55	46.69	36625.97	2.10E+05	47	27.68	2.92	1.47
SZ57	157.84	5.69	463.55	46.69	36625.97	2.10E+05	47	27.74	2.94	1.25
SZ58	158.78	5.61	463.55	46.69	36625.97	2.10E+05	47	28.29	2.92	1.45
SZ59	206.98	6.50	463.55	46.69	36625.97	2.10E+05	47	31.83	2.24	1.90
SZ60	207.67	6.63	463.55	46.69	36625.97	2.10E+05	47	31.33	2.23	1.94
SZ61	206.63	6.81	463.55	46.69	36625.97	2.10E+05	47	30.35	2.24	1.76
SZ62	231.57	7.34	463.55	46.69	36625.97	2.10E+05	47	31.55	2.00	0.63
SZ63	231.27	7.34	463.55	46.69	36625.97	2.10E+05	47	31.51	2.00	0.52
SZ64	231.95	7.19	463.55	46.69	36625.97	2.10E+05	47	32.27	2.00	0.58
SZ65	305.82	9.55	463.55	46.69	36625.97	2.10E+05	47	32.02	1.52	2.01
SZ66	305.36	9.58	463.55	46.69	36625.97	2.10E+05	47	31.89	1.52	1.99
SZ67	305.99	9.53	463.55	46.69	36625.97	2.10E+05	47	32.13	1.51	2.00

F.2   Shakir-Khalil (1993)
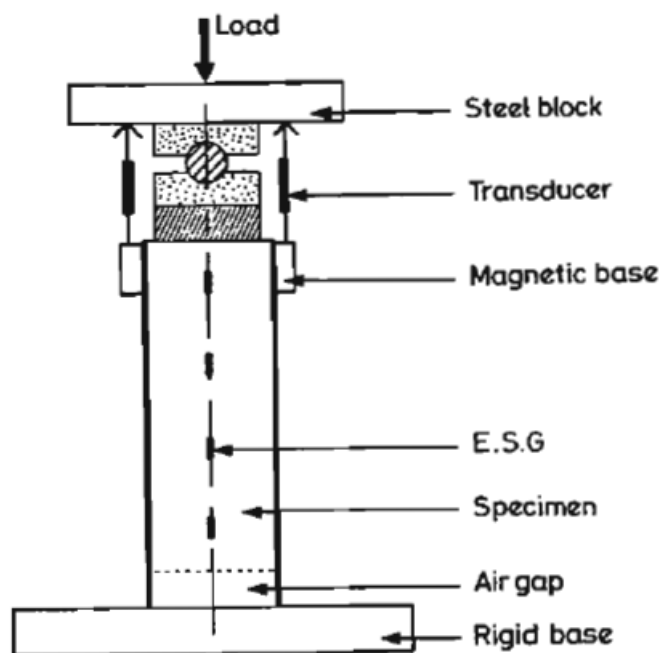
Figure F.2: Test set-up by Shakir-Khalil (1993).

Table F.2: Representative test results by Shakir-Khalil (1993).

Test Specimen	D_D [mm]	t_D [mm]	L [mm]	F_{ck} [N/mm²]	E_c [N/mm²]	E_s [N/mm²]	Age [days]	D_D/t_D [-]	L/D_D [-]	f_b [N/mm²]
Y4a	168.30	5.00	202.00	48.80	37044.79	2.10E+05	28	33.66	1.20	0.88
Y4b	168.30	5.00	203.00	48.80	37044.79	2.10E+05	28	33.66	1.21	0.93
Y5a	168.30	5.00	399.00	48.80	37044.79	2.10E+05	28	33.66	2.37	0.79
Y5b	168.30	5.00	400.00	48.80	37044.79	2.10E+05	28	33.66	2.38	0.80
Y6a	168.30	5.00	600.00	48.80	37044.79	2.10E+05	28	33.66	3.57	0.72
Y6b	168.30	5.00	599.00	48.80	37044.79	2.10E+05	28	33.66	3.56	0.65

F.3   Roeder et al. (1999)
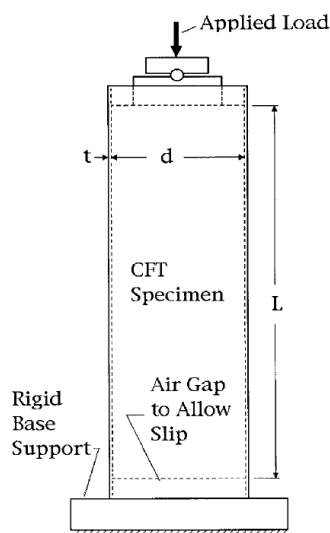
Figure F.3: Test set-up by Roeder et al. (1999).

Table F.3: Representative test results by Roeder et al. (1999).

Test Specimen	D_p [mm]	t_p [mm]	L [mm]	F_{ck} [N/mm²]	E_c [N/mm²]	E_s [N/mm²]	Age [days]	D_p/t_p [-]	L/D_p [-]	f_b [N/mm²]
II-5	355.62	7.11	1064.00	47.30	36748.55	2.10E+05	28	50.01	2.99	0.28
II-6	355.62	7.11	1064.00	47.30	36748.55	2.10E+05	24	50.01	2.99	0.36
II-7	355.62	7.11	1775.00	43.90	36055.61	2.10E+05	29	50.01	4.99	0.18
II-8	355.62	7.11	1775.00	43.90	36055.61	2.10E+05	29	50.01	4.99	0.19
II-9	609.58	5.59	1927.00	44.90	36262.64	2.10E+05	25	109.05	3.16	0.15
II-10	609.58	5.59	1927.00	47.20	36728.60	2.10E+05	25	109.05	3.16	0.18

F.4   Nezamian et al. (2002)
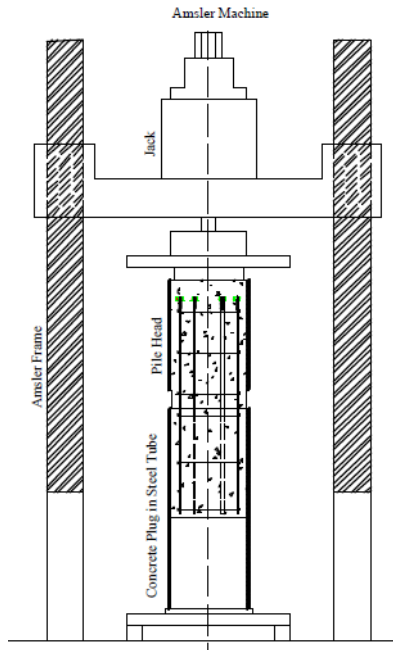
Figure F.4: Test set-up by Nezamian et al. (2002).

Table F.4: Representative test results by Nezamian et al. (2002).

Test Specimen	D_p [mm]	t_p [mm]	L [mm]	F_{ck} [N/mm²]	E_c [N/mm²]	E_s [N/mm²]	Age [days]	D_p/t_p [-]	L/D_p [-]	f_b [N/mm²]
S1000-1	237.00	11.50	1000.00	50.00	37277.87	2.10E+05	28	20.61	4.22	2.02
S1000-2	237.00	11.50	1000.00	50.00	37277.87	2.10E+05	28	20.61	4.22	2.00
S500-1	237.00	11.50	500.00	50.00	37277.87	2.10E+05	28	20.61	2.11	2.06
S500-2	237.00	11.50	500.00	50.00	37277.87	2.10E+05	28	20.61	2.11	2.02

F.5   Aly et al. (2009)
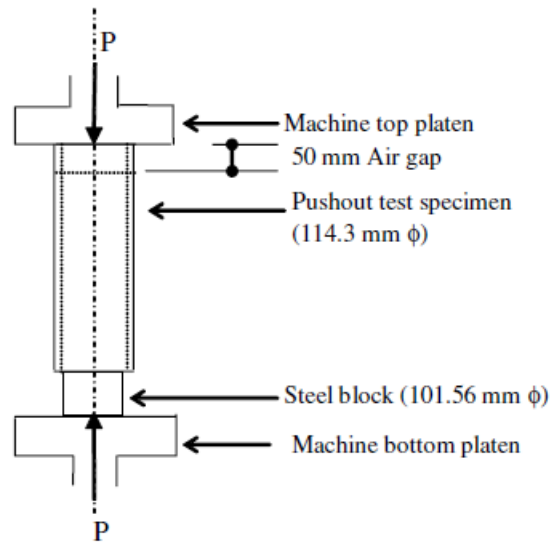
Figure F.5: Test set-up by Aly et al. (2009).

Table F.5: Representative test results by Aly et al. (2009).

Test Specimen	D_p [mm]	t_p [mm]	L [mm]	F_{ck} [N/mm^2]	E_c [N/mm^2]	E_s [N/mm^2]	Age [days]	D_p/t_p [-]	L/D_p [-]	f_b [N/mm^2]
A1	114.30	3.20	522.00	71.00	40898.82	2.10E+05	66	35.72	4.57	1.03
B1	114.30	3.20	522.00	41.00	35439.00	2.10E+05	64	35.72	4.57	1.19
C1	114.30	3.20	522.00	69.00	40585.41	2.10E+05	32	35.72	4.57	0.92
D1	114.30	3.20	522.00	64.00	39776.12	2.10E+05	56	35.72	4.57	1.18
F1	114.30	3.20	522.00	41.00	35439.00	2.10E+05	33	35.72	4.57	1.23
H1	114.30	3.20	522.00	70.00	40742.82	2.10E+05	98	35.72	4.57	1.00

Comparative Study Shear Keys: Pile-Sleeve Standards

Similar to the bond stress, the influences of the parameters on the shear key capacity are determined. These influences cannot be verified with testing for the plug connection due to the lack of test data. Instead, this appendix starts with a comparison between the test results of pile-sleeve specimens and the calculated results from the formulations.

G.1 Comparison

A comparison is made between data of pile-sleeve test specimens and the outcome of the equations. Test data from Lamport et al. (1991) is used for this analysis. They tested eighteen specimens, all with a pile diameter (D_p) of 457mm with a thickness (t_p) of 15.9mm and a sleeve (D_s) of 533mm with 12.7mm wall thickness (t_s). More specifications are given in Table G.1 and Figure G.1.

Table G.1: Test specimens by Lamport et al. (1991).

Sample	L [mm]	h/s [-]	Age [days]	Fck [N/mm²]	Eg [N/mm²]
UTA1	850.90	0.016	20	27.08	19981
UTA2	876.30	0.016	22	27.35	19981
UTA3	906.78	0.016	21	27.70	15158
UTM1	891.54	0.016	23	30.18	19981
UTM2	901.70	0.017	23	28.25	15158
UTM3	881.38	0.018	26	28.94	15158
UTA4	777.24	0.016	21	41.27	25493
UTA5	784.86	0.017	23	39.82	25493
UTA6	769.62	0.017	25	45.54	25493
UTA13	459.74	0.016	21	33.97	22048
UTM5	452.12	0.016	23	37.76	22048
UTM6	469.90	0.015	25	39.07	22048
UTA7	878.84	0.017	21	32.80	22737
UTA8	866.14	0.015	23	34.52	22737
UTA9	871.22	0.017	25	36.86	22737
UTA10	480.06	0.016	2	45.68	24115
UTA11	472.44	0.017	22	76.62	32383
UTA12	474.98	0.017	23	73.59	32383
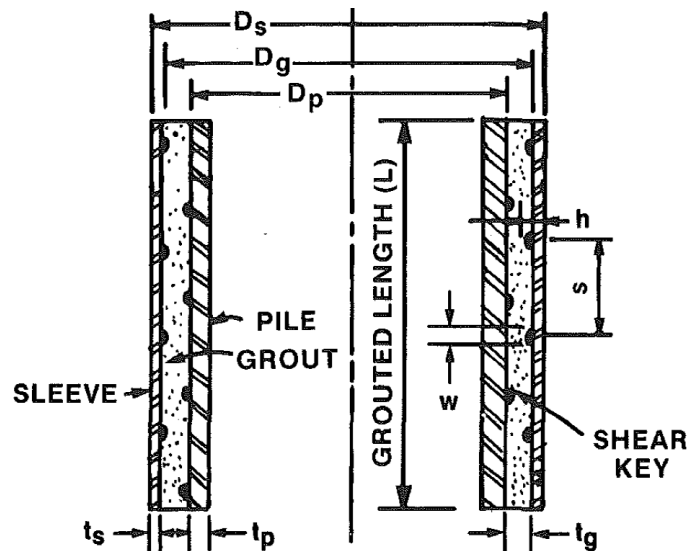
Figure G.1: Definitions for the pile-sleeve connection (Lamport et al. (1991)).

For all eighteen specimens, the axial strength (bond and shear keys) have been calculated. The results including design factors are given in Table G.2. All four standards calculated lower strength compared to the measured axial capacity. The differences are considered really large; differences up to 775% are found. Similar to the plug connections, the Norsok predicts the largest values. For the pile-sleeve connections, it is advised to use this standard in design.

Table G.2: Results of the four design standards.

Sample	Measured capacity [MPa]	OT (2002) [MPa]	API (2003) [MPa]	DNV (2013) [MPa]	Norsok (2012) [MPa]
UTA1	3.53	0.46	0.57	0.58	1.38
UTA2	3.56	0.46	0.58	0.58	1.38
UTA3	3.27	0.43	0.58	0.58	1.34
UTM1	3.51	0.48	0.61	0.60	1.41
UTM2	3.84	0.45	0.61	0.62	1.39
UTM3	4.04	0.48	0.65	0.66	1.43
UTA4	4.36	0.61	0.76	0.69	1.54
UTA5	4.91	0.62	0.77	0.72	1.58
UTA6	4.60	0.67	0.85	0.76	1.62
UTA13	3.52	0.53	0.66	0.63	1.45
UTM5	5.86	0.56	0.71	0.66	1.48
UTM6	4.85	0.54	0.70	0.63	1.45
UTA7	4.35	0.54	0.67	0.66	1.50
UTA8	3.78	0.51	0.64	0.60	1.42
UTA9	3.93	0.58	0.73	0.70	1.53
UTA10	3.46	0.63	0.82	0.71	1.56
UTA11	4.71	0.94	1.28	0.94	1.88
UTA12	4.52	0.92	1.24	0.92	1.86

G.2   Comparative study shear keys

Similar to the bond capacity, a comparative study is conducted. The same example as in section D.5 and 9.1 is used with the stiffness factor proposed by Nezamian (2003). The given values include the design factors as presented in section D.3.

G.2.1   Shear keys: shear key height/spacing

For the same example as before, the axial strength is obtained for all standards. However, this time shear keys are adopted. Within the limits of the expressions, the capacity is plotted against the ratio of the shear key height over the spacing in Figure G.2. The Eurocode, the British standard and the expression by Roeder et al. (1999) do not include shear keys and are for that reason disregarded.

The OT formulation uses the smallest range for the h/s ratio of just 0 to 0.04. Within this range, the calculated values are very similar to the API and DNV. The Norsok standard is the only one which does not use a linear relation between the capacity and h/s. This shows in the purple line which is slightly curved. The difference between Norsok and DNV is rather large at the higher h/s ratios. This is attributed to the lower design factor which is adopted.
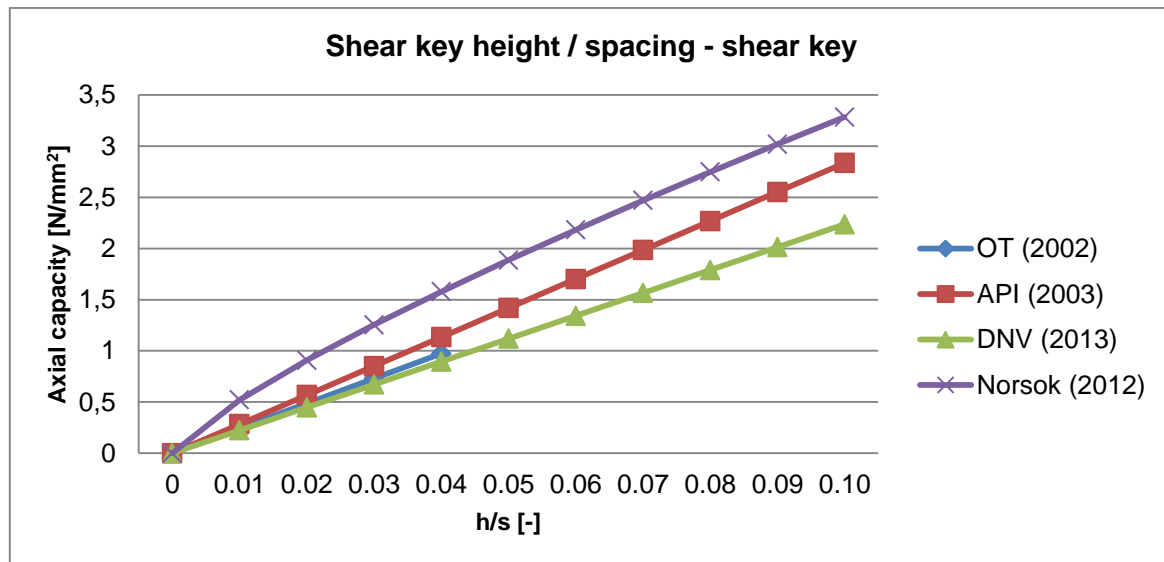
Figure G.2: Effect of the ratio between shear key height and spacing.

G.2.2   Shear keys: concrete compressive strength

The axial capacity due to shear keys is directly related to the compressive strength, as seen in section D.1.1. Therefore, it is expected that the concrete class will have a large influence on the capacity. The maximum values for the h/s ratios are used for the making of Figure G.3. This means a value of 0.04 for the OT and 0.10 for Norsok, DNV and API. The outcomes of the OT are considerably lower than the ones from the other three codes. The mutual differences are much larger than the difference in the previous section.
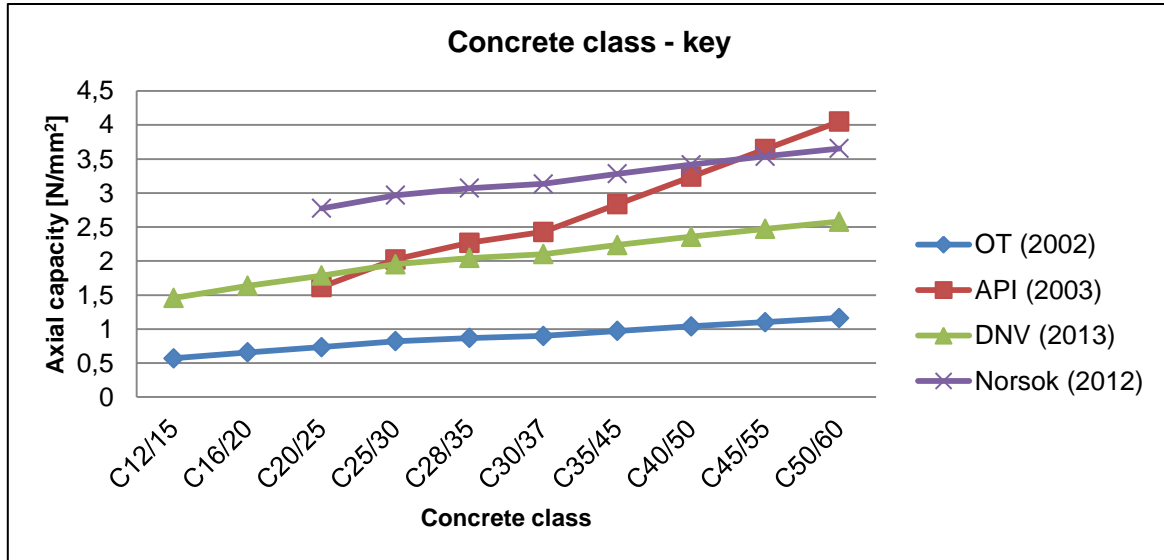
Figure G.3: Effect of the concrete compressive strength on the axial capacity.

G.2.3 Shear keys: diameter over thickness

Within the limits of the standards, the effect of the D_p/t_p is given in Figure G.4. Remarkable detail is the constant value of the API. None of the geometrical properties of the pile are taken into account, so a constant value is given. The other three standards tend to follow the same curve as for the bond capacity. DNV tends to give very high values for low ratios and low values for higher ratios.
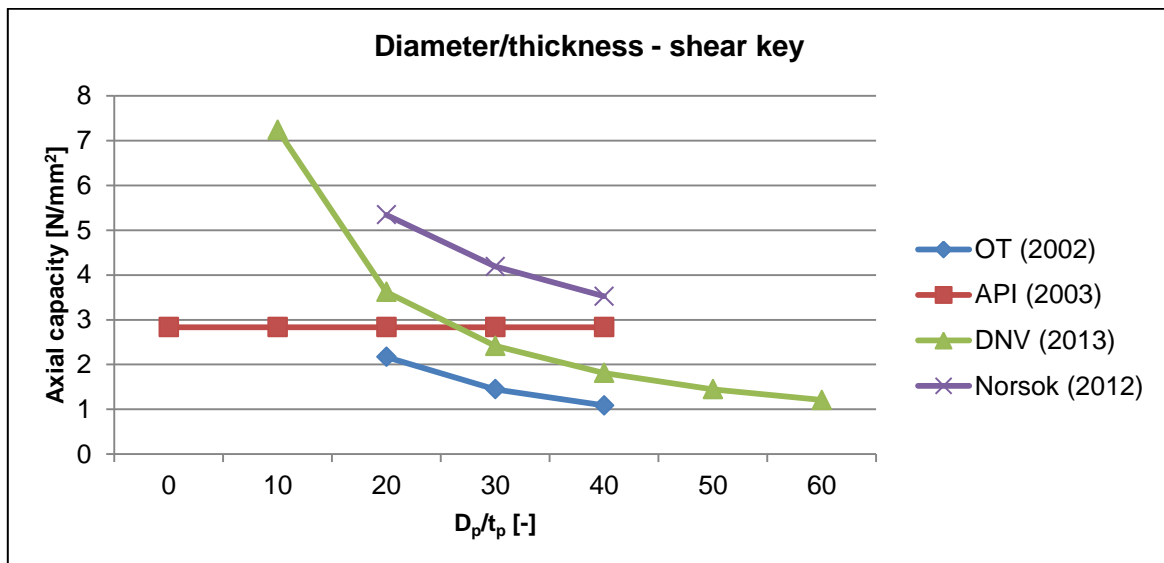
Figure G.4: Effect of the D_p/t_p on the shear key capacity.

G.3 Conclusion

A comparison between the pile-sleeve formulations is performed. These expressions are conservative when they are used for a pile-sleeve connection. However, Appendix D showed that high values are predicted for the bond capacity. Furthermore, a comparative study regarding the h/s ratio, the concrete class and the D_p/t_p ratio is performed. Just like in case of the bond capacity, the mutual differences are very large for the design values. The Norsok design standard tends to give the largest values. It is pointed out that the material factor of 3.0 is used for the DNV code since the grout exceeds the thickness of the pile-sleeve systems.

Costs Comparison

For the given example of Chapter 9, the costs comparison is made whether to choose shear keys or rely solely on bond. The difference in costs will arise due to two reasons namely the positioning of the shear keys and the amount of required concrete. The geometry of the example is given in Table H.1.

Table H.1: The geometry for the given example.

Element	Unit	Shear keys	Bond
h	mm	25	
w	mm	40	
s	mm	600	
L	mm	1200	6034
R_p	mm	457	457
N	shear keys	2	

H.1   Standardized values

Since this is a general comparison, standardized values are used. Table H.2 is composed with the help of an expert of Ballast Nedam. It is assumed that the wages are West-European and that distances to suppliers are reasonable. All required materials and labour is present.

Table H.2: Standardized values which are used in this analysis.

Element	Unit	Values
Steel:		
Weight steel	kg/m^3	7800
Price	€/ton	1500
Welding:		
Welder	€/Hr	50
Help	€/Hr	35
Wage (welder + help)	€/Hr	67.5
Welding rate	m/Hr	1
Generator	€/Hr	25
Material	€/m	8
Concrete:		
Price C35/45	€/m^3	140
Pumping charges	€/m^3	10
Temp control	€/m^3	0
Reinforcement:		
Amount	kg/m^3	200
Costs	€/ton	700
Bending, cutting, installation	€/ton	350

Transport:		
Pontoon	€/day	1500
Tug Boat	€/day	2500
Fuel	€/day	500
Labour (pontoon)	€/day	1400
Trucks	€/m^3	100
Pump	€/m^3	15
No. plugs keys per day	plugs/day	20
No. plugs without keys per day	plugs/day	12

H.2   Example (axial load 3000kN)

In the example, an axial load of 3000kN is assumed. For this load, the length for the plain plug connection is calculated at a length of 6050mm. With the standardized values of Table H.2, the costs are given in Table H.3. When the costs for the shear keys are set to 100%, the costs for the plain connection are equal to 104%.

Table H.3: Costs comparison for the example of Chapter 9 with an axial load of 3000kN.

Element	Unit	Shear keys	Bond
Steel:			
Amount steel	m^3	0.006	
Weight	ton	0.045	
Total:	**€/plug**	**67**	
Welds:			
Temporary facilities	€/plug	150	
testing welds	€/plug	75	
Welders	€/plug	775	
Generator	€/plug	287	
Material	€/plug	46	
Total:	**€/plug**	**1333**	
Concrete:			
Amount concrete	m^3	0.79	3.96
Price material	€/plug	79	396
Temp control	€/plug	0	0
Pumping charges	€/plug	8	40
Total:	**€/plug**	**87**	**436**
Reinforcement:			
Steel costs	€/plug	110	504
bending, cutting installation	€/plug	55	252
Total:	**€/plug**	**165**	**756**
Transport:			
Transport:	€/plug	295	492
trucks + pump	€/plug	90	455
Total:	**€/plug**	**385**	**947**
Formwork:			
Total:	**€/plug**	**500**	**500**
Total:	**€/plug**	**2537**	**2637**
		100%	**104%**

H.3   Example (axial load 2500kN)

When the analysis is performed again only now with an axial load of 2500kN, the results completely change (Table H.4). The interface length of the plain connection reduces to 4850mm instead of the 6034mm from the previous section. With this new length, the plain connection will be cheaper (91% of the shear key connection). The plug of the shear key connection cannot be shortened since the reinforcement bars need an appropriate anchorage length.

Table H.4: Costs comparison for the example of Chapter 9 with an axial load of 2500kN.

Element	Unit	Shear keys	Bond
Steel:			
Amount steel	m^3	0.006	
Weight	ton	0.045	
Total:	**€/plug**	**67**	
Welds:			
Temporary facilities	€/plug	150	
testing welds	€/plug	75	
Welders	€/plug	775	
Generator	€/plug	287	
Material	€/plug	46	
Total:	**€/plug**	**1333**	
Concrete:			
Amount concrete	m^3	0.79	3.17
Price material	€/plug	79	317
Temp control	€/plug	0	0
Pumping charges	€/plug	8	32
Total:	**€/plug**	**87**	**349**
Reinforcement:			
Steel costs	€/plug	110	404
bending, cutting installation	€/plug	55	202
Total:	**€/plug**	**165**	**606**
Transport:			
Transport:	€/plug	295	492
trucks + pump	€/plug	90	365
Total:	**€/plug**	**385**	**857**
Formwork:			
Total:	**€/plug**	**500**	**500**
Total:	**€/plug**	**2537**	**2312**
		100%	**91%**

Glossary

List of Symbols

a	Adhesion
A_c	Concrete surface
Acc	Concrete area in compression
Asc	Steel area in compression
Ast	Steel area in tension
b	Correction factor
b_{fr}	Friction factor
c	Cover on the longitudinal RC
C_c	Compressive force concrete
C_f	Radial flexibility factor
C_I	Surface irregularities (=0.084mm)
C_L	Length parameter
C_p	Diameter scale factor
C_s	Surface condition factor
C_s	Radial Stiffness (Norsok)
C_s	Compressive force steel
D_g	Outer diameter grout
D_o	Outside diameter annual ring
D_p	Mean pile diameter
D_s	Outer diameter sleeve
E_c	Modulus of elasticity concrete
E_g	Modulus of elasticity grout
E_s	Modulus of elasticity steel
f_{axial}	Total capacity (bond and shear keys)
f_b	Bond stress
f_{ck}	Char. concrete compressive strength
f_{ck}^*	Crushing strength concrete
f_{EXX}	Min. tensile strength weld material
$f_{friction}$	Friction between pile and plug due to necking of the pile
f_{key}	Max stress keys
f_r	Tensile strength concrete
f_{sk}	Shear key axial capacity
f_u	Ultimate tensile capacity pile
$f_{u,sk}$	Bond strength including shear keys
$g_{rt}(x)$	Resistance model
h	Outstand of the shear keys
h_o	Fictitious height
H	Horizontal force on the cap
m	Modular ratio (E_s/E_g)
$M_{s,d}$	Bending moment on the plug

k	Stiffness connection (Eurocode)
k_∞, k_n	Fractile factors
k_{API}	Ratio f_{ck}^*/f_{ck}
K	Radial stiffness
K_{DNV}	Stiffness factor DNV
$K_{Nezamian}$	Proposed stiffness factor
K_{OT}	Stiffness factor offshore technology
l_e	Embedment length
L	Interface length
L_{pile}	Pile length above firm soil
$M_{shear\ key}$	Moment capacity per shear key
M_{sk}	Bending moment capacity of all keys
$M_{tot,plug}$	Total bending moment capacity
M_{wr}	Bending moment capacity wrenching
$M_{\mu,wr}$	Bending moment capacity friction
N	Number of shear keys
p	Pressure induced by necking
$p_{contact}$	Contact pressure
p_{local}	Local stress at the top of the plug
p_{nom}	Nominal allowed stress
P	Vertical force on the piles
P_o	Maximum force on the piles
P_u	Axial capacity plug
R	Ratio R_c/R_p^2
$R_{b,i}$	Resultant force in batter pile
R_c	Radius plug
R_i	Inner radius concrete cylinder
r_k	Resistance function with factor
R_P	Radius steel pile
s	Shear key spacing
s_Δ	Standard deviation
t	Time in days
t_g	Thickness grout
t_p	Thickness pile
t_r	Thickness of concrete layer between pile and longitudinal RC
t_s	Thickness sleeve
T_s	Tensile force steel
u	Perimeter concrete
V_i	Vertical force piles
V_r	Variance including product function

V_{xi}	Variance resistance factors
V_{δ}	Variance test data
w	Shear key width
W	Weld size

Greek Symbols

α_{rt}, α_{δ}	Weighing factors
α, β, κ	Empirical parameters Kelvin model
β_{as}	Time factor autogenous shrinkage
$\beta_{ds}(t,t_s)$	Time factor chemical shrinkage
δ_{DNV}	Surface condition DNV ($0.0037R_p$)
δ_i	Specimen dispersion
Δ	Difference in radial displacements
$\bar{\Delta}$	Average dispersion
Δ_1	Enlargement of the steel tube
Δ_2	Shrinkage
Δ_3	Rugosity of the tube
Δ_c	Radial displacement concrete
Δ_i	Logarithm of dispersion terms
Δ_s	Radial displacement steel
$\varepsilon_{ac}(\infty)$	Final autogenous shrinkage
$\varepsilon_{cd}(t)$	Chemical shrinkage

$\varepsilon_{c,\theta}$	Circumferential strain concrete
$\varepsilon_{s,\theta}$	Circumferential strain steel
κ	Early age reduction factor (DNV)
μ	Coulomb-friction coefficient (=0.5)
μ_s	Surface irregularities tube (=0.05)
μ_{DNV}	Surface interface DNV (=0.4-0.6)
υ_c	Poisson ratio concrete
υ_s	Poisson ratio steel
ρ_v	Amount of shear RC
$\sigma_{c,n}$	Radial pressure on the concrete
$\sigma_{c,\theta}$	Circumferential stress concrete
$\sigma_{c,z}$	Longitudinal stress concrete
$\sigma_{s,n}$	Radial pressure on the steel tube
$\sigma_{s,\theta}$	Circumferential stress steel tube
$\sigma_{s,z}$	Longitudinal stress steel tube
τ	Shear strength concrete
τ_A	Axial shear due to normal force
τ_M	Axial shear due to bending moment
τ_{kg}	Shear strength grout
φ	Angle

List of Acronyms

API	American Petroleum Institute
BS	British Standard
CFT	Concrete Filled Tube
DF	Derived Formulation
DNV	Det Norske Veritas
EC	Eurocode
FE	Finite Element
MOE	Modulus of Elasticity
NSC	Normal Strength Concrete
OT	Offshore Technology
PSDM	Plastic Stress Distribution Method
RC	Reinforcement
SD	Standard Deviation
SCF	Stress Concentration Factor
STM	Strut and Tie Model